IGRF-13 candidate evaluations by GFZ

M. Korte[1], F. Vervelidou[2,1], M. Rother[1]

November 22, 2019

[1] Helmholtz Centre Potsdam, GFZ German Research Centre for Geosciences, Telegrafenberg, 14473 Potsdam, Germany.

[2] Université de Paris, Institut de Physique du Globe de Paris, CNRS, F-75005 Paris, France.

Contents

1 Candidates Overview

The following table designates a capital letter (used as model ID everywhere), a color and a line type or symbol (used in sections 5 to 7 and appendix A). The model IDs A – O agree with Patrick's suggestion. The $\oplus$-sign shows if the candidate type is available.

ID	Colour	Line type, Symbol	Designat	15	20	SV
A	black	solid line, star	BGS	$\oplus$	$\oplus$	$\oplus$
B	orange		CEA/CSES		$\oplus$	
C	green		CU/NCEI	$\oplus$	$\oplus$	$\oplus$
D	red		DTU	$\oplus$	$\oplus$	$\oplus$
E	blue		GFZ	$\oplus$	$\oplus$	$\oplus$
F	brown		IPGP	$\oplus$	$\oplus$	$\oplus$
G	purple		ISTerre	$\oplus$	$\oplus$	$\oplus$
H	gray		IZMIRAN	$\oplus$	$\oplus$	$\oplus$
I	black	dashed line, circle	Japanese Consortium			$\oplus$
J	orange		Leeds			$\oplus$
K	green		MPS (Max Planck)			$\oplus$
L	red		NASA_GSFC	$\oplus$	$\oplus$	$\oplus$
M	blue		Uni Potsdam/Max Planck	$\oplus$	$\oplus$	$\oplus$
N	brown		Spanish Team	$\oplus$	$\oplus$	$\oplus$
O	purple		U Strasbourg et al.	$\oplus$	$\oplus$	$\oplus$
X	gray		arithmetic mean model			

We confirmed that all our arithmetic mean and median models agree with the means and medians that Patrick distributed at the end of October.

2 Assessment of candidate models

The following assessment is based on inter-comparison analyses described in sections $3-8$, and appendix B. Most of these analyses follow methods and plots performed by the 2015 evaluation paper (Thébault et al., EPS, doi:10.1186/s40623-015-0273-4). In addition, section 9 contains a comparison of the candidate models to data from several ground observatories.

2.1 DGRF 2015

All models seem valid representations of the geomagnetic field 2015, with varying amounts of external field leakage. Deviation from the arithmetic mean does not tell about deviation from the true (core) field, the true pure core field contribution is unknown in all three cases (2015, 2020, SV).

The mean vector field differences ${}_{i,j}R$ range between 4.34 and 9.17 nT and are mostly in the same range, though overall slightly larger, than had been the case for `DGRF2010` (see 3.1 and the separate Excel sheet). Models D, M and F show the closest consistency with the mean among all models. Models G, H and O show the strongest deviations from the mean, the median and from all other models. There also is no consistency among these three "outliers", i.e. they differ from the mean in very different ways. This is apparent in the difference maps shown in section 4.1 or appendix A.1 and the Lowes and azimuthal power spectra shown in section 6.1. In particular, in agreement with the differences in the spatial domain (section 4.1), model G has the largest difference with respect to the mean and median models over low degrees, but is quite consistent in degrees 8 and higher (see 5.1 and appendix A.1). Models H and O have the largest differences over higher degrees. However, while models H and O are the ones that differ most from the mean and medians models in terms of degree correlation (see section 7.1), model G shows a higher degree of agreement than other models. But overall, the degree correlation is very high for all degrees among the different models, especially up to degree 8.

Model N has the most different power distribution, SH degrees 2, 4 and 9 are quite consistent, while other degrees are quite different from the mean (see 6.1). Although model G comes with uncertainty estimates on the coefficients, for many of them, in particular the low degree ones, the uncertainty estimates do not reach to the majority of the other models (Appendix A.1). The uncertainties of other models that provide them are much lower for the low degree coefficients than those of model G, for higher degrees the uncertainty estimates of model N are large and often include many other models.

As far as the sensitivity matrices are concerned (see section 8.1), models H and O, together with model N, show the largest difference with respect to mean and median models, while model G shows again a higher degree of agreement.

Systematic deviations from the mean that might be interpreted as specific external field influence (see section 4.1 and appendix section B.1):

- Models A, C, H, and particularly L and N have some geomagnetic latitudinal structures. For A and C this is mainly a difference between equatorial and higher latitudes, for H several latitudinal stripes are seen. In L and N the B_Z difference from the mean or median has a clear north-south hemispheric pattern, interestingly of opposed sign in the two models, and appearing as stripes over all latitudes when downward continued to the CMB. In other components the differences at the surface are most pronounced at high latitudes.

- Models D and F show weak hemispheric deviations in Z with lower values in the north and higher in the south, while an opposite pattern is found in model E.

- Models D, F, N seem to have somewhat lower global intensity than the mean, while models G, L and E seem somewhat higher in this respect.

2.2 IGRF 2020

All models seem valid representations of the geomagnetic field 2020, with varying amounts of external field leakage. As expected, the differences with respect to the mean and median models are larger than in the case of DGRF 2015.

The mean vector field differences $_{i,j}$R range between 8.93 and 16.84, in the same range as was the case for IGRF2015 (see 3.2 and the separate Excel sheet).

Models D, M, A and F are most consistent with the mean and among them. Models O, B, E and N differ most strongly from the mean and are also not consistent among them (seen also in appendix A.2, or the difference maps in 4.2 and B.2). In three cases, individual (regional) differences from the mean or median exceed +/-20nT. For models E and N, this is due to long tails in the histograms, while the distribution for model O is closer to normally distributed (see section 4.3. According to the Lowes power spectra, model E carries significantly more energy over degrees 3-6 than the other models. However, this difference is not visible anymore when plotting the azimuthal power spectra. In terms of degree correlation, same as for DGRF, the models show a high degree of agreement with the mean and median models, with models B, H, N and O being the ones with the smallest degree of agreement.

Not surprisingly, the scatter in coefficients is larger for 2020 than for 2015 and outliers in individual coefficients are less obvious (see section 5.2 and appendix A.2). Models G (for low degrees only) , E (mainly for intermediate degrees), N, O (mainly for higher degrees) and B (for a few coefficients of various degree) seem to be the ones differing most strongly from the others. In terms of sensitivity matrices, the models B, N and O are the ones that show the largest differences with respect to the mean and median models. Uncertainty estimates mostly overlap at least with some of the other models. A few coefficients of models E and O are the main exceptions of outlying coefficients (without uncertainty estimates) that do not fall within uncertainty estimates from one of the models that have them.

Systematic patterns are also less pronounced while the models in general differ more strongly than in the DGRF 2015 case (see section 4.2 and appendix B.2):

- Geomagnetic latitudinal structures in the differences are seen for models C, F, L and N, for C and N with very similar pattern to the DGRF 2015 case (appendix B.2)
- Models D and F have somewhat lower global intensity than the mean, while models B, L and N have higher global intensity.
- Models F and L show hemispheric (north-south) differences from the mean with opposite sign.
- Model G has a distinct large-scale deviation from the mean, manifesting as a zonally hemispheric deviation with larger values over the Americas and much of the Pacific and smaller values over Europe, Africa and Asia in intensity compared to the mean.

2.3 SV 2020 - 2025

Future SV clearly is the most difficult quantity to estimate, and consequently nearly all models differ notably from the mean or median.

The mean vector field differences ${}_{i,j}R$ (see 3.3) lie between 11.49 and 32.95 nT/yr, a much larger spread than it was the case 5 years ago. Model D is the closest to the mean. Models L, O, I and C differ most strongly from the mean, again also without being consistent among this group. In particular models L, O and I differ by more than 20 nT/yr from most other models and the mean, L and O differ from each other by 40 nT/yr. For model O, the difference (see section A.3) mainly comes from the dipole coefficients, for L a large part comes from equatorial dipole and quadrupole. Model L is the only one where several B_r values deviate from the mean and median by more than $\pm$40 nT/yr, reaching up to -45 nT/yr and +48 nT/yr (4.4 and 4.3). The corresponding deviation values of models O and I are about $\pm$30 nT/yr. However, the distribution of differences for model O is far from normally distributed, with a larger fraction of large differences than in the other models (see 4.3). Model L appears most obviously as outlying also in coefficient differences (see 5.3), power spectra, both Lowes and azimuthal (see 6.3), and sensitivity matrix (8.3). In terms of degree correlation it stands out for degrees 2 and especially 3, the same as in the Lowes power spectrum. This shows that the observed excessive energy, with respect to the mean and median models, is mainly carried by these degrees. Model O stands out for degree 1, model I for degree 5 and model J for degree 7. Models L, I and O are the ones that differ most from the other models according to the azimuthal power spectra. For nearly all models the spectral difference (see section 6.3 and appendix B.3) tends to be larger for low degree coefficients (though dipole often a bit smaller than quadrupole) and smaller for higher degrees, with the exceptions of models J (nearly opposite) and N (close to flat spectral difference). The sensitivity matrices underline the fact that there is a much better agreement between the DGRF and IGRF models than the SV models. In addition to the already discussed outliers L, I and O, models C, E, H and N appear to have also large differences with respect to the mean and median models, at least over some degrees.

We don't really spot any interpretable spatial patterns in the differences from the mean (see appendix section B.3), perhaps excluding some more zonal structures in models A and H (but not agreeing in amplitudes and sign all over Earth), and a hemispheric structure in model O with weaker SV prediction for the northern and stronger for the southern hemisphere than estimated by the arithmetic mean model.

2.4 Suggestions for final models

We have no way to determine the *best* model. It seems likely that the *truth* is close to where solutions tend to cluster, in particular if they come from models derived from different data sets and with different modelling techniques. Systematic patterns indicate that several models seem to suffer from external field leakage in various forms, but at least for DGRF 2015 and IGRF 2020 we do not consider it justified to reject complete models based on the findings

from the comparisons. In our opinion the weighted averaging as done for the previous DGRF 2010 and IGRF 2015 is a good solution. We would indeed consider weighted averaging of individual coefficients as wrong, because we assume there are correlations among each model's coefficients. So we are in favour of last time's practice of averaging the B_r surface field values with assigned Huber weights.

For SV, we find it a more difficult decision. On the one hand, there is one very clear outlier (model L) and one or two more models that differ substantially from mean or median (models O and I). All three of these also show large differences to each other, which might justify a complete rejection of these from the final SV product. On the other hand, due to the variability of SV, we expect the mean or median to be less meaningful and we assume that the chances that apparently outlying values turn out to be correct are much higher here than would be the case in the DGRF or IGRF case. That would argue for including these models. We also note that due to the large differences in spatial patterns, averaging all models at the surface might lead to significantly subdued SV estimates compared to the unknown reality, which might be reflected better in one of the individual models (that in this case could be even one of the outliers). However, as we have no way to tell at the present time, we consider the previous solution of also averaging all these model values at Earth's surface with Huber weights a reasonable solution. It might be worth checking how much influence the one to three outlying models (L, O and I) have by building weighted averages with and without these models and deciding upon evaluation.

3 Vector field differences

The following plots are visualisations of the RMS vector field differences $_{i,j}$R provided in units of nT (nT/yr for SV) between all pairs of models and to the arithmetic mean model X. The top row shows the mean value of each column. There are blank rows and columns if the corresponding candidate model does not exist. Apart from the extra *Mean (A-O)* row the matrices are of course symmetric. The values plotted here are provided in the separate Excel sheet (generally equivalent to tables 3, 5 and 7 from the 2015 evaluation paper).

3.1 RMS vector field differences DGRF 2015

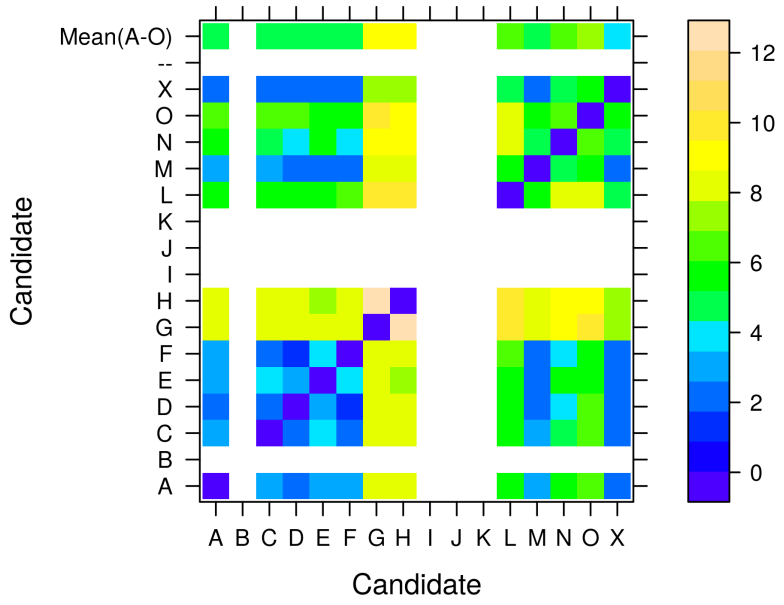

3.2 RMS vector field differences IGRF 2020

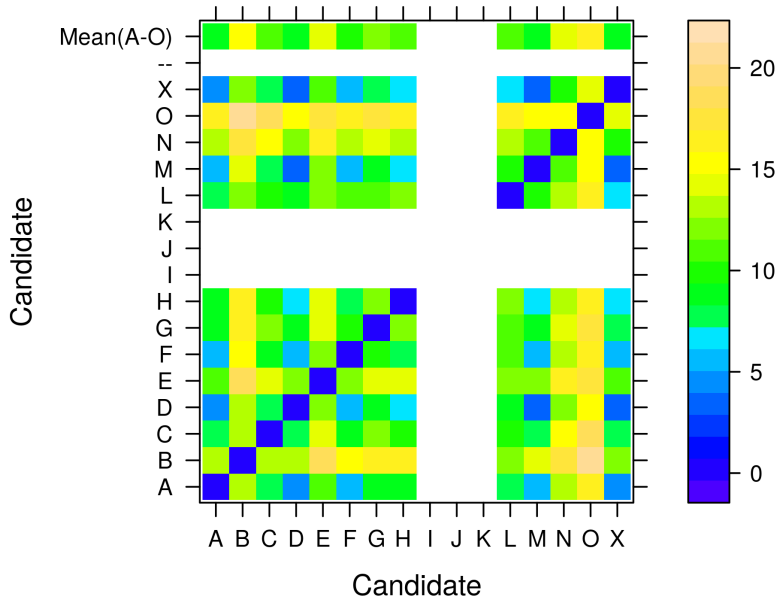

3.3 RMS vector field differences SV 2020-2025

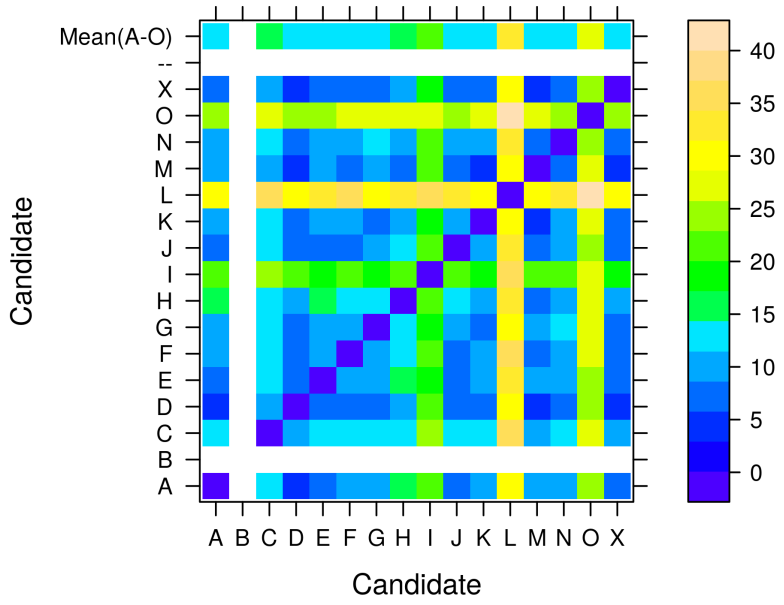

4 Maps

The following maps show the difference in nT of the down B_z component between each candidate model and the arithmetic mean or median (see figure titles) for DGRF 2015, IGRF 2020 and SV. The color scale goes from -15 to 15 nT for DGRF 2015 for all models, from -20 to 20 nT for IGRF 2020 for all models, and from -30 to 30 nT for the SV for all models except for model L, for which it goes from -50 nT to 50 nT.

It is saturated (higher absolute values) in several cases.

4.1 DGRF 2015, Mean and Median

Mean

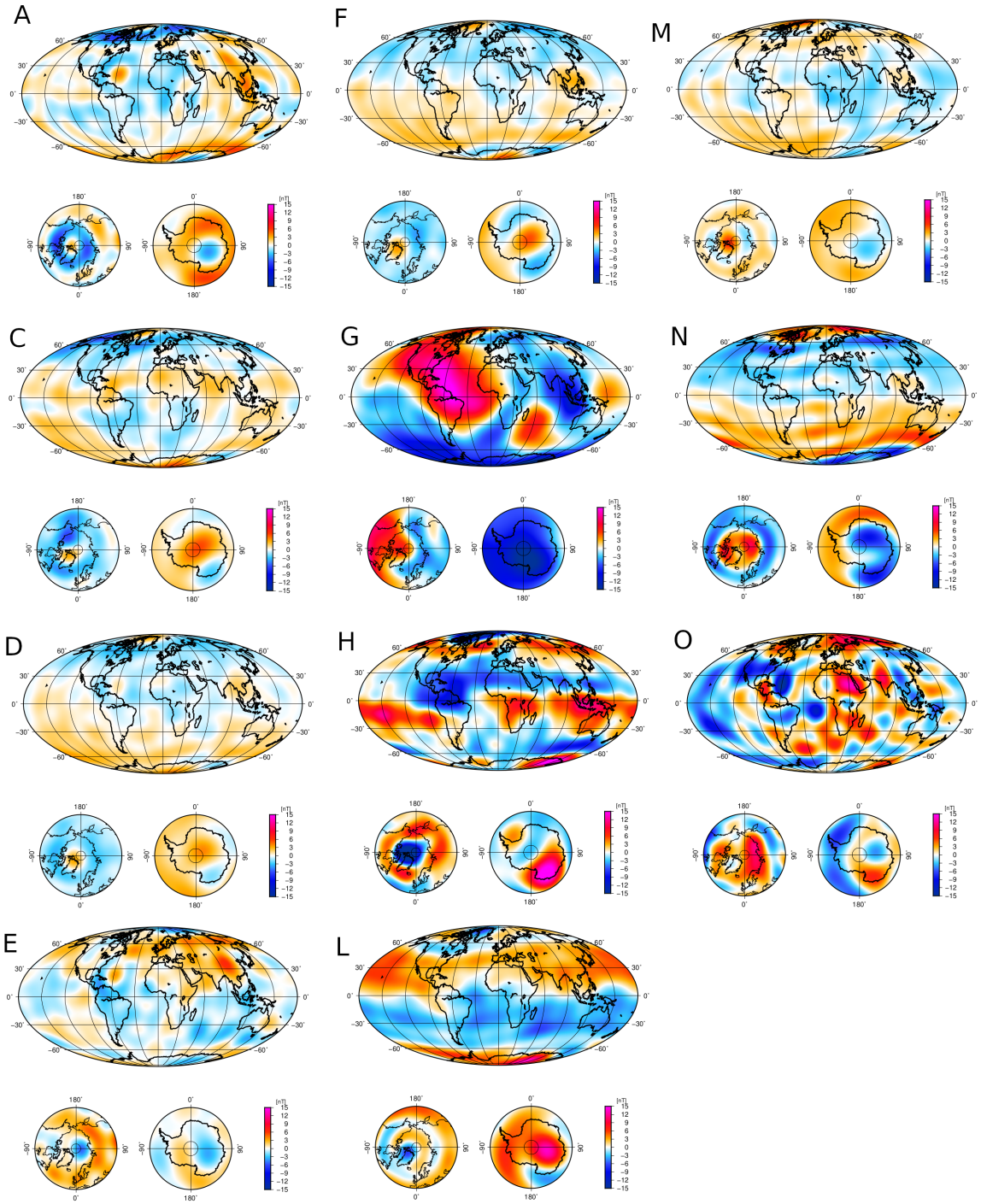

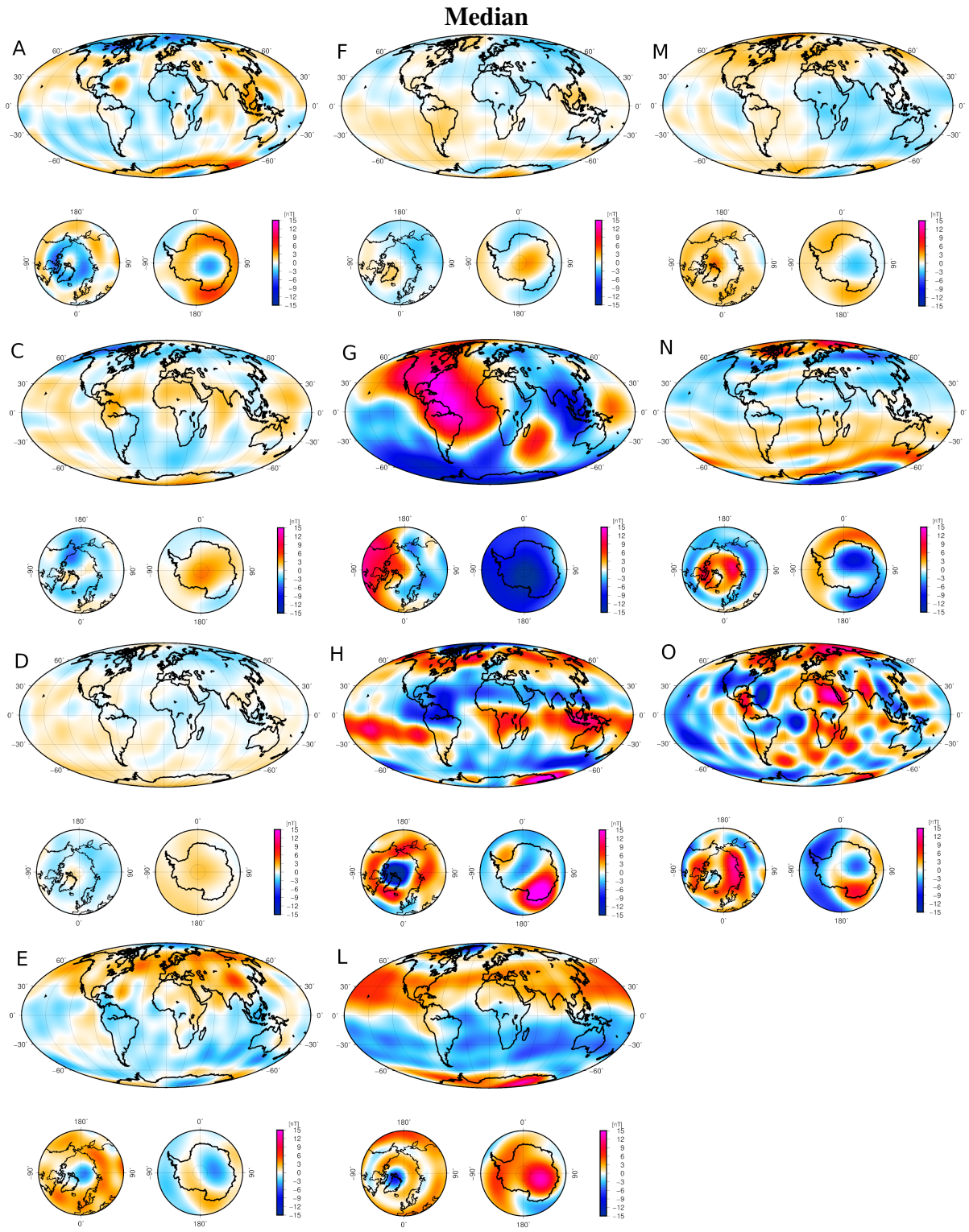
Median
A
F
M
C
G
N
D
H
O
E
L
[nT]
15
12
9
6
3
0
−3
−6
−9
−12
−15

4.2 IGRF 2020, Mean and Median

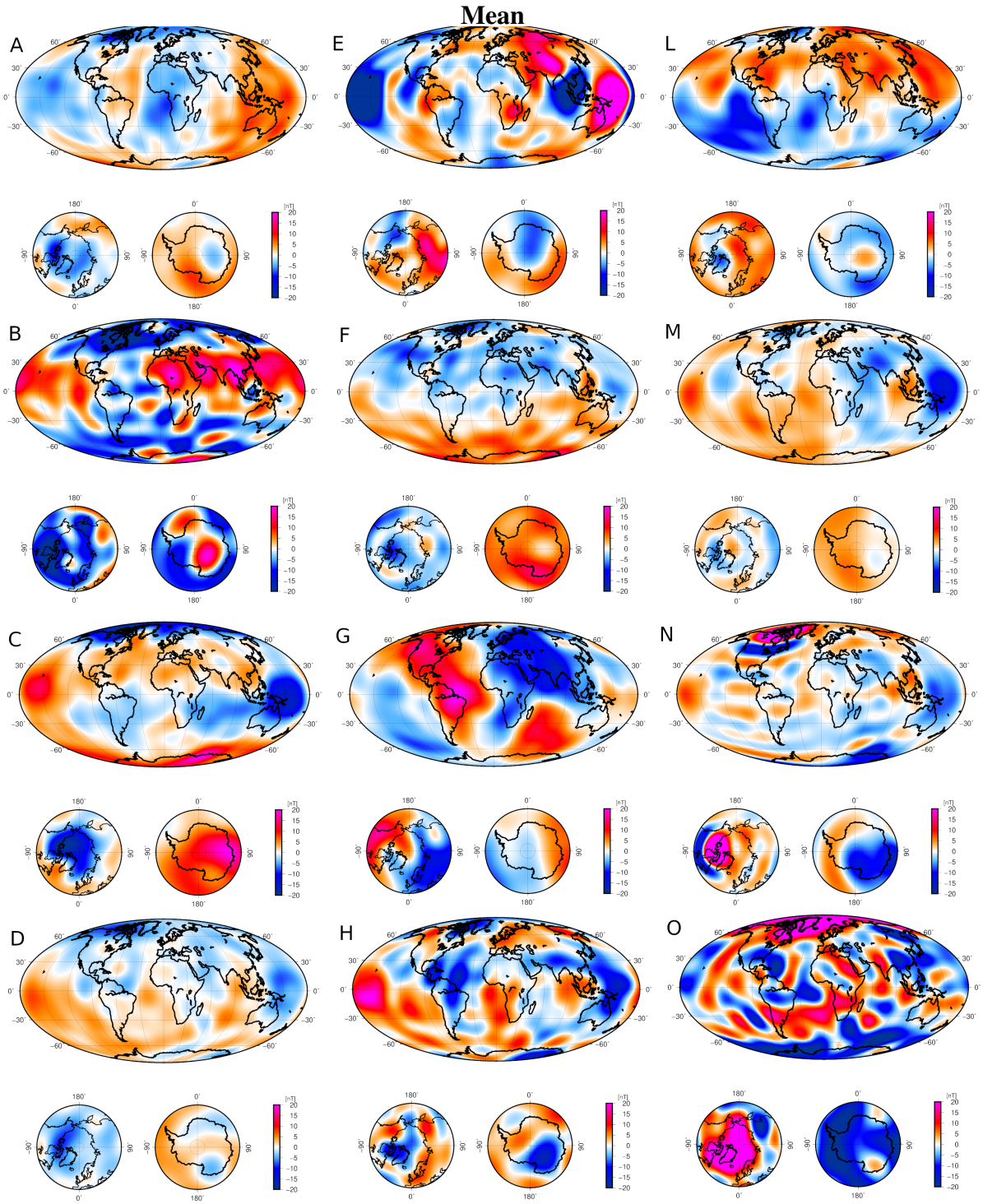

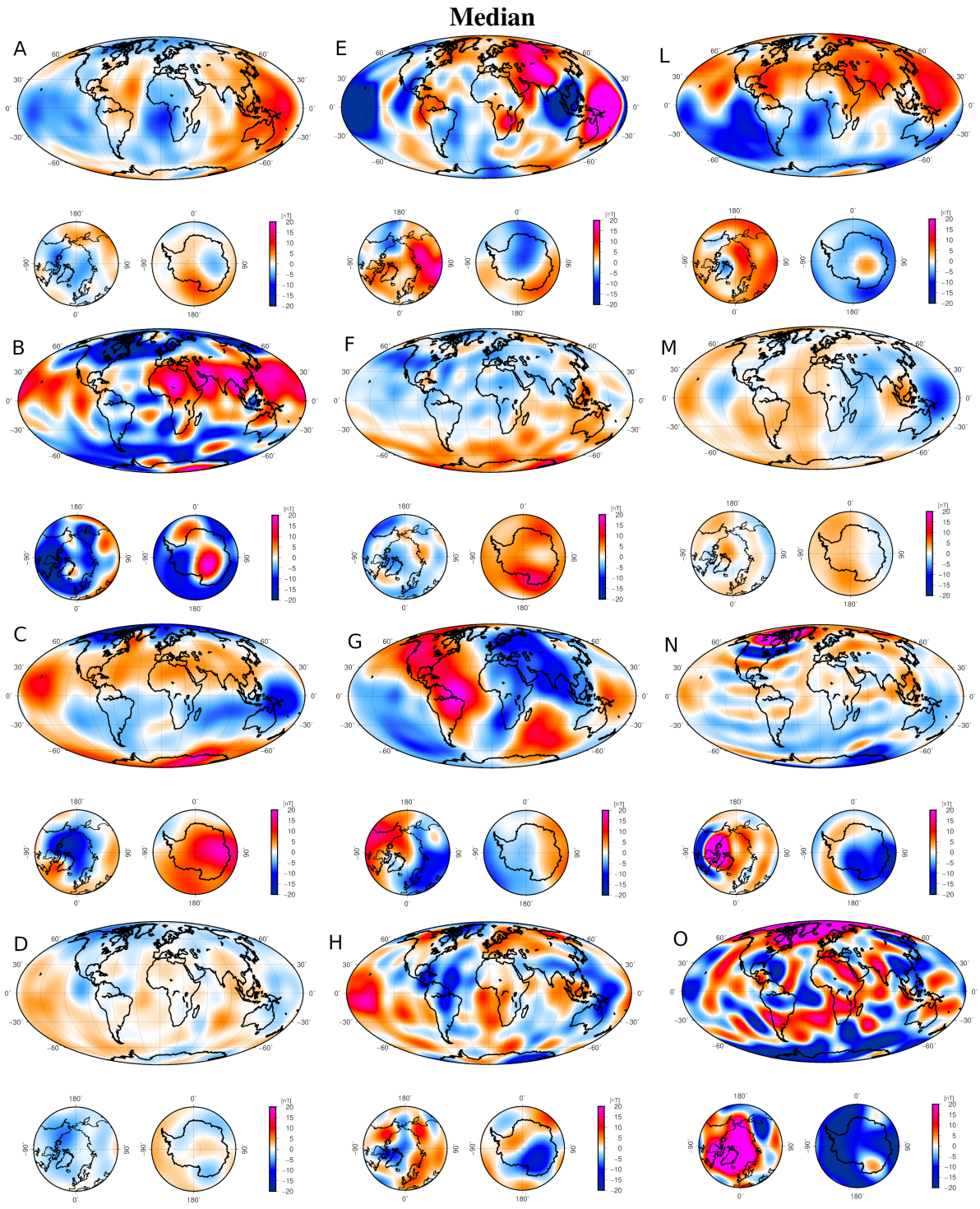
Median
A
E
L
B
F
M
C
G
N
D
H
O
[nT]
20
15
10
5
0
−5
−10
−15
−20

4.3 Difference histograms

The following figure shows histograms of the differences between the Bz component of the IGRF candidate models and the Bz component of the mean (top) and median (bottom) models, for the three candidate models with differences that sporadically go significantly beyond +/-20 nT.

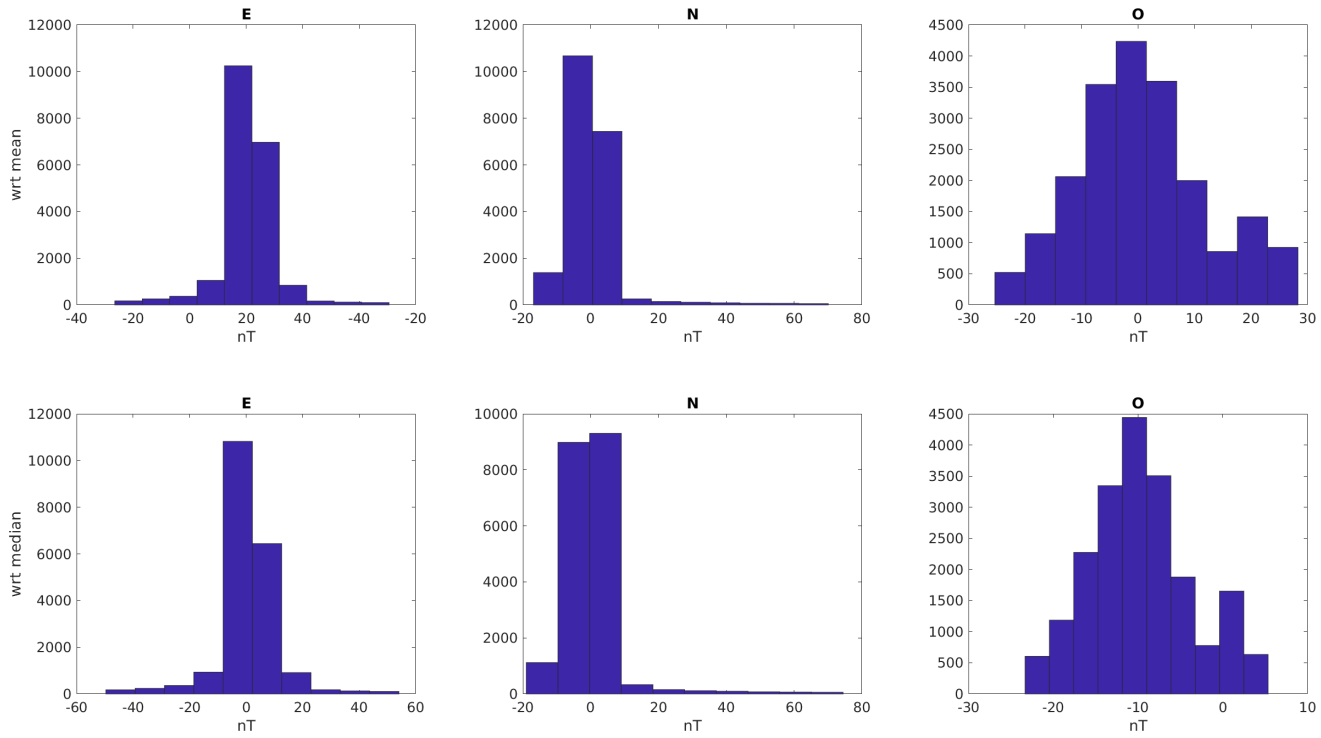

4.4 SV 2020–2025, Mean and Median

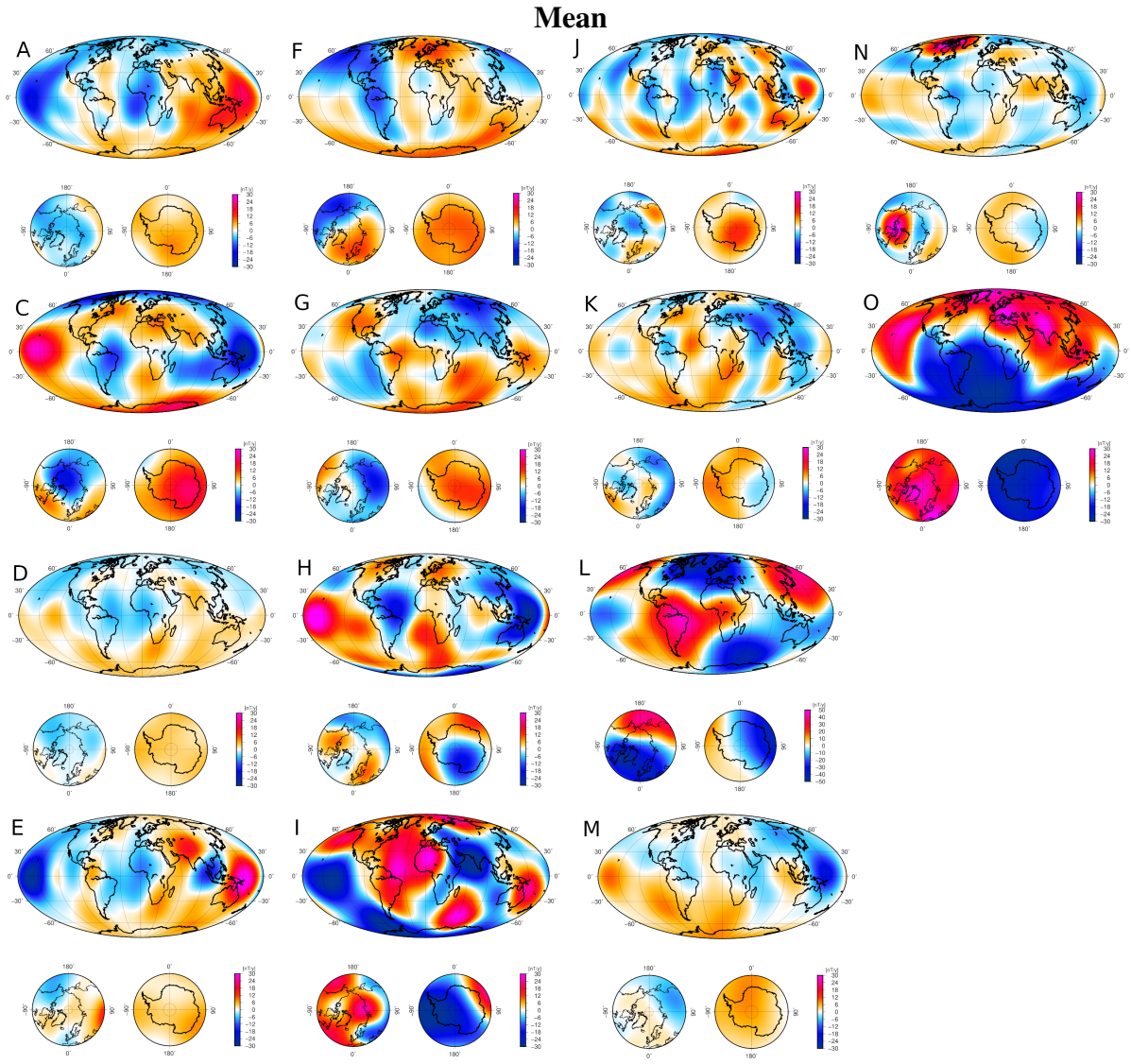

Median

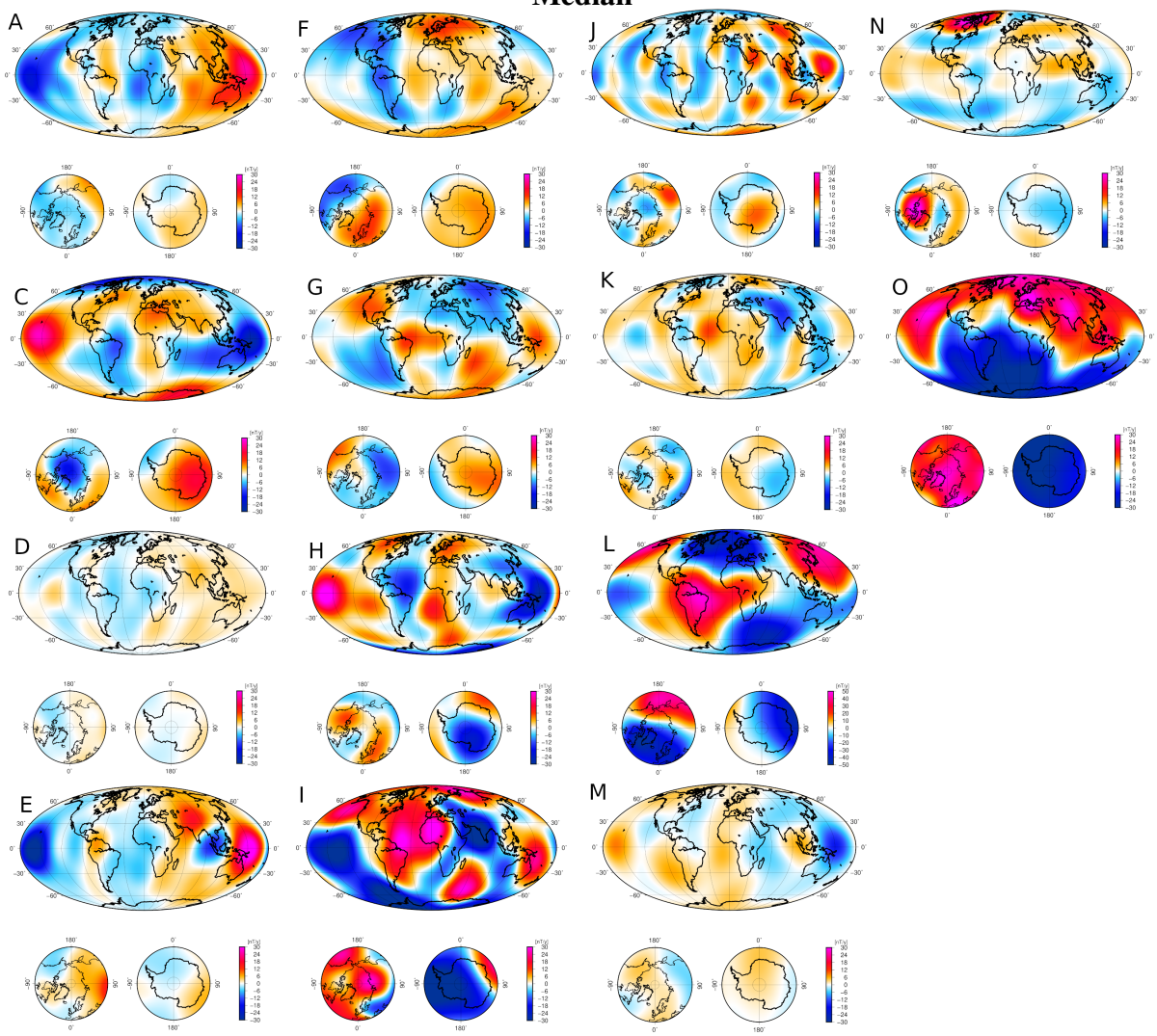

4.5 Difference histograms

The following histograms show histograms of the differences from the mean (top) or median (bottom) plotted in section 4.4 for the three most outlying SV candidate models.

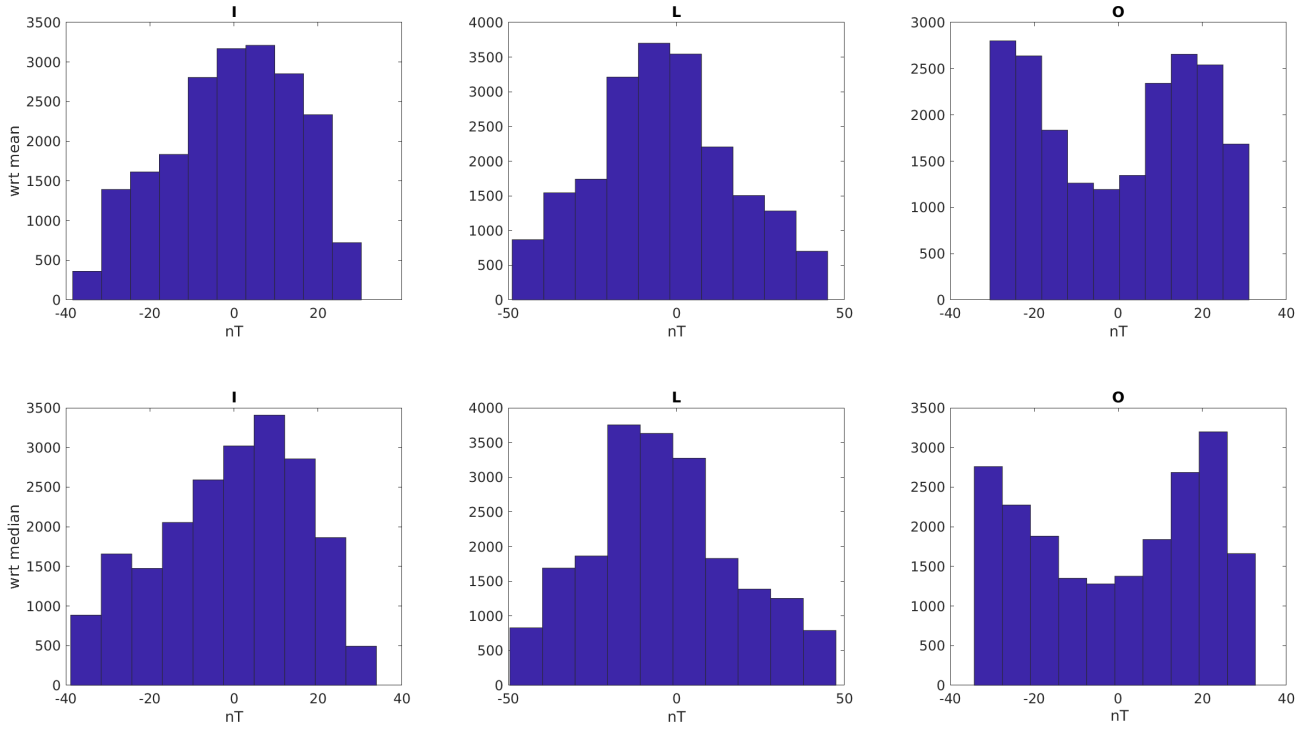

5 Coefficient differences

The following plots show the differences $_{i,j,}g_n^m$ between the candidate models and the mean (top) or median (bottom) model as a function of the spherical harmonic coefficient for DGRF 2015, IGRF 2020 and the SV prediction as in Figs. 1, 5 and 8 of the 2015 evaluation paper. The vertical black lines mark the zonal coefficients (m=0) of each SH degree. See also appendix A for a comparison plot of the individual coefficients.

5.1 DGRF 2015

Mean

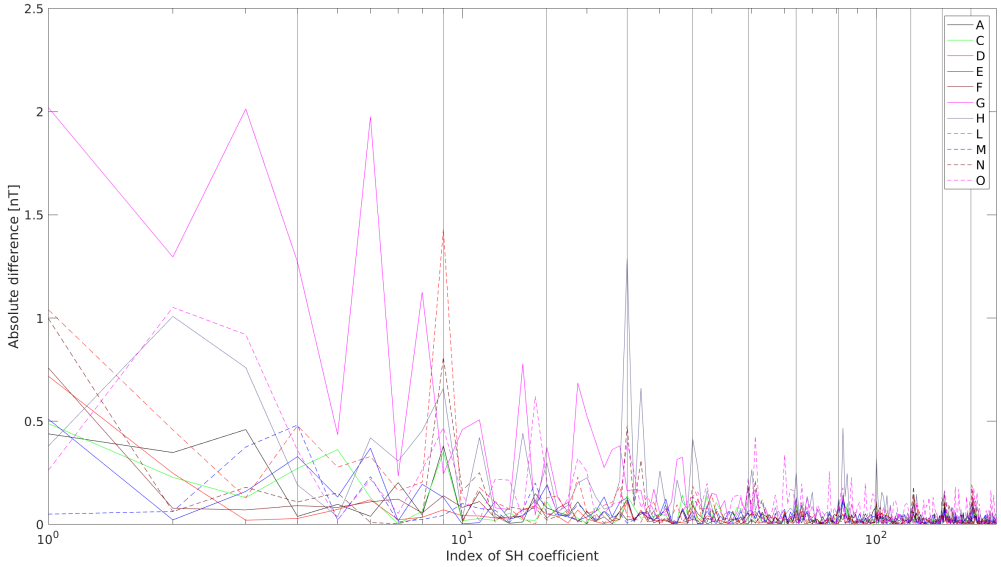

Median

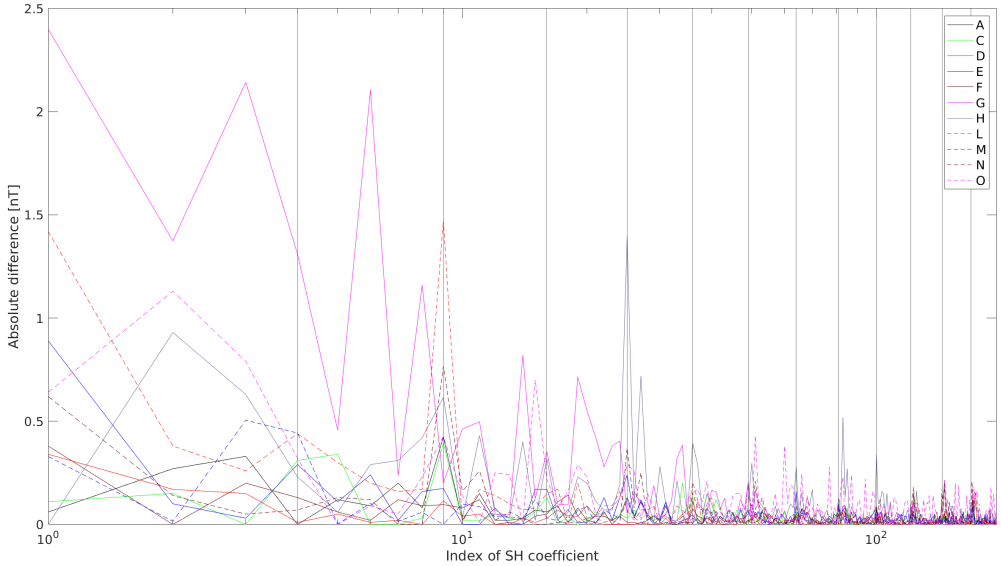

5.2 IGRF 2020

Mean

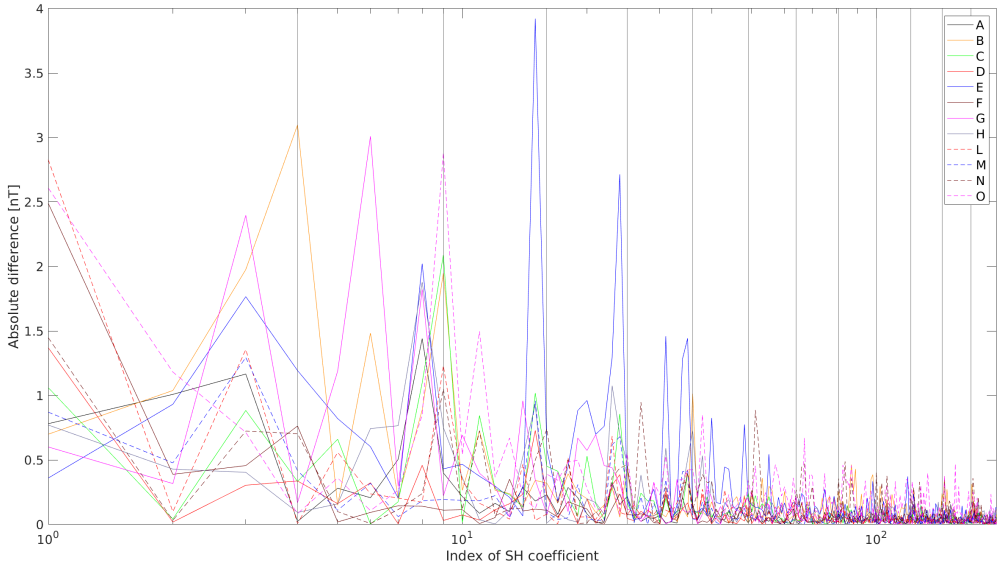

Median

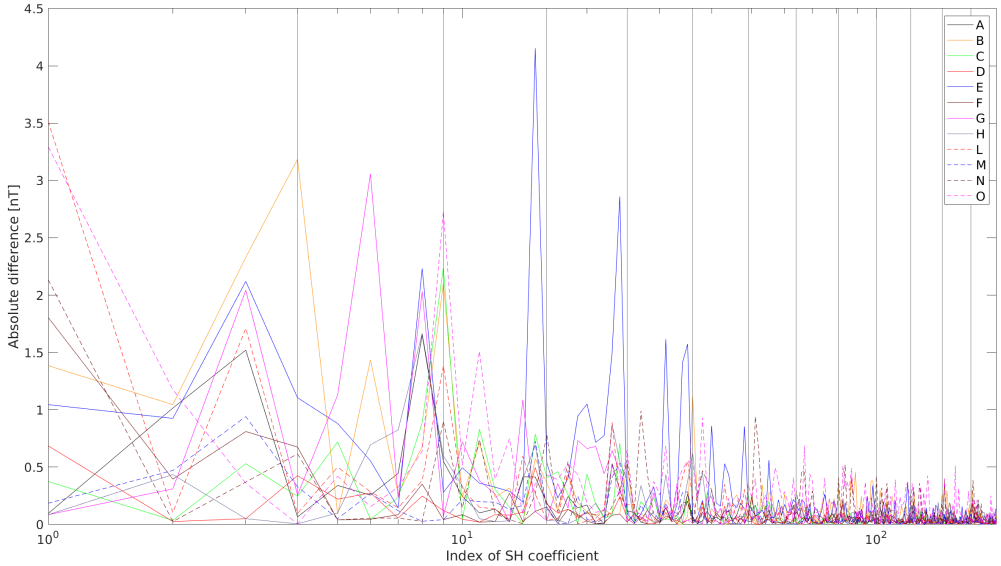

5.3 SV 2020–2025

Mean

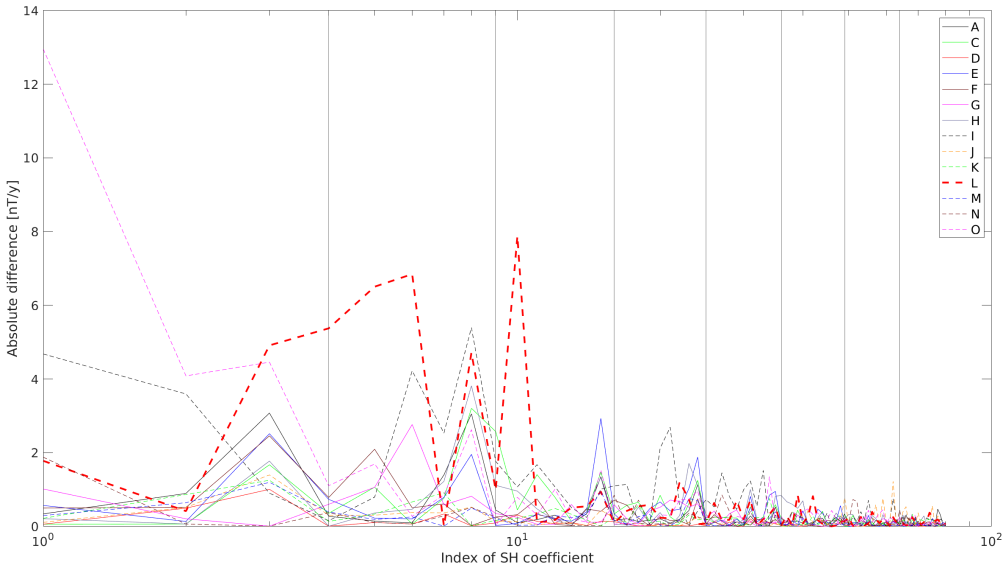

Median

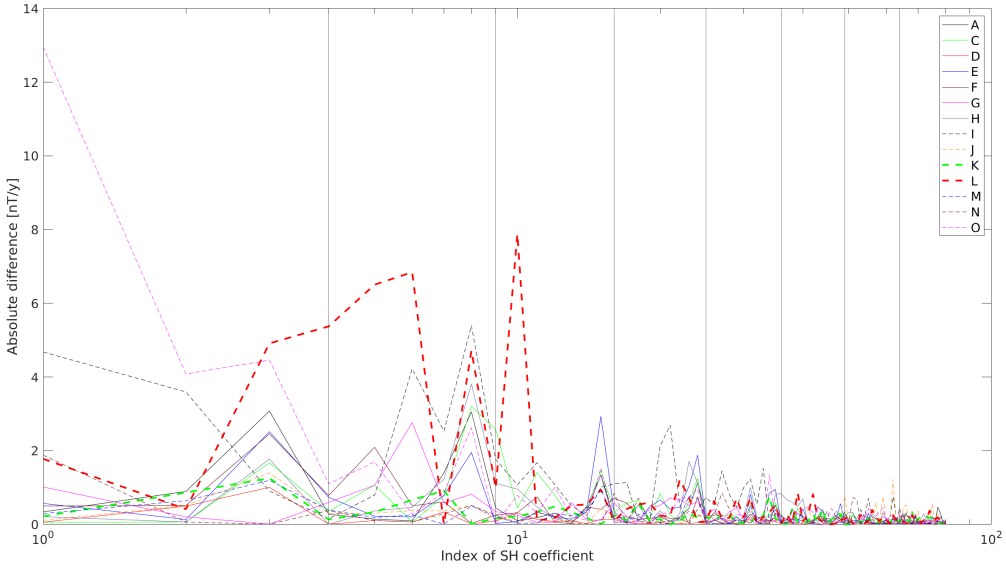

6 Power Spectra

The following plots show the geomagnetic power spectra and the azimuthal power spectra (see subsection titles) of the differences between the candidate models and the mean (top) or median (bottom) for DGRF 2015, IGRF 2020 and SV (see section titles).

6.1 DGRF 2015

6.1.1 Difference Power Spectra (Lowes)

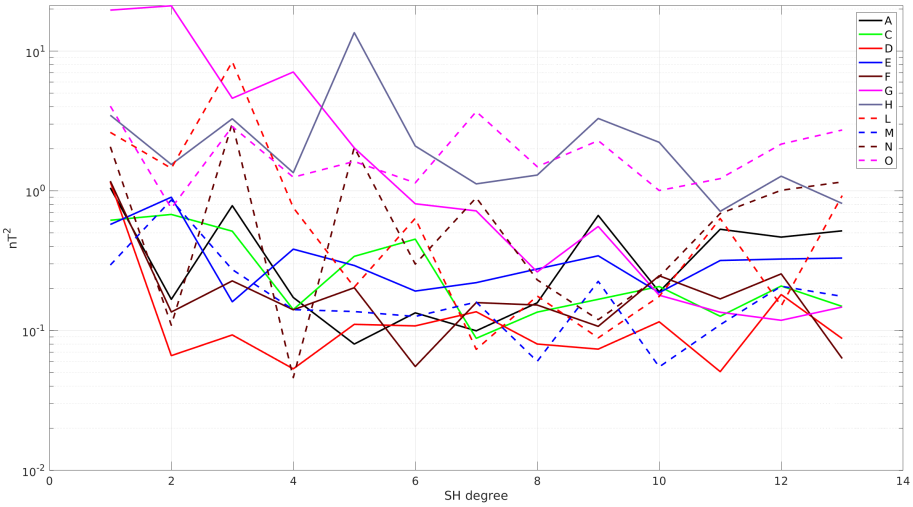

Mean

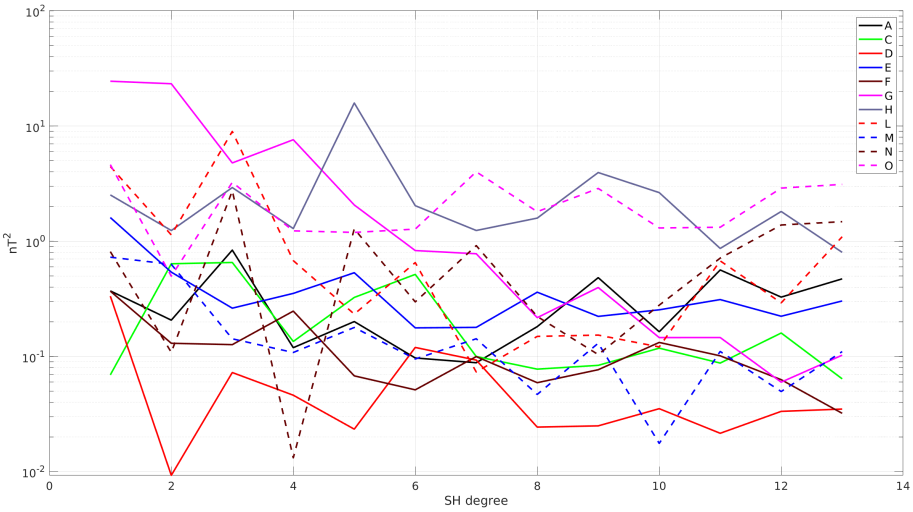

Median

6.1.2 Difference Power Spectra (Azimuthal)

Mean

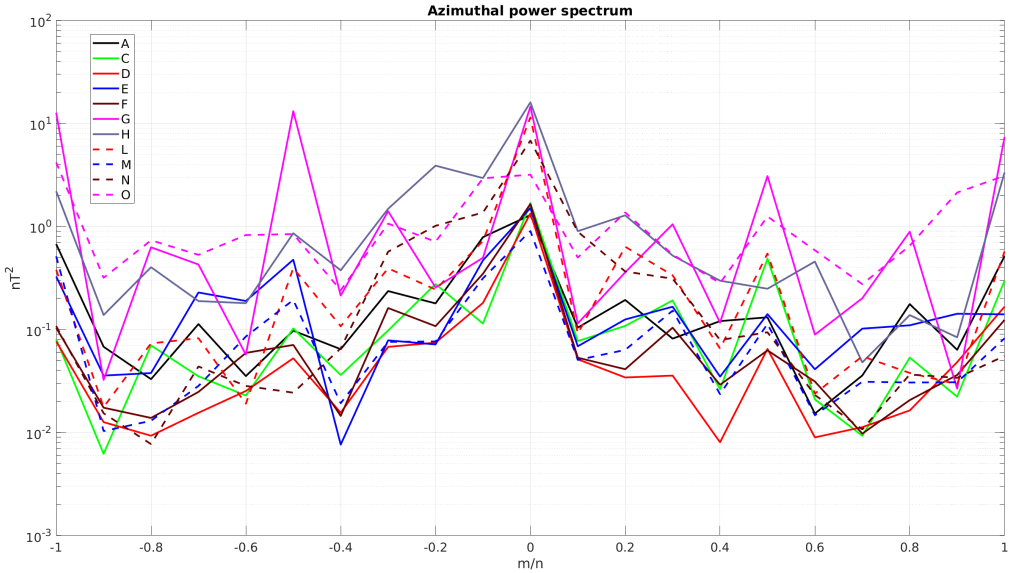

Median

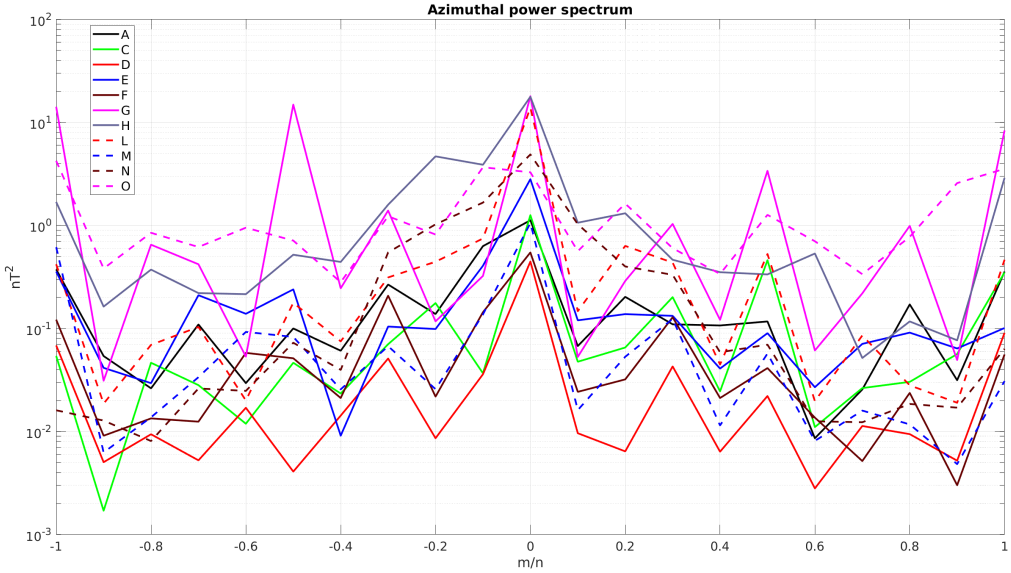

6.2 IGRF 2020

6.2.1 Difference Power Spectra (Lowes)

Mean

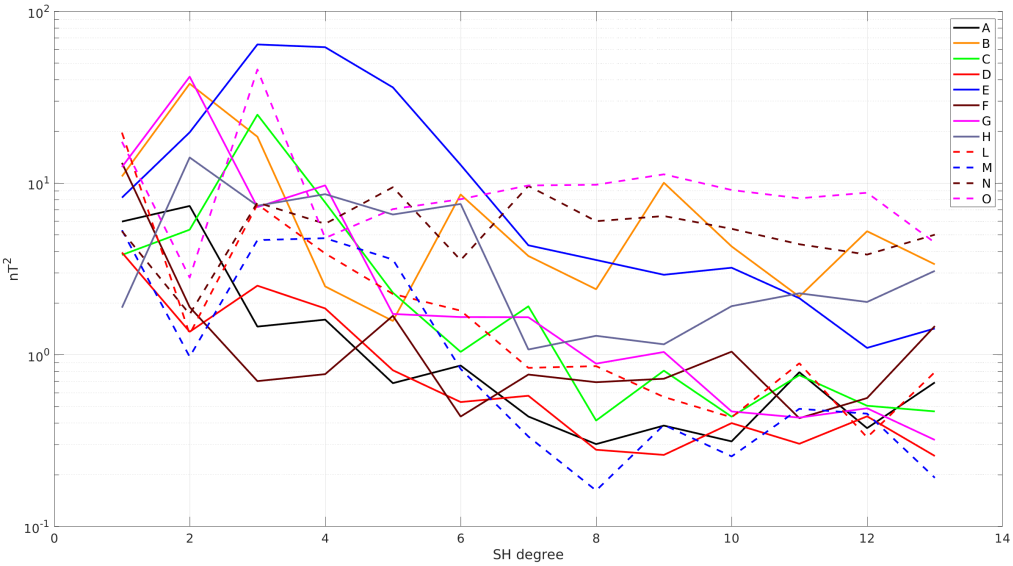

Median

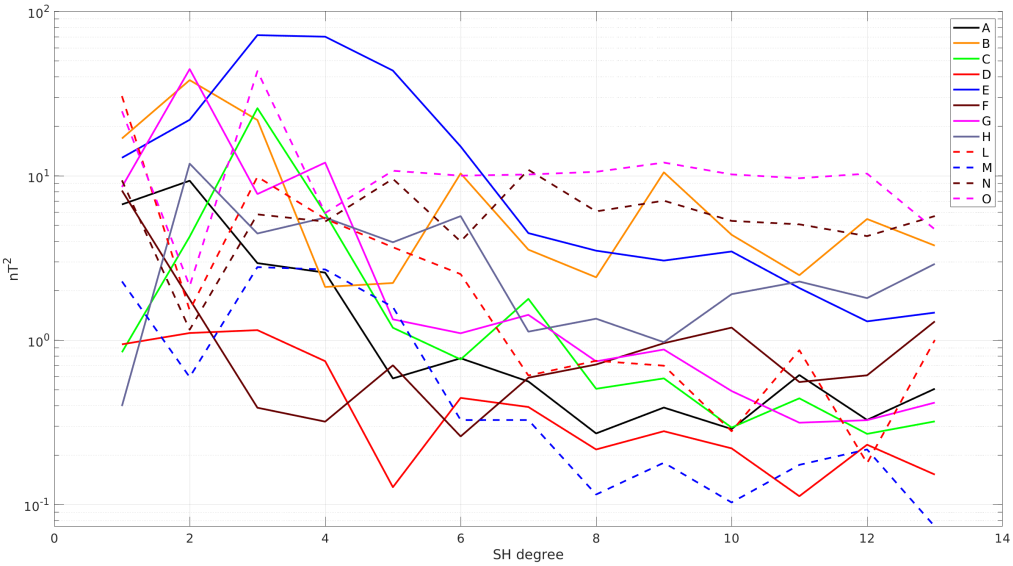

6.2.2 Difference Power Spectra (Azimuthal)

Mean

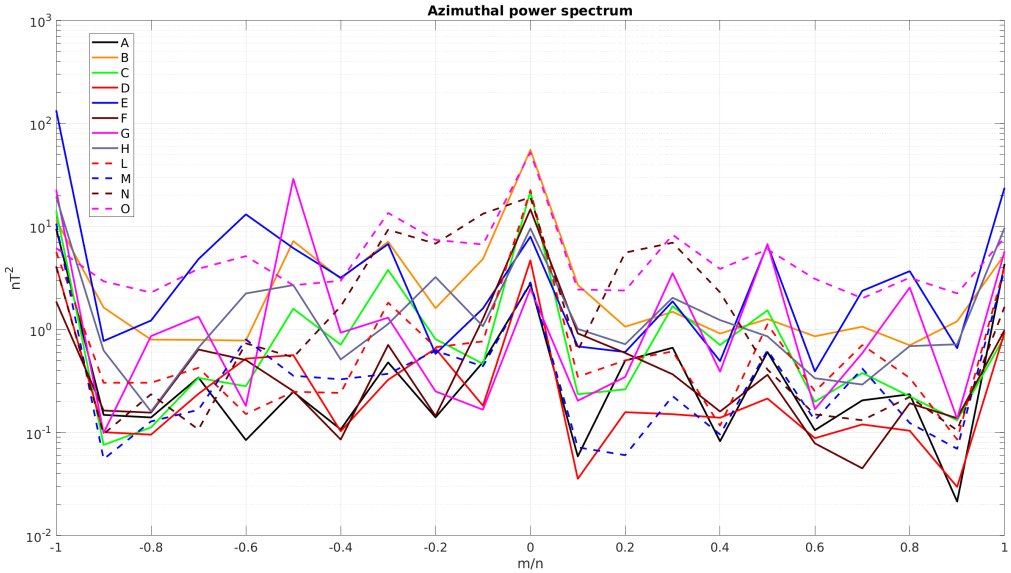

Median

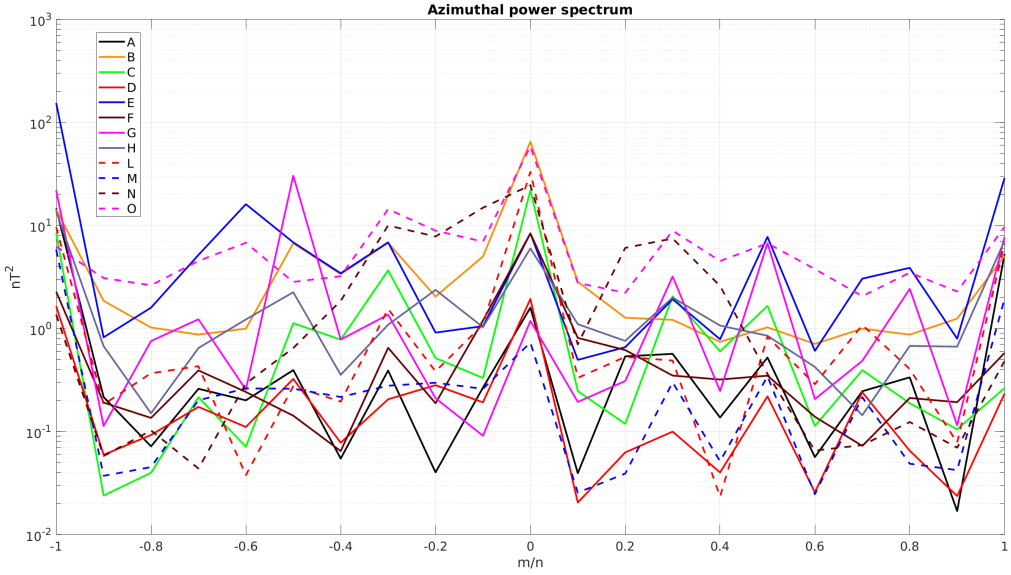

6.3 SV 2020–2025

6.3.1 Difference Power Spectra (Lowes)

Mean

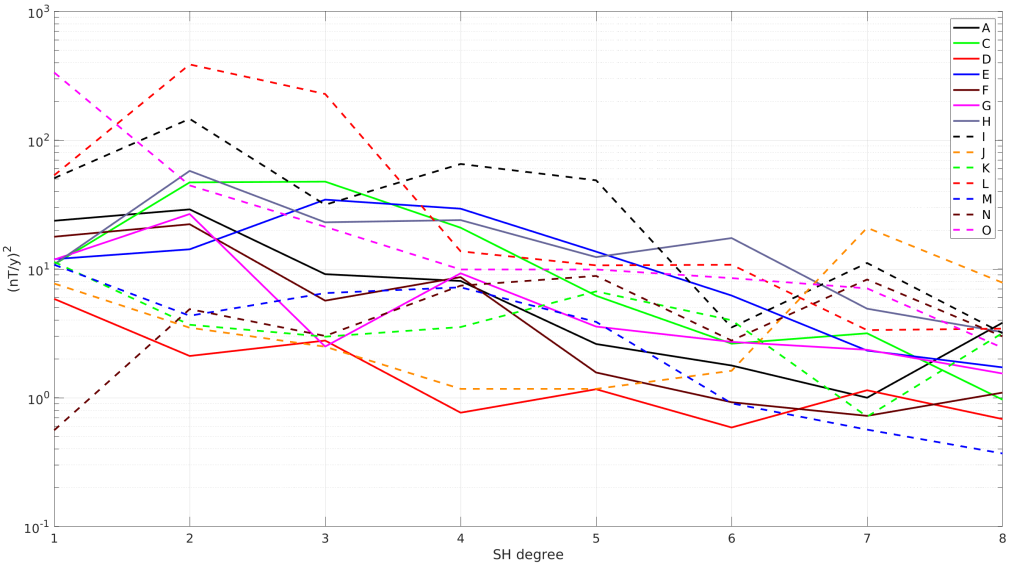

Median

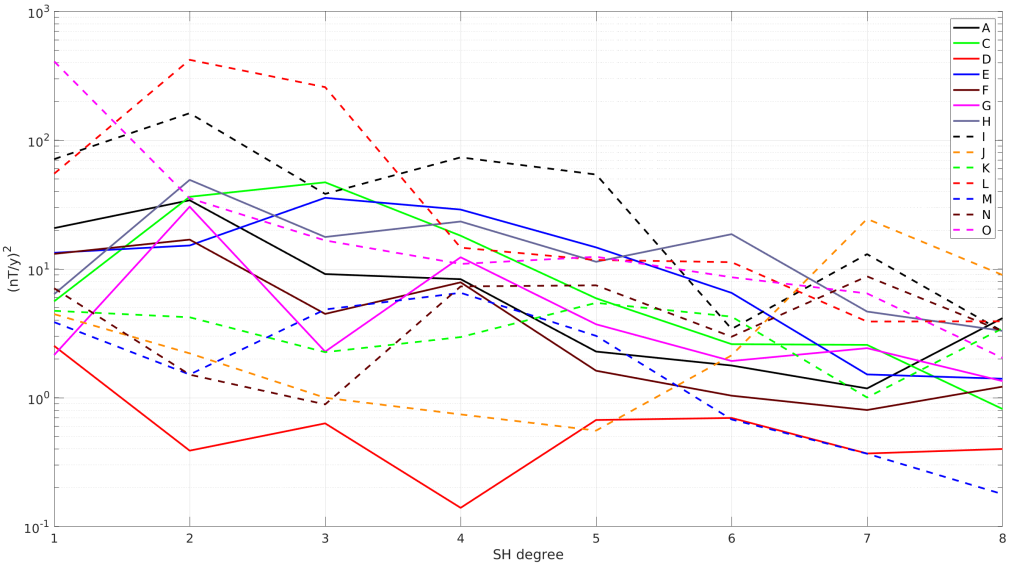

6.3.2 Difference Power Spectra (Azimuthal)

Mean

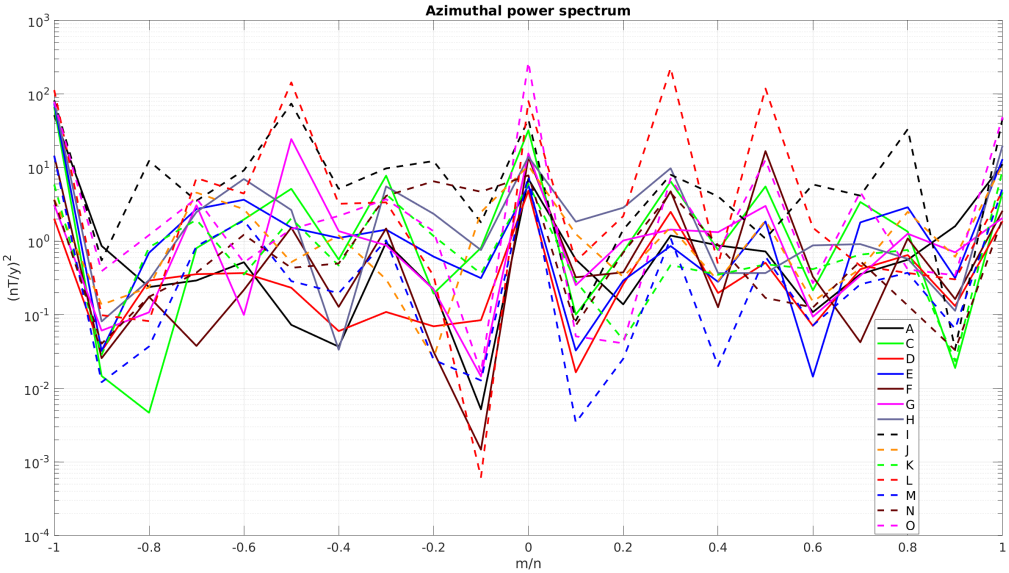

Median

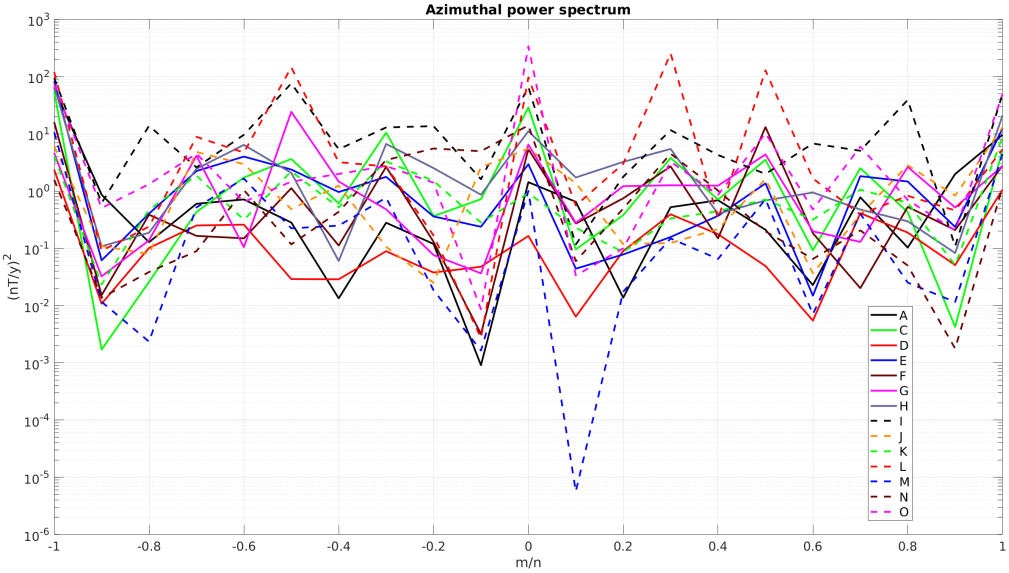

7 Correlations

The following plots show the SH degree correlation of each candidate with the mean (top) or median (bottom) according to Fig. 5 of the 2015 evaluation paper for DGRF 2015, IGRF 2020 and SV.

7.1 DGRF 2015

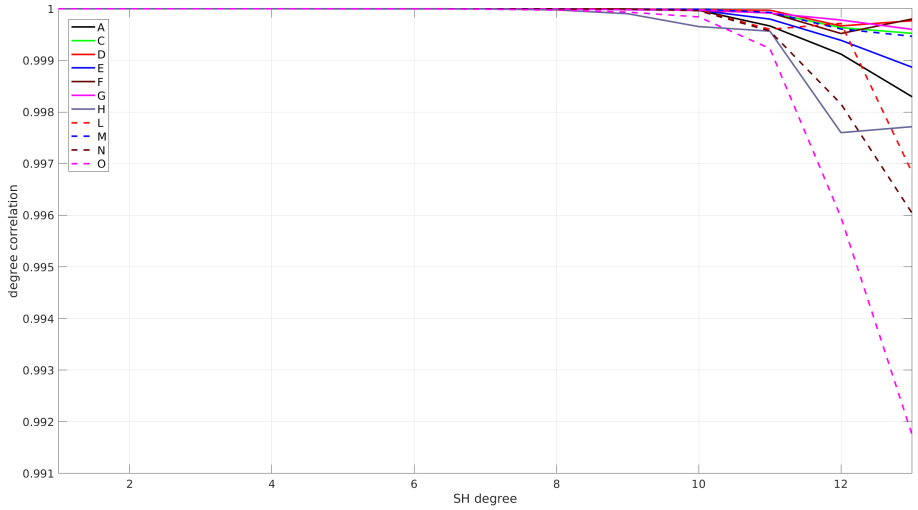

Mean

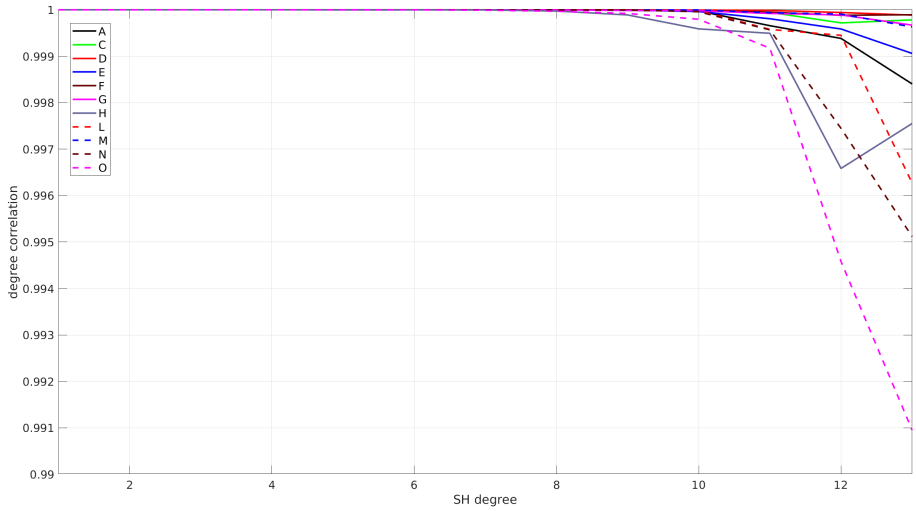

Median

7.2 IGRF 2020

Mean

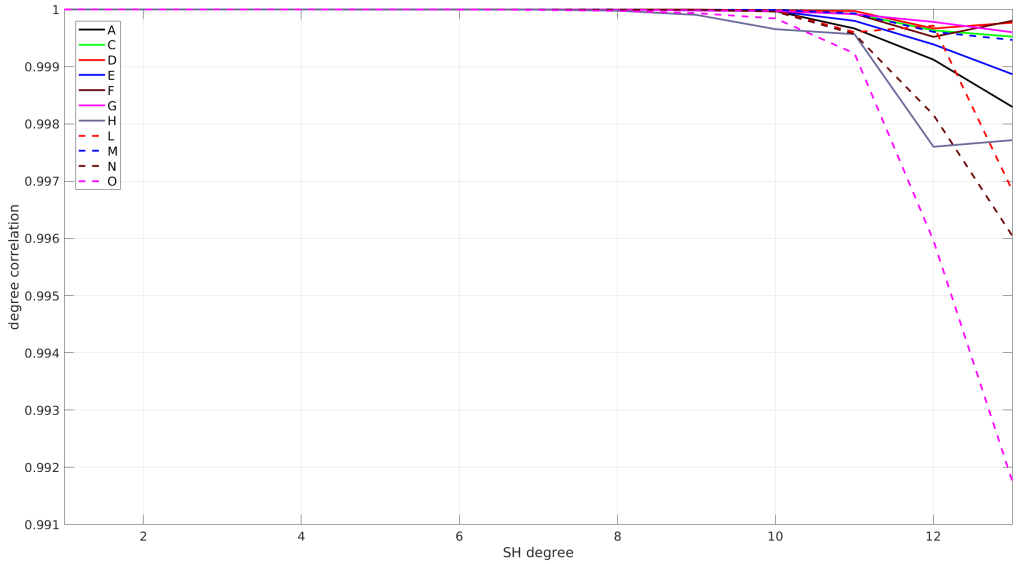

Median

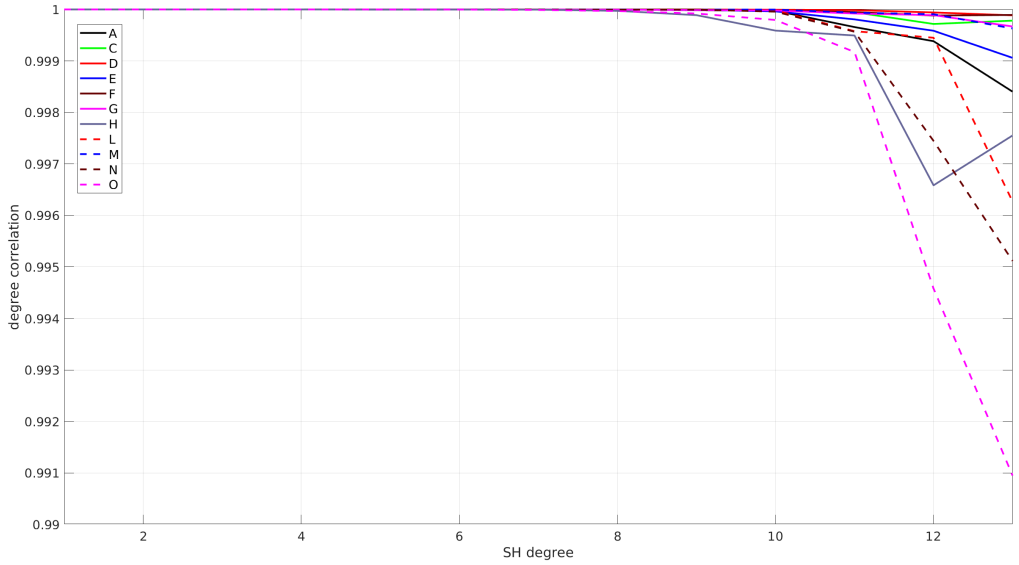

7.3 SV 2020–2025

Mean

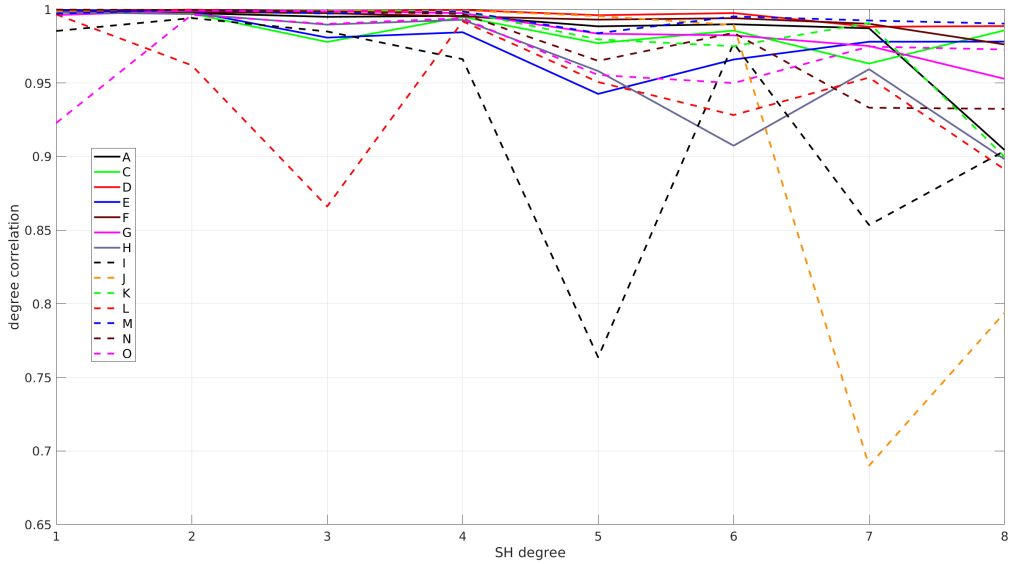

Median

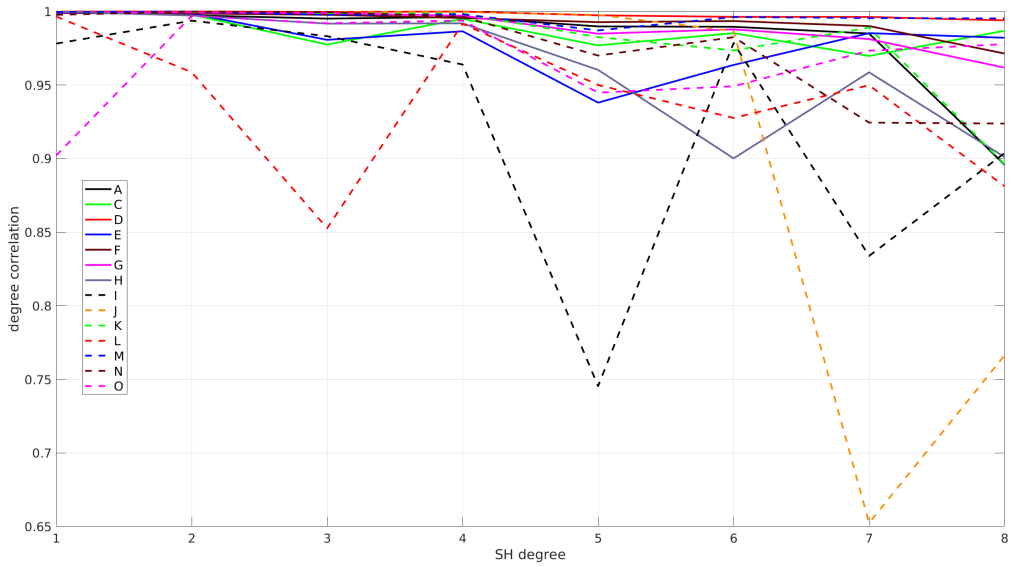

8 Sensitivity Matrices

The following show the sensitivity matrices S(n,m) of the differences in percent between the mean (left) or median (right) and each of the candidate models for DGRF 2015, IGRF 2020 and SV.

8.1 DGRF 2015

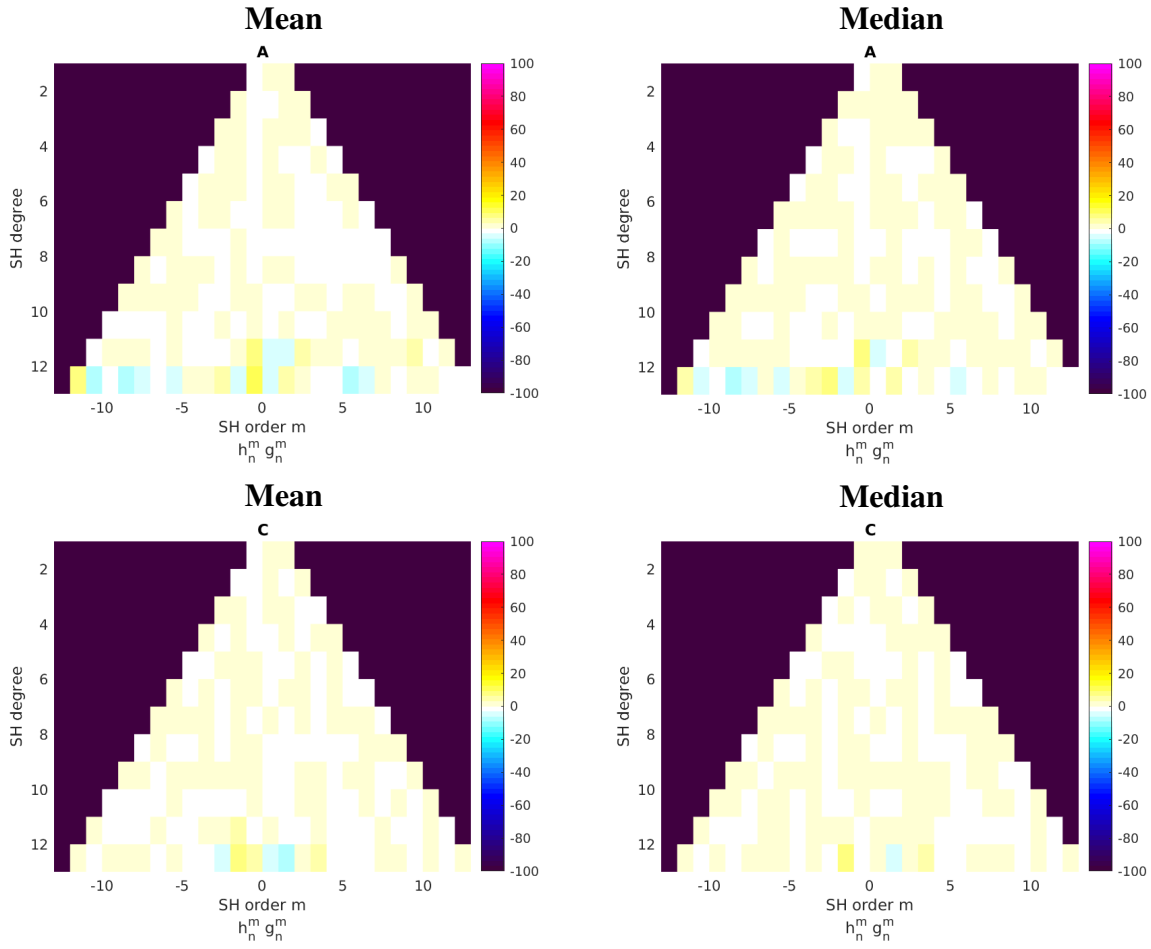

Mean

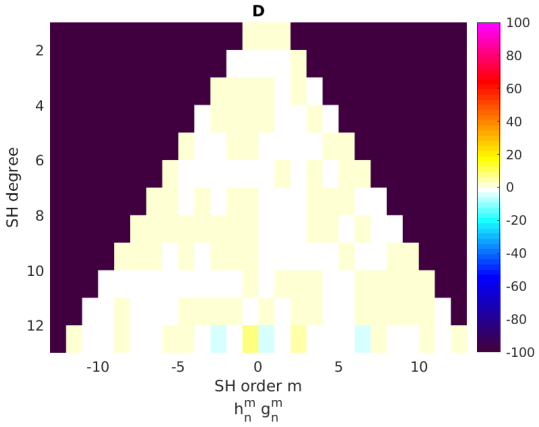

Median

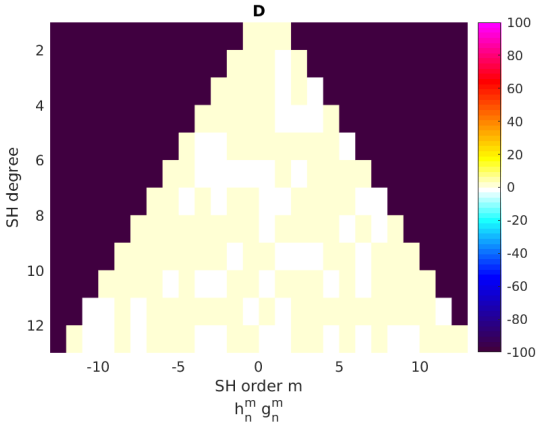

Mean

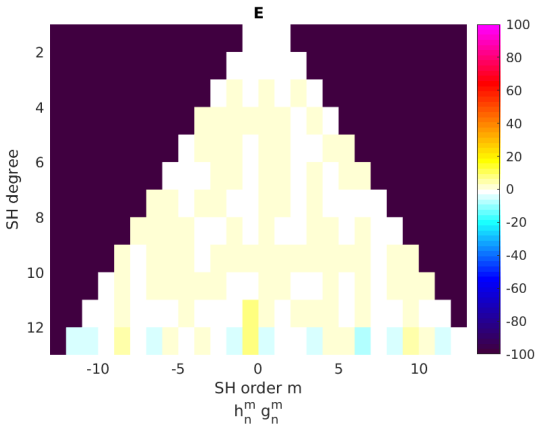

Median

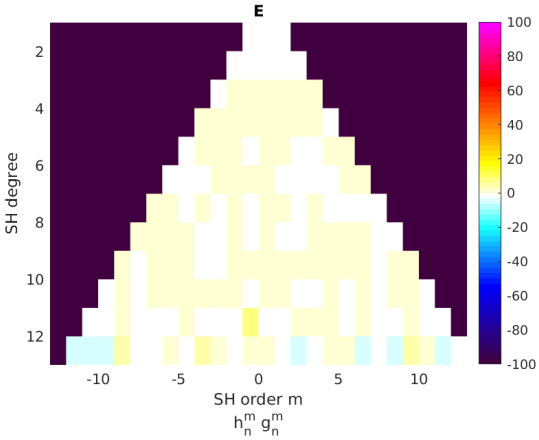

Mean

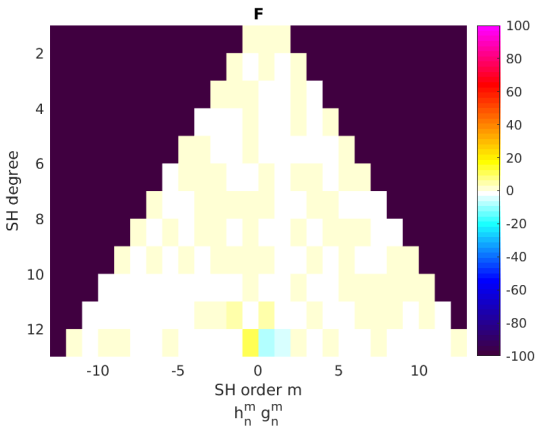

Median

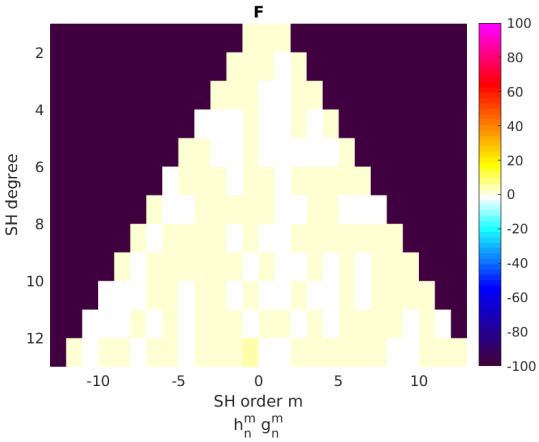

Mean

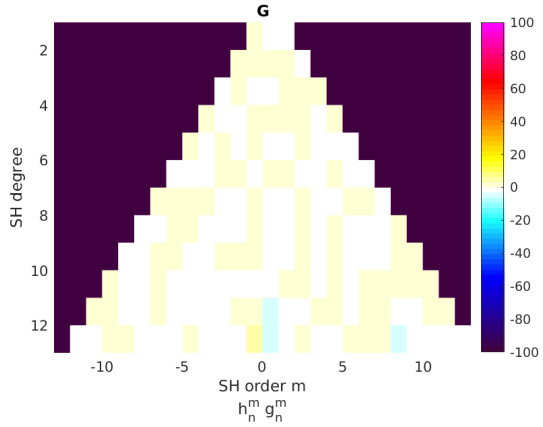

Median

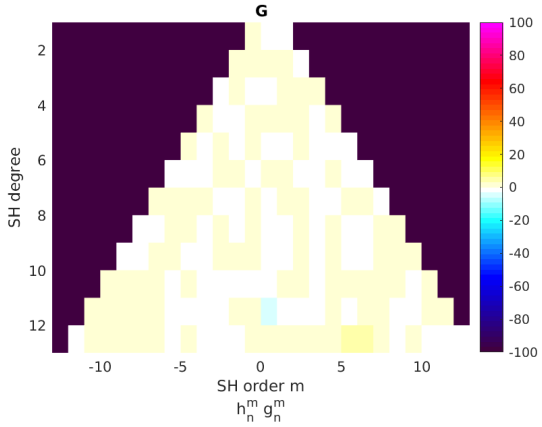

Mean

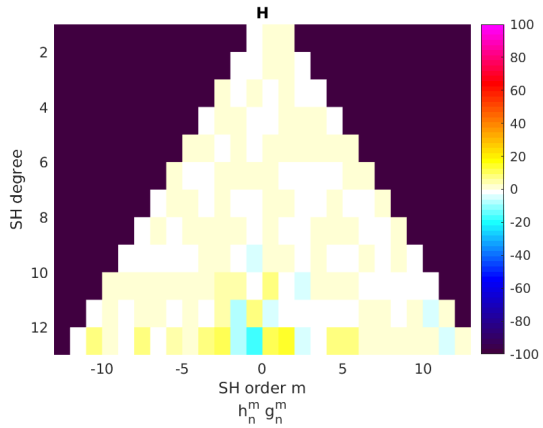

Median

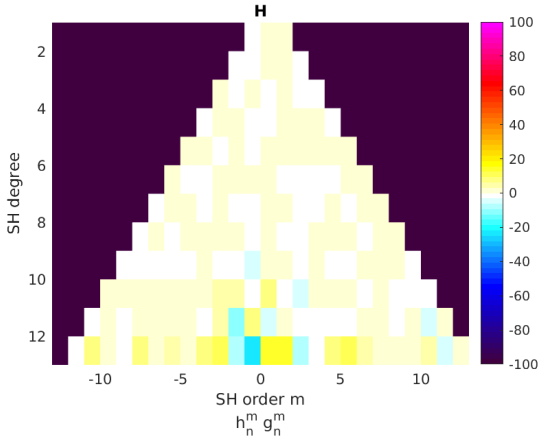

Mean

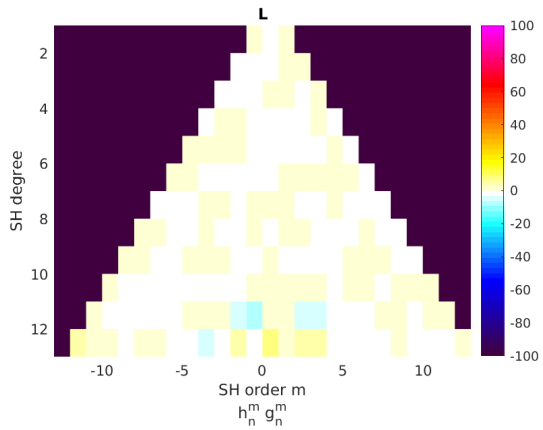

Median

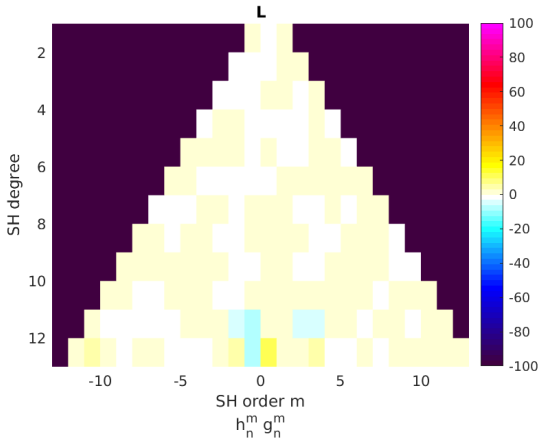

Mean

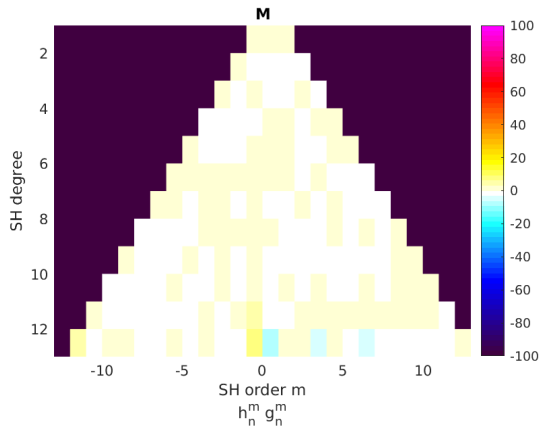

Median

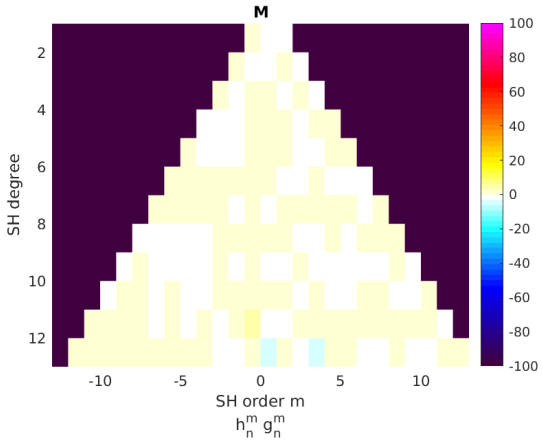

Mean

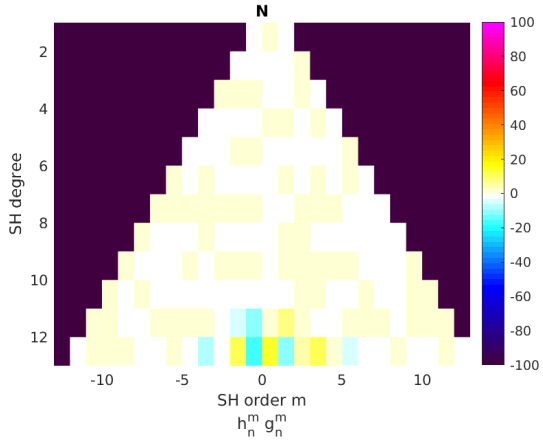

Median

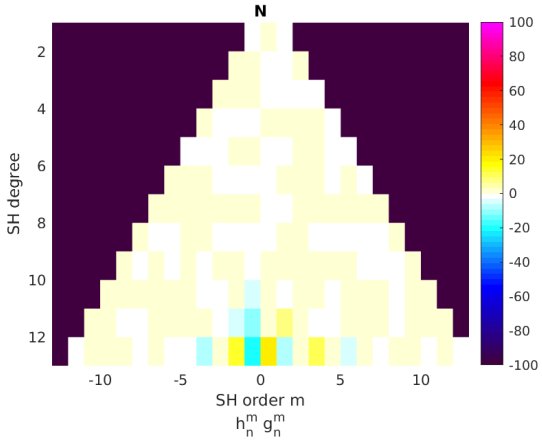

Mean

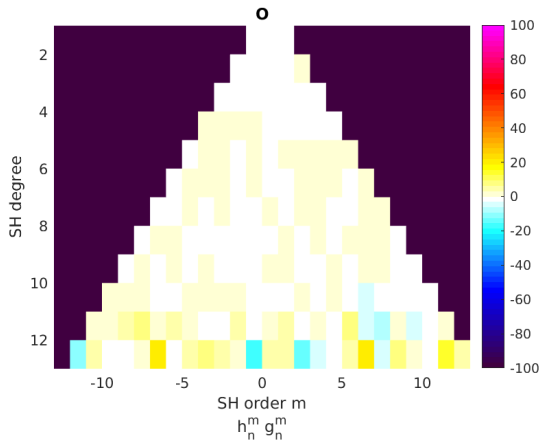

Median

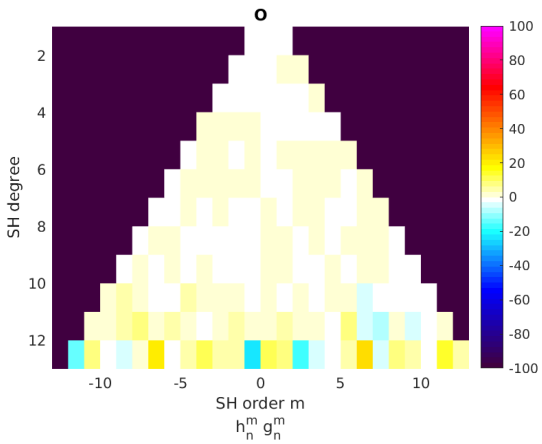

8.2 IGRF 2020

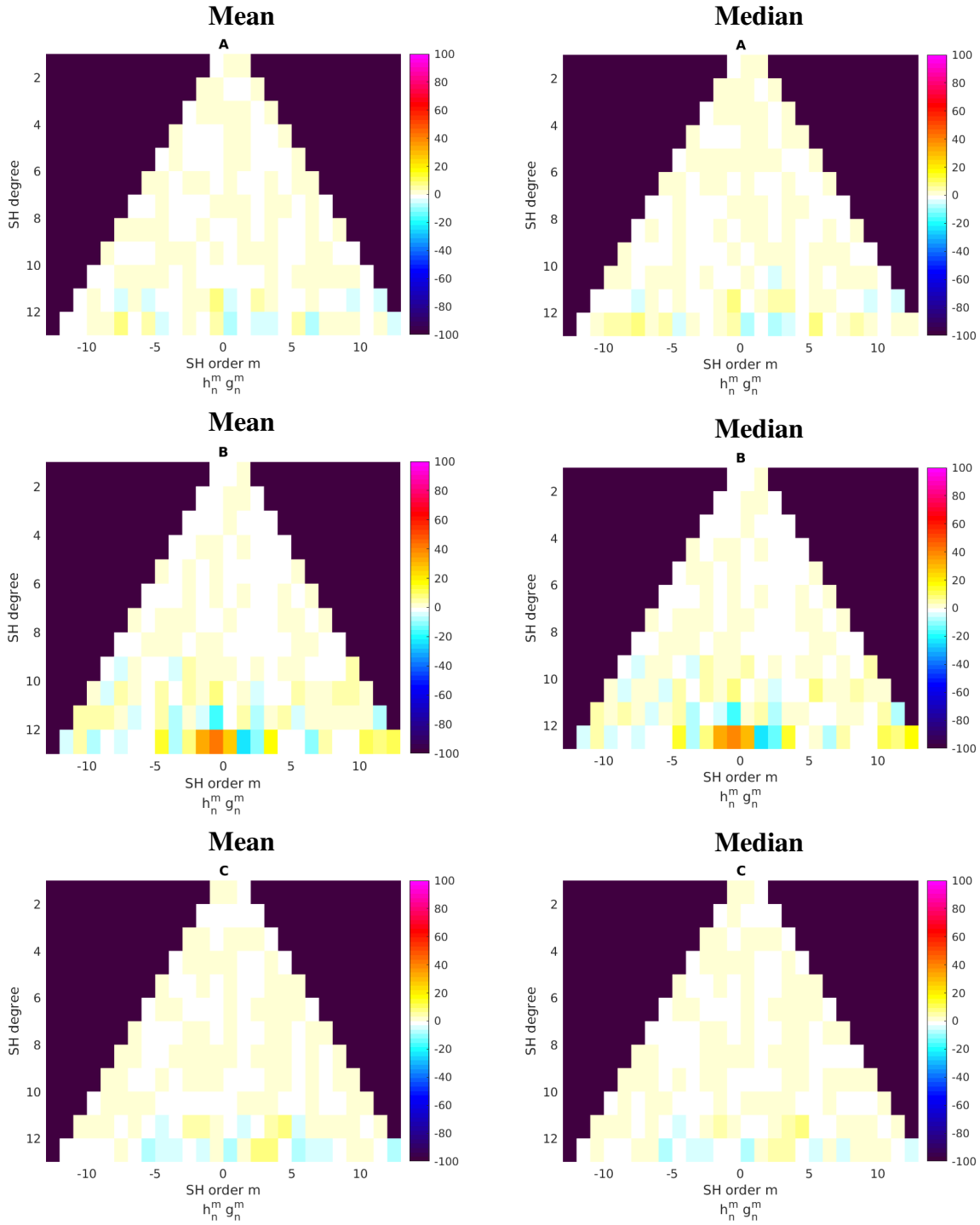
Mean
A
SH degree
SH order m
h_n^m g_n^m
Median
A
SH degree
SH order m
h_n^m g_n^m
Mean
B
SH degree
SH order m
h_n^m g_n^m
Median
B
SH degree
SH order m
h_n^m g_n^m
Mean
C
SH degree
SH order m
h_n^m g_n^m
Median
C
SH degree
SH order m
h_n^m g_n^m

Mean

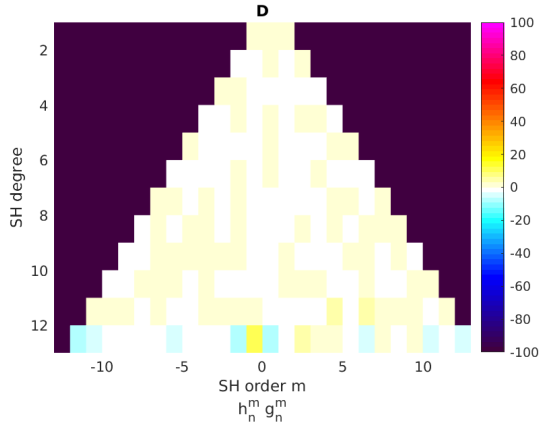

Median

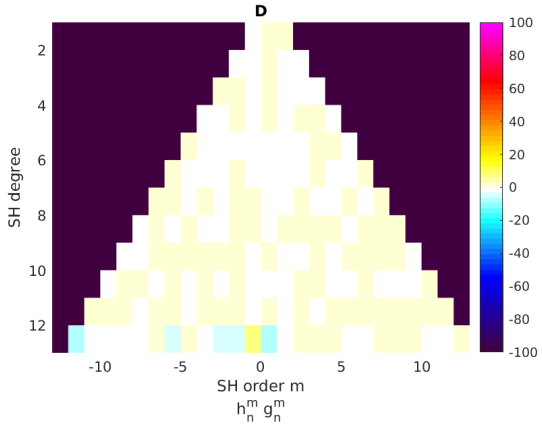

Mean

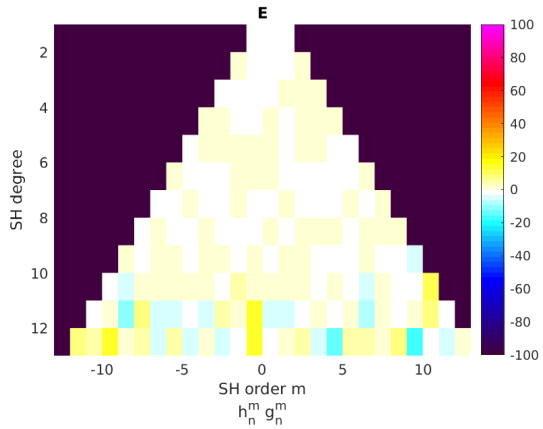

Median

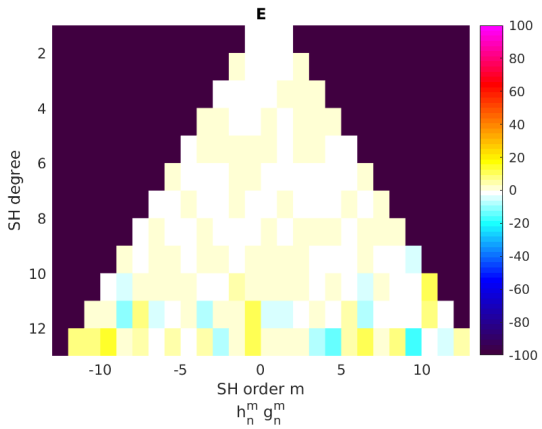

Mean

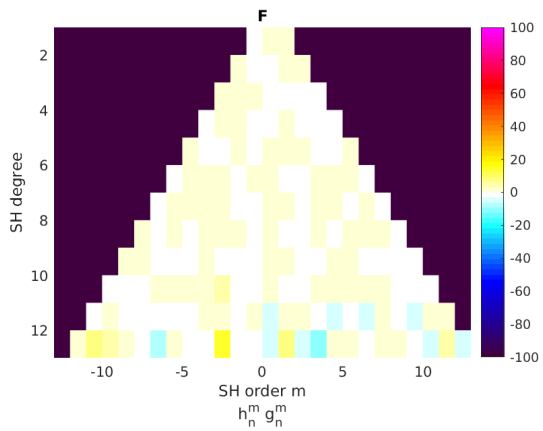

Median

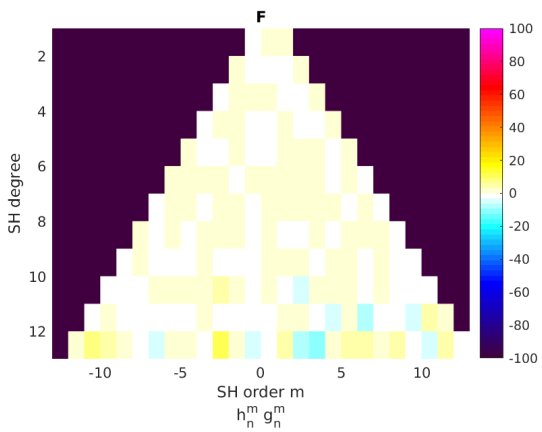

Mean

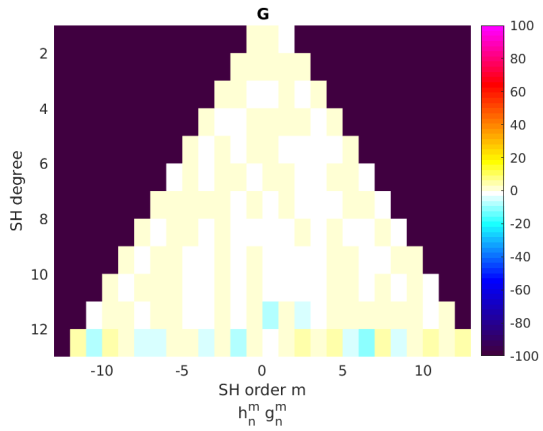

Median

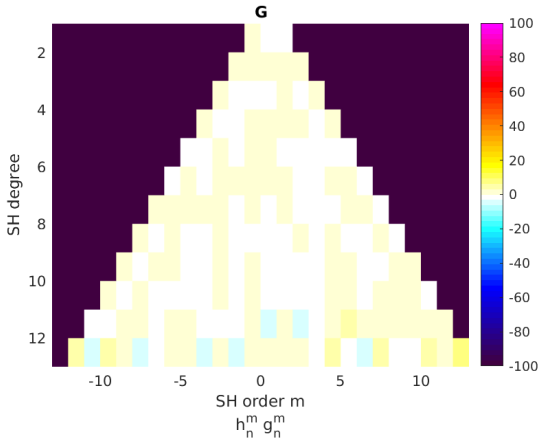

Mean

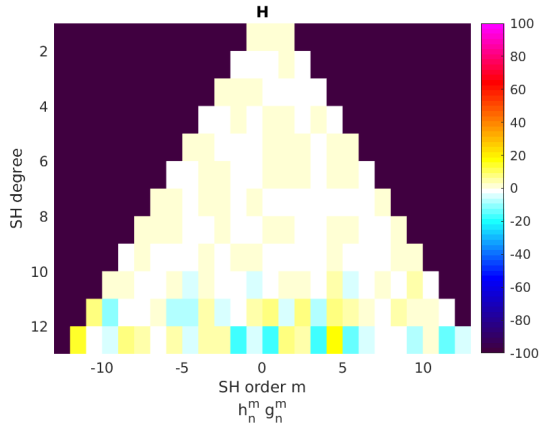

Median

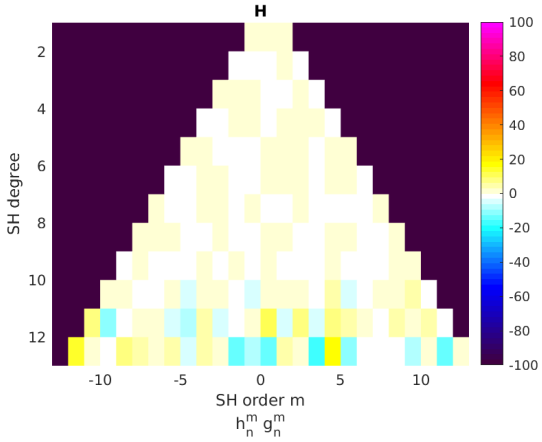

Mean

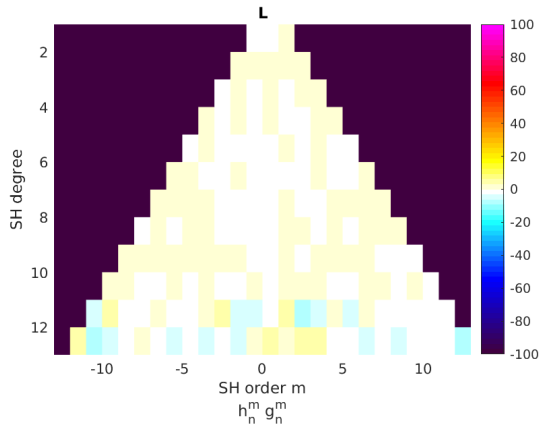

Median

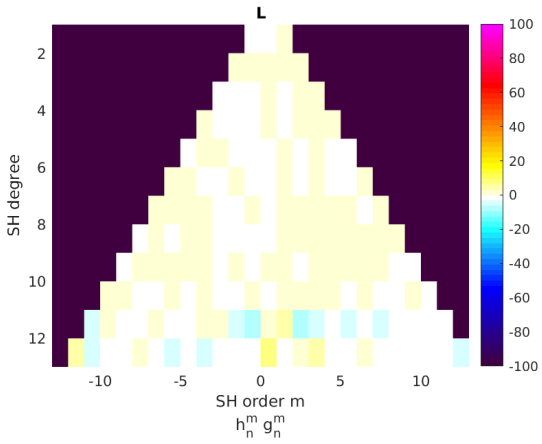

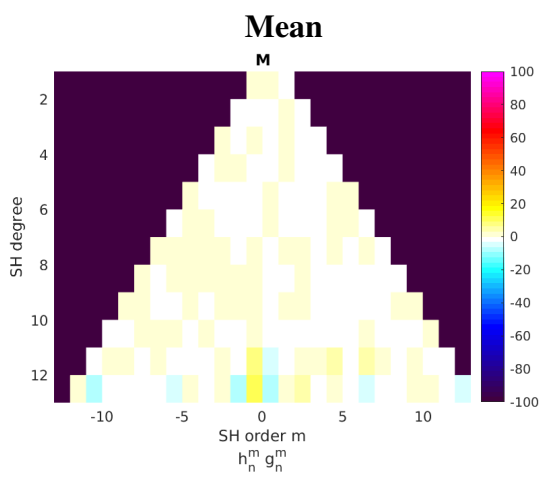
Mean
M
SH degree
SH order m
h_n^m g_n^m

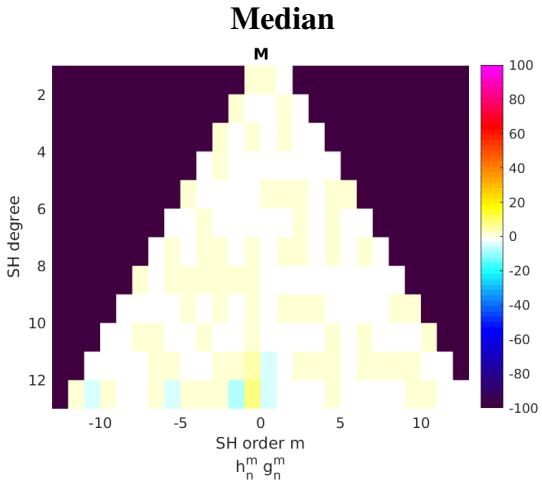
Median
M
SH degree
SH order m
h_n^m g_n^m

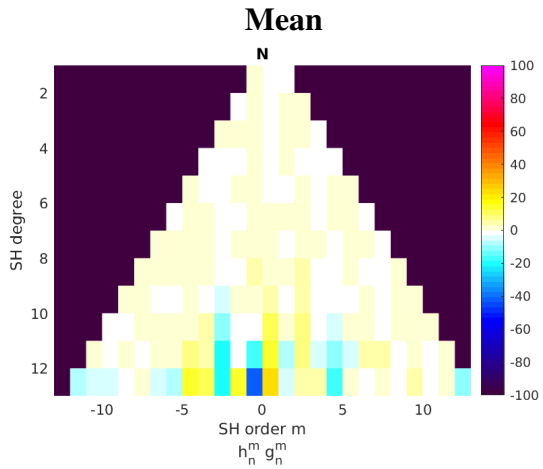
Mean
N
SH degree
SH order m
h_n^m g_n^m

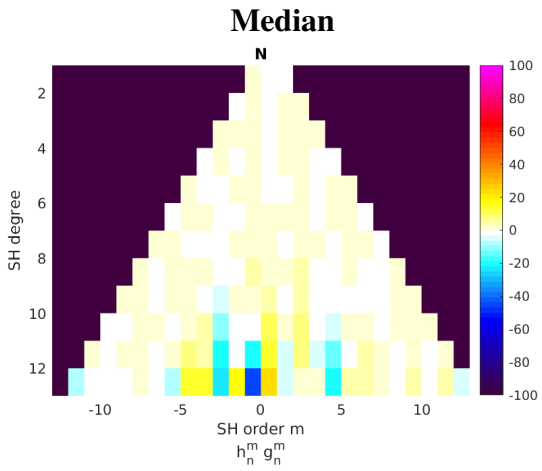
Median
N
SH degree
SH order m
h_n^m g_n^m

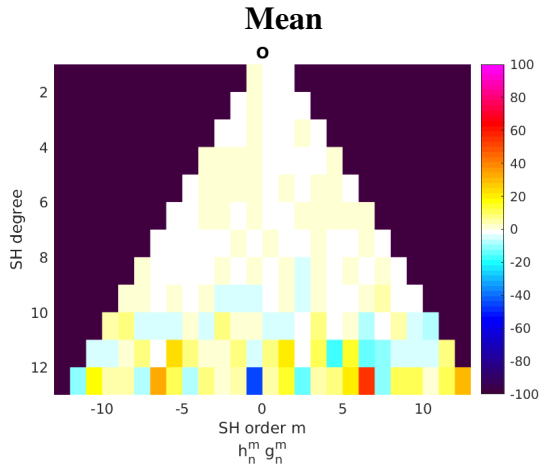
Mean
O
SH degree
SH order m
h_n^m g_n^m

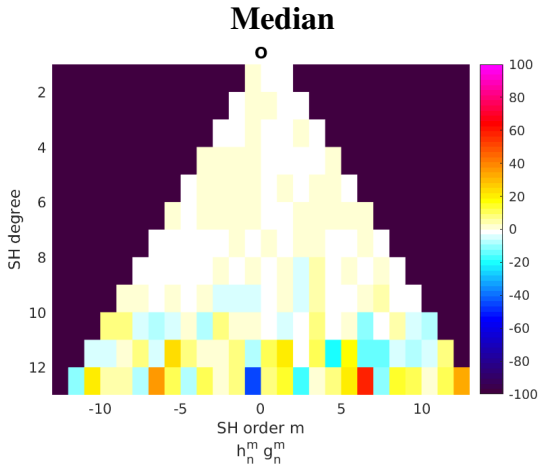
Median
O
SH degree
SH order m
h_n^m g_n^m

8.3 SV 2020–2025

Mean

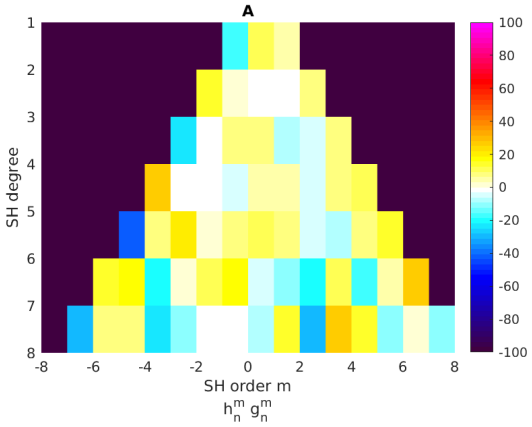

Median

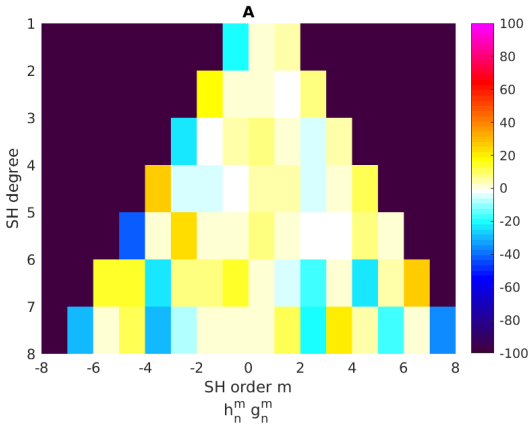

Mean

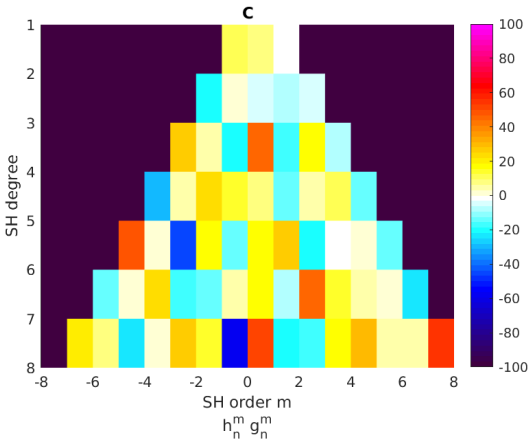

Median

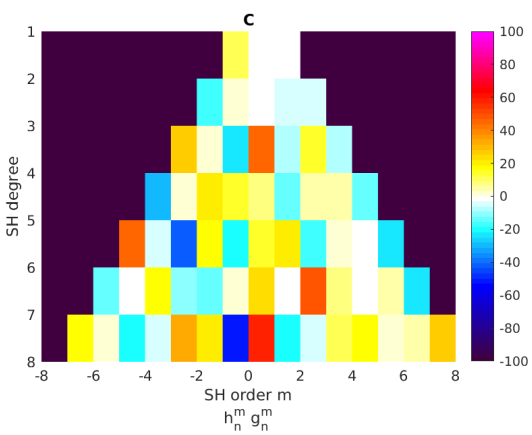

Mean

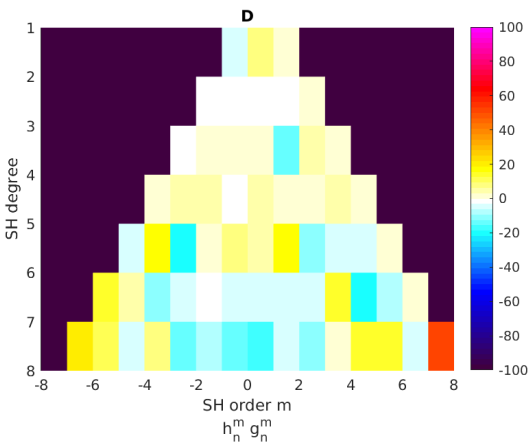

Median

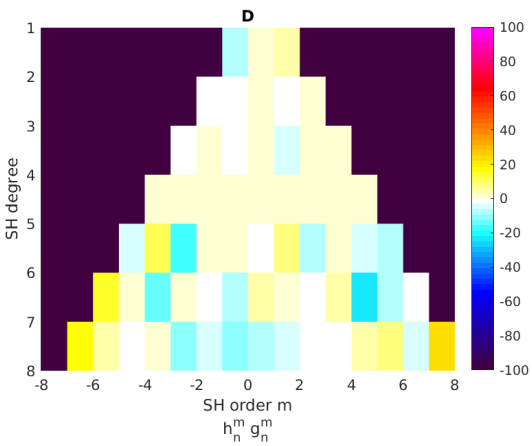

Mean

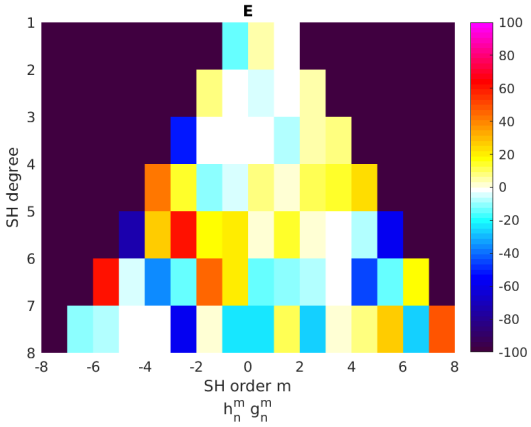

Median

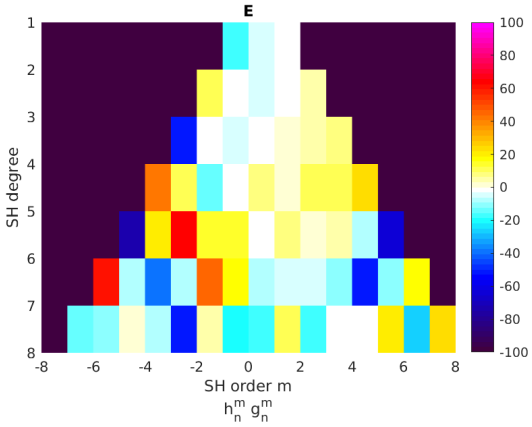

Mean

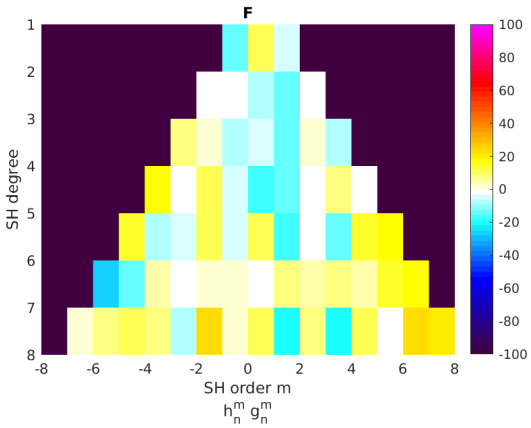

Median

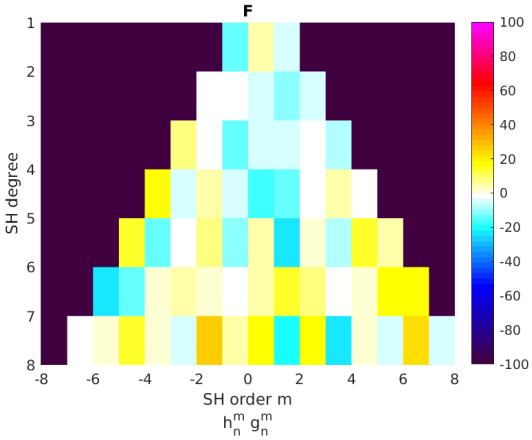

Mean

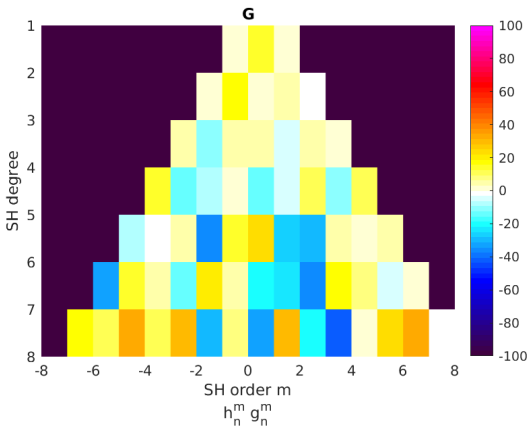

Median

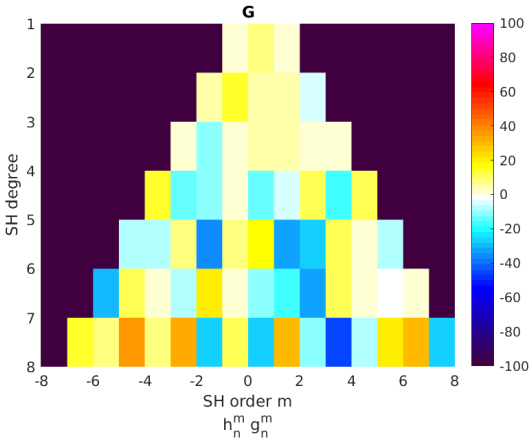

Mean

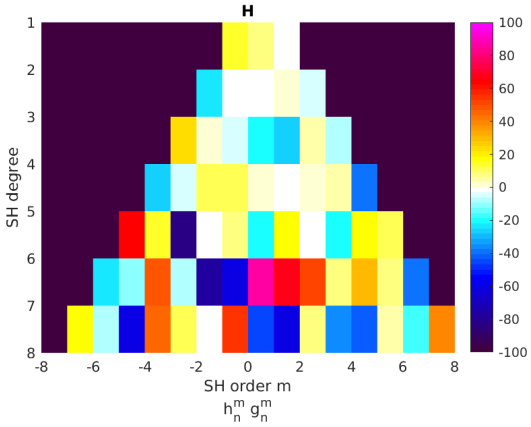

Median

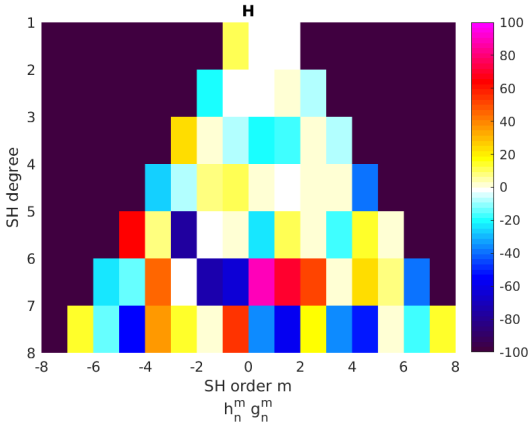

Mean

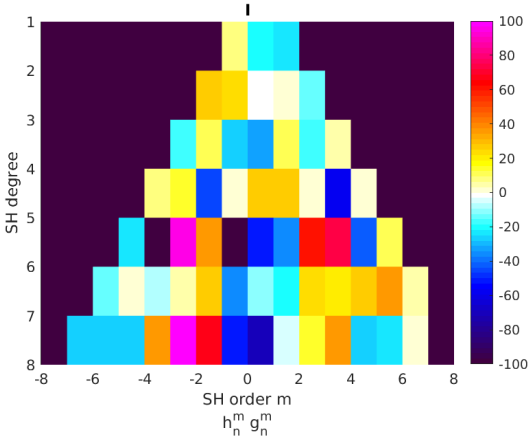

Median

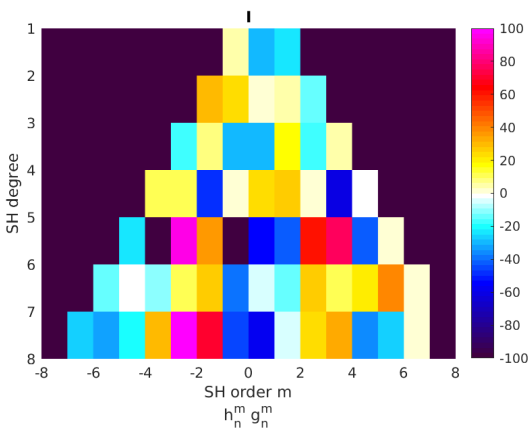

Mean

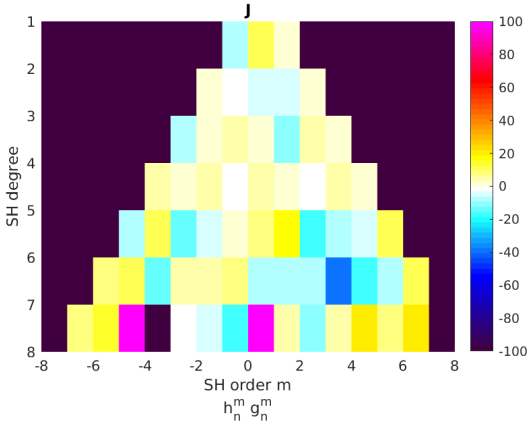

Median

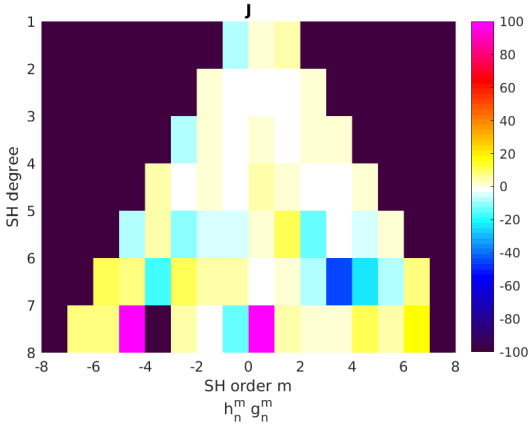

Mean

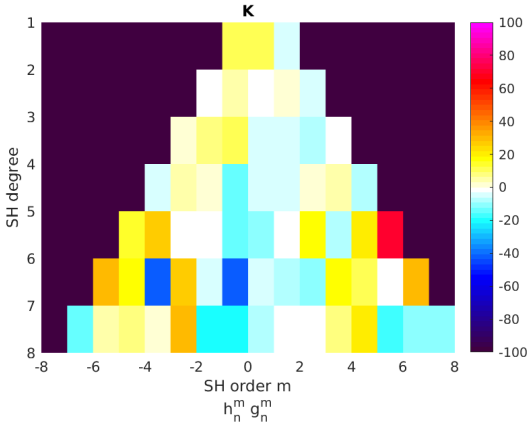

Median

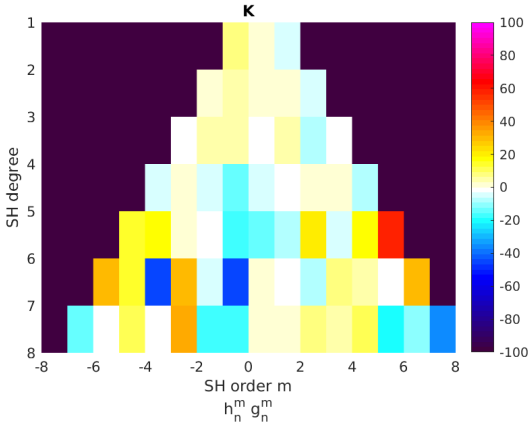

Mean

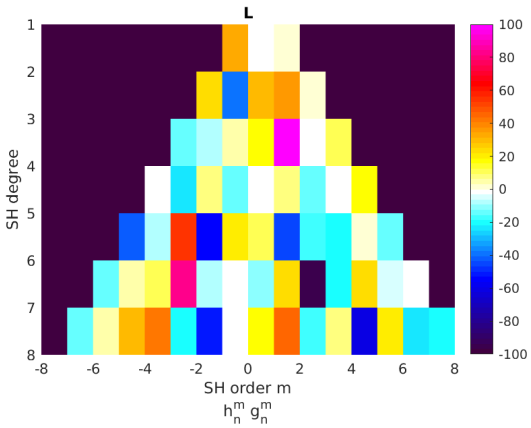

Median

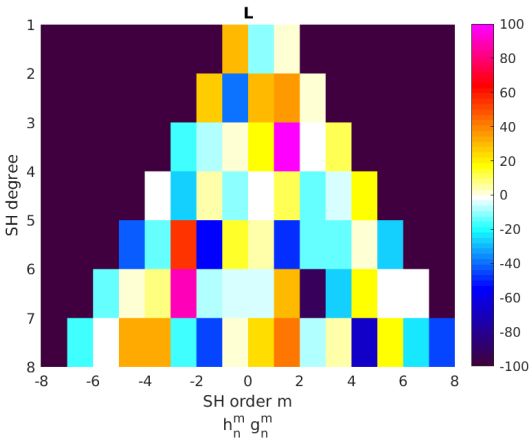

Mean

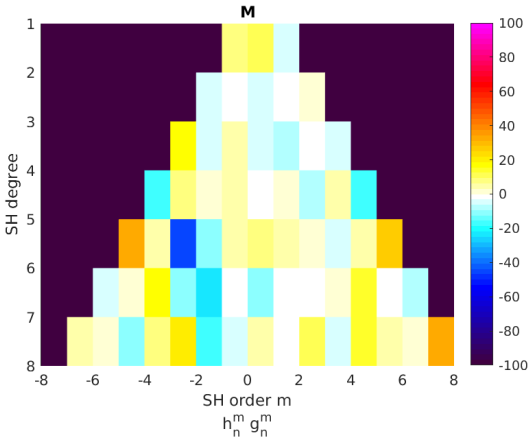

Median

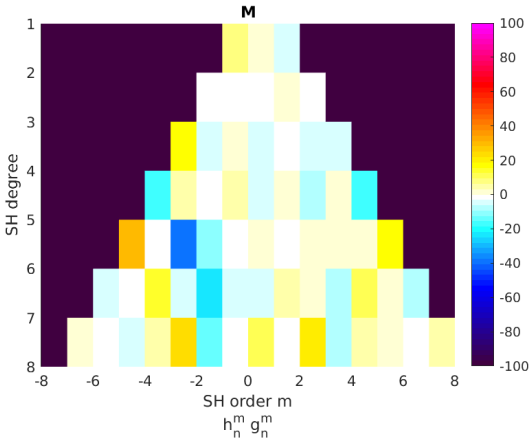

Mean

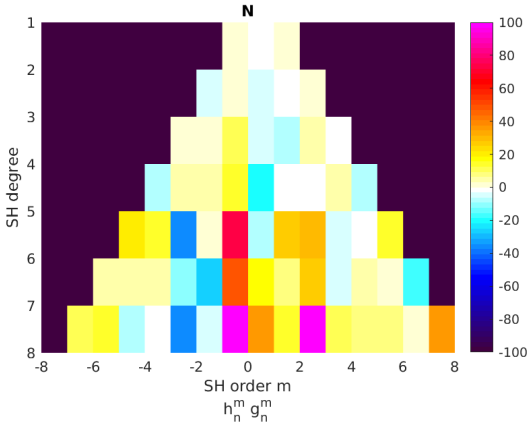

Median

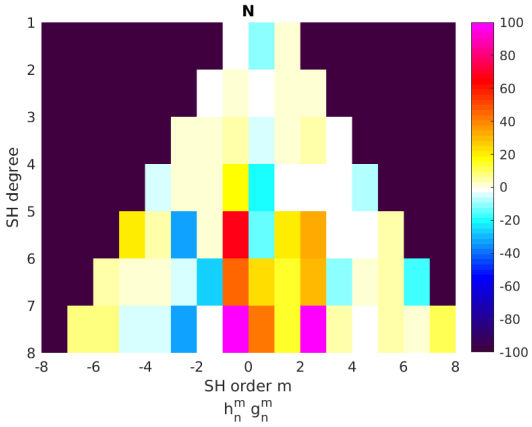

Mean

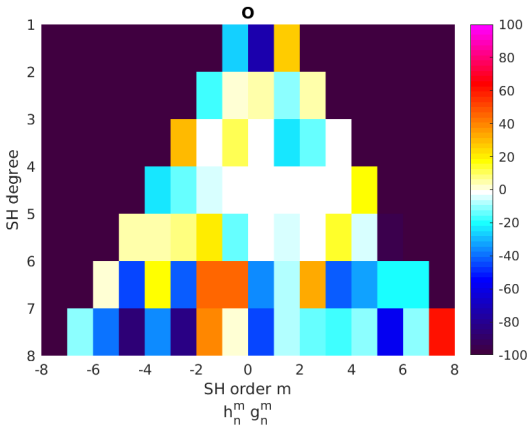

Median

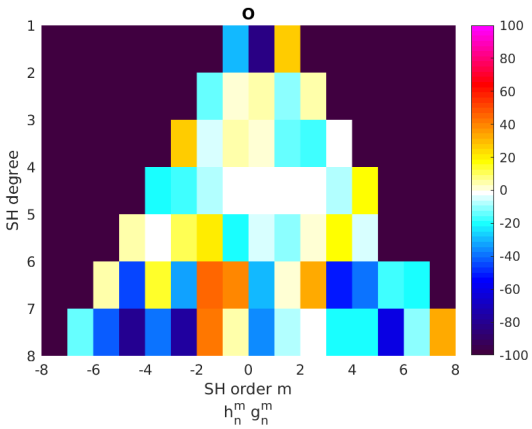

9 Comparison against observatory data

This section compares time series of linearly interpolated candidate models between 2015-2020 with Niemegk and other observatory data. Colour and letter coding is as indicated on page 5.

9.1 NGK

Figure on page 47, upper row: Magnetic field evolution

- *Orange scatter:* observatory hourly data
- *red line:* smoothed version of hourly data
- *bright greenish line:* `CHAOS-6` model (no observatory bias estimate applied)
- *dashed black line:* `Mag.num`-model (parent model of the GFZ candidate, observatory bias estimate applied)
- *thin short and straight lines in the 2015-2020 interval:* candidate models as linear interpolation between the DGRF 2015 and IGRF 2020 type, where applicable.

Since observatory offsets are not known for the candidate models, shifts to nullify the differences of the averages are calculated, subsequently only the slopes varies.

Figure on page 47, lower row: `SV` evolution

- *Scattering orange line:* observatory data `SV` estimation
- *long black straight line:* a fitted long term trend of this scattering observatory `SV` data points
- *bright greenish line:* `CHAOS-6` model (`SV`)
- *dashed dark curved line:* the `Mag.num` classic model (`SV`)
- *dotted curve:* a `Mag.num` delta data only model version (`SV`), as an alternative `Mag.num` model of higher variability in time.

The slopes from the frames in the upper row of the figure in the 2015 - 2020 interval are now constant horizontal short straight lines. They cannot follow the short-period behaviour of the observatory `SV` estimate like the forward modelled time series for less restricted models.

The `NGK` overview figure at page 47 also show the candidate forecasted `SV`s (where applicable), drawn as short straight lines for the time period 2020 to 2025, which is not covered by observatory data yet. That gives an visual idea about the variability of the candidates compared to the given scatter and drift in the field components and the corresponding observatory `SV` estimate.

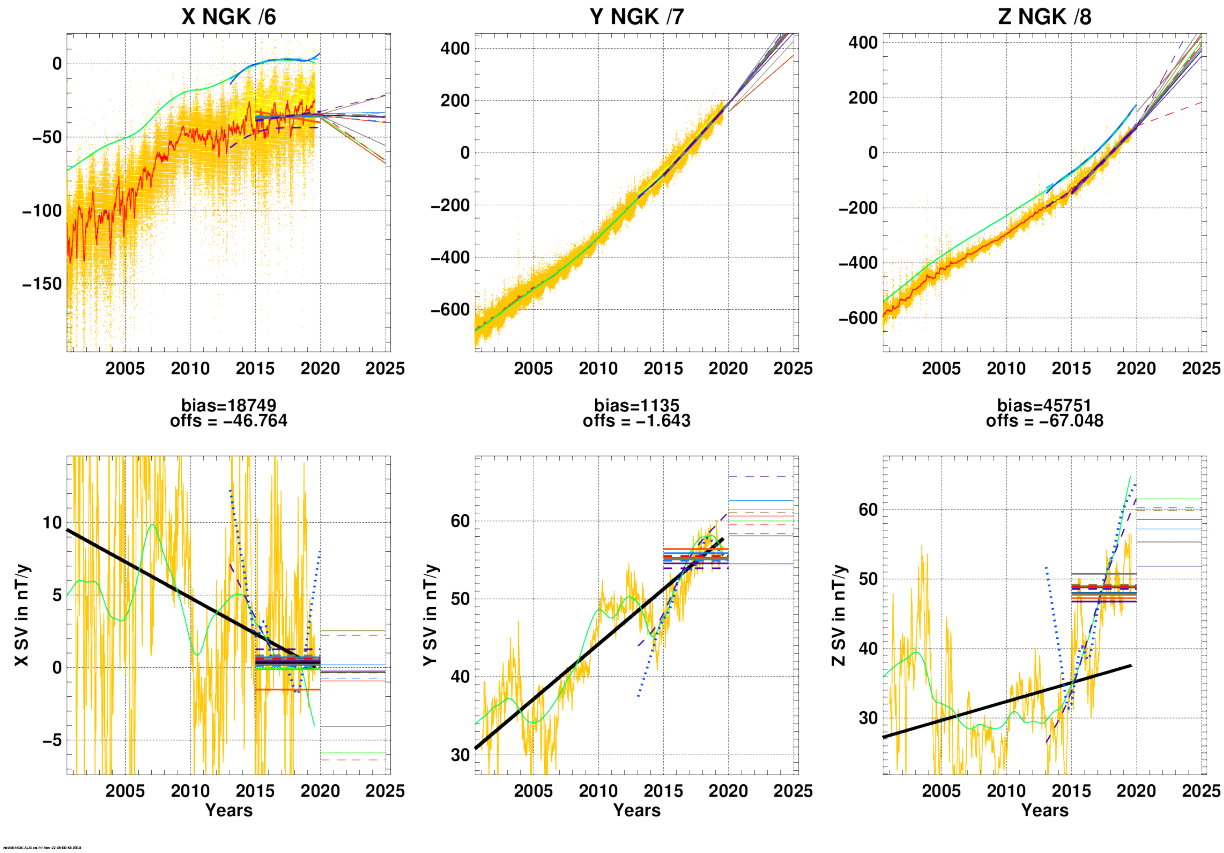

9.2 Candidate comparisons for selected observatories

The figures on pages 49 - 51 show the RMS between data from different observatories in the field (X, Y, Z) and the estimated SV (X′, Y′, Z′). While NGK (Niemegk) is located in an area well covered by observatories, the other selected observatories are located in remote areas.

The figures show RMS calculated for available data in the interval between 2015 to 2020. The respective RMS values are displayed in matrix-like level-plots.

As demonstrated in the figure (page 47) for NGK, large scatter and large drift of the SV can occur. Therefore, the RMS values can be larger than the differences between the candidate estimates. Subsequently, to indicate more clearly a better or worse fit, the columns in these summarising level-plot images (the station names and location are indicated at the figures) are recentered by subtracting the median of the corresponding column.

The colour scale is fix. For cases with blue colours the RMS is lower than the column median RMS value, for red colours larger. The absolute deviation from the column-median value is smaller for pastel colours.

- For observatory HRN the candidate O seems to have an exceptional result for Z′, while the

other candidates shows small deviations.

- Observatories MCQ and MAW show low absolute values for the deviation from the component-wise medians.
- Candidate H shows mostly above-median results on the more diverging cases.
- The Z (and the Z′) component stands out clearly for candidate E in the CKI observatory, while the candidate shows otherwise a good fit, maybe diverging for observatories CTA and GUA.
- All candidate models show clear deviations in the Z and Z′ column for GUA (a somewhat isolated observatory in the Pacific Ocean), for the Australian observatory CTA and, less prominent, for the station ASP.
- The Y component generally shows the closest agreement in absolute terms for all candidates and all the selected observatories.

Niemegk, Germany,
Colat. 37.93°, Long. 12.68°, Elev. 78 m

NGK

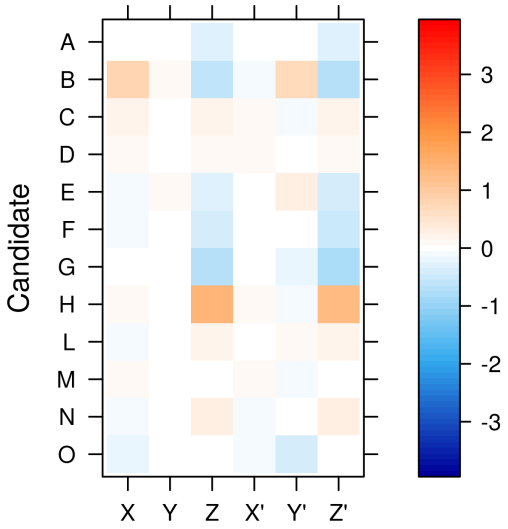

RMS, median centered

Macquarie Isl. Tasmania,
Colat. 144.5°, Long. 158.95°, Elev. 4 m

MCQ

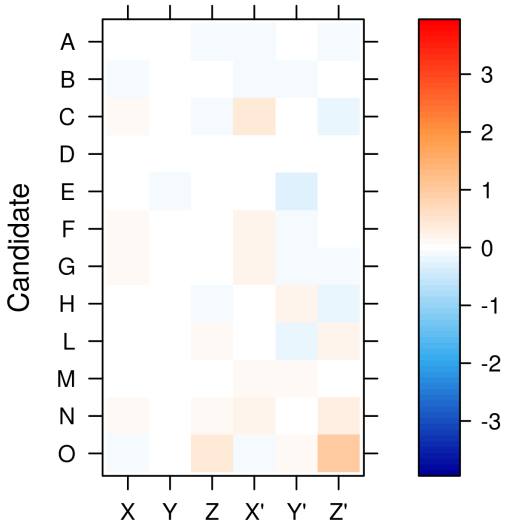

RMS, median centered

Ascension Isl., South Atlantic,
Colat. 97.5°, Long. 345.62°, Elev. 177 m

ASC

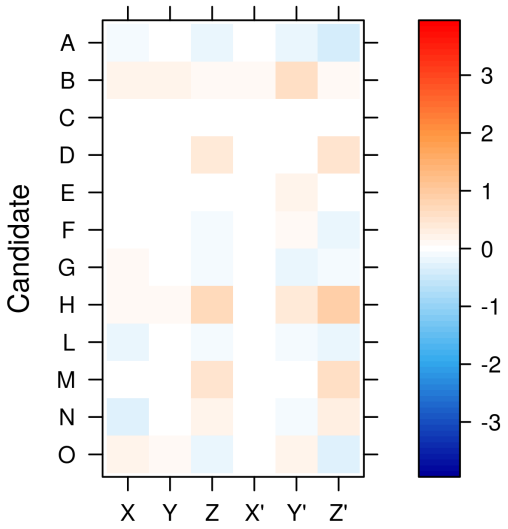

RMS, median centered

Mawson Station, Antarctic
Colat. 157.6°, Long. 62.88°, Elev. 12 m

MAW

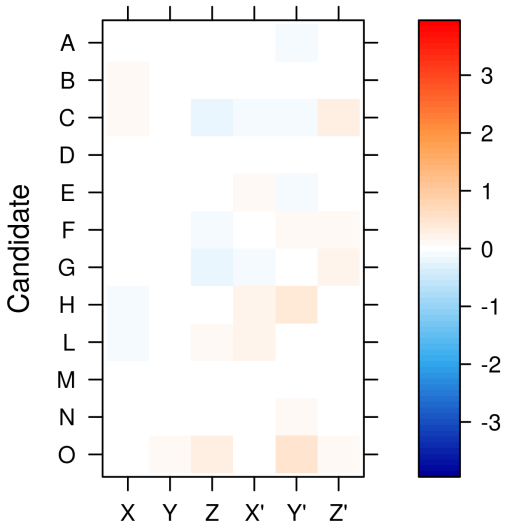

RMS, median centered

Guam, Marianna Islands,
Colat. 76.41°, Long. 144.87°, Elev. 140 m

GUA

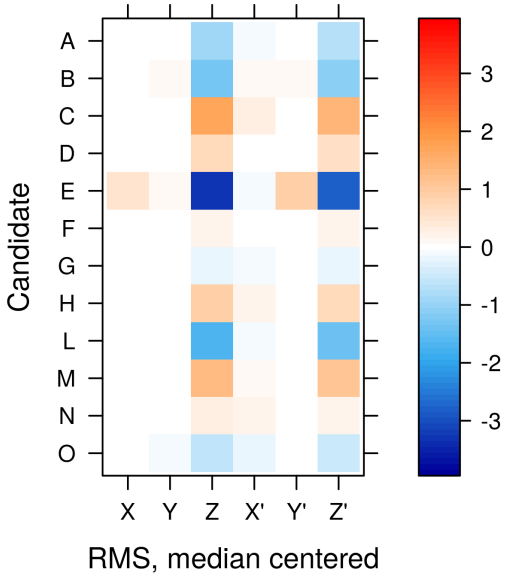

RMS, median centered

Charters Towers, Australia,
Colat. 110.10°, Long. 146.3°, Elev. 370 m

CTA

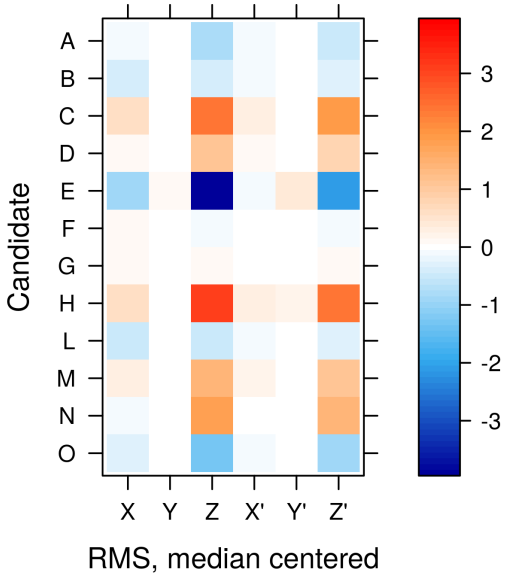

RMS, median centered

Cocos Keeling Isl., Australia,
Colat. 102.18°, Long. 96.83°, Elev. 2.7 m

CKI

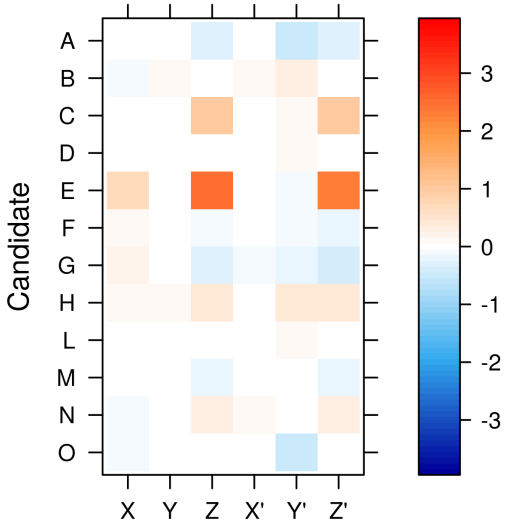

RMS, median centered

Barrow, Alaska,
Colat. 18.68°, Long. 203.38°, Elev. 12 m

BRW

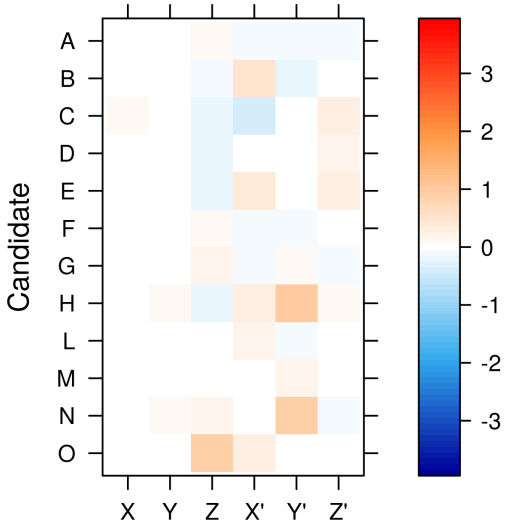

RMS, median centered

Alice Springs, Australia,
Colat. 113.77°, 133.88°, Elev. 557 m

ASP

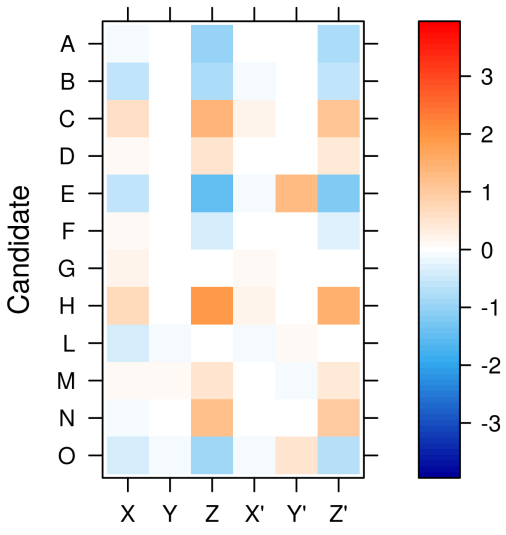

Casey Station, Antarctica,
Colat. 156.283°, Long. 110.533°, Elev. 40 m

CSY

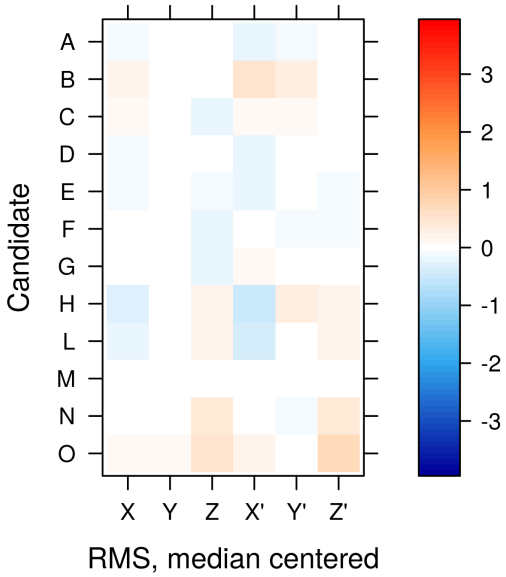

Gingin, Western Australia,
Colat. 121.356°, 115.715°, Elev. 50 m

GNG

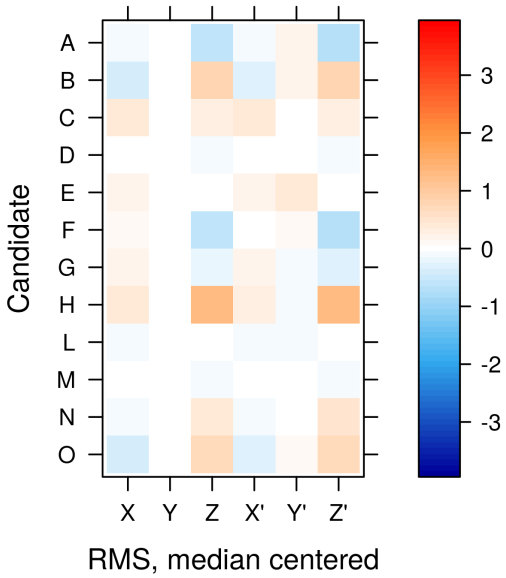

Hornsund, Norway,
Colat. 13.0°, Long. 15.37°, Elev. 15 m

HRN

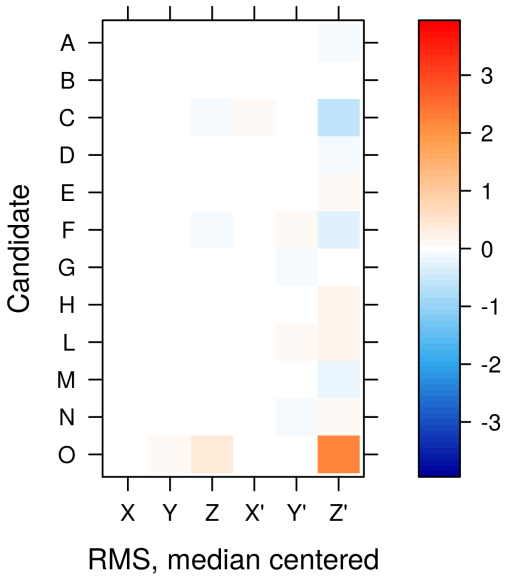

A Overviews of individual coefficients (selected subset)

The following plots show individual coefficients from all candidate models and the mean in units of nT (with uncertainty estimates where given) for DGRF 2015, IGRF 2020 and SV 2020–2025. Each small panel shows the coefficients of one degree and order as labelled above the panel, the labels on the horizontal axes are meaningless and should be ignored. For colours and symbols refer to section 1. For each of the three products, the first line contains all dipole and quadrupole coefficients. Coefficients of SH degrees 3 to 9 are in lines two to eight, always with the zonal coefficient (m=0) in the first column, so that degrees 4 to 9 are more and more incomplete with only as many coefficients as fit into one line.

A.1 DGRF 2015

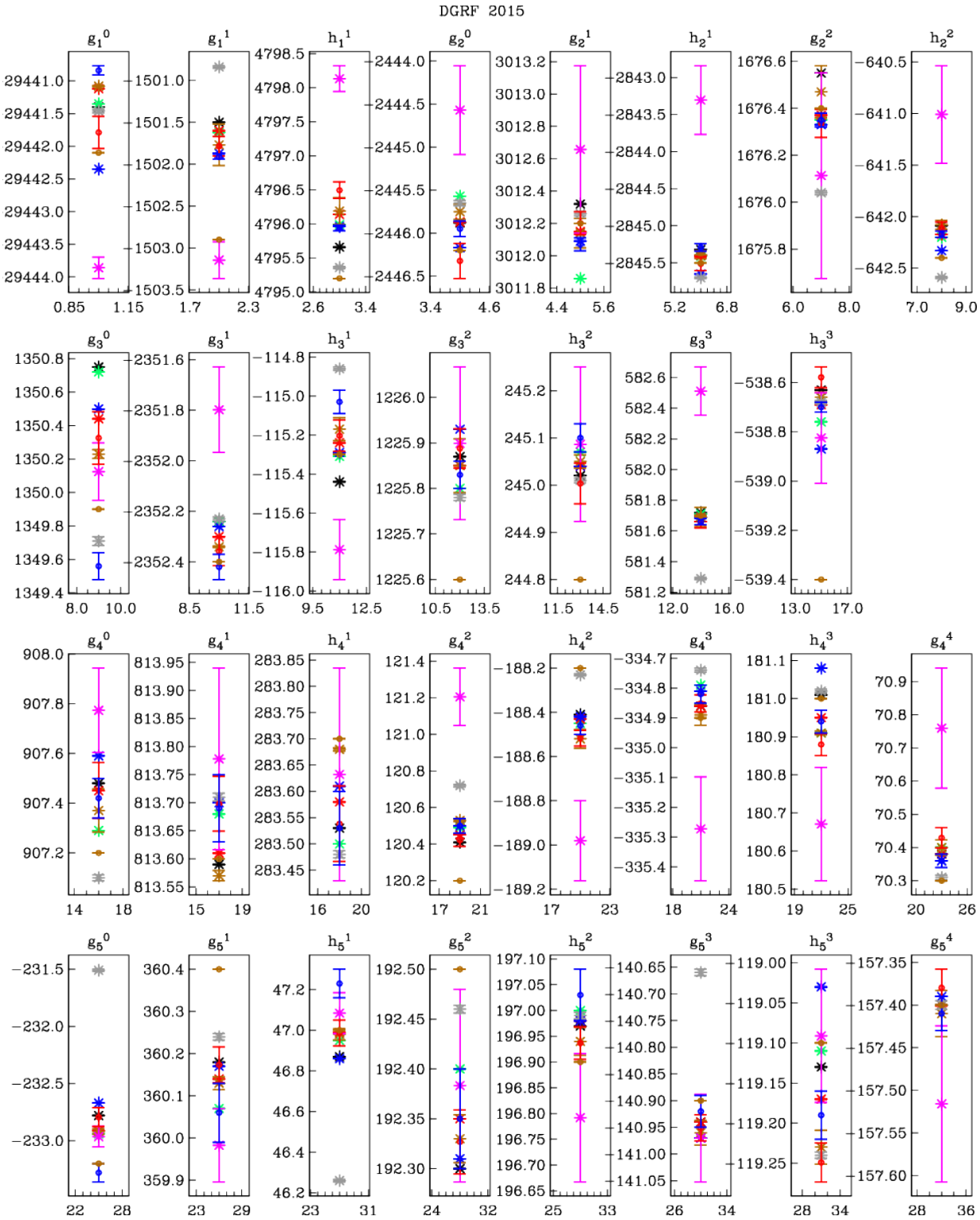
DGRF 2015
g1 0
g1 1
h1 1
g2 0
g2 1
h2 1
g2 2
h2 2
g3 0
g3 1
h3 1
g3 2
h3 2
g3 3
h3 3
g4 0
g4 1
h4 1
g4 2
h4 2
g4 3
h4 3
g4 4
g5 0
g5 1
h5 1
g5 2
h5 2
g5 3
h5 3
g5 4

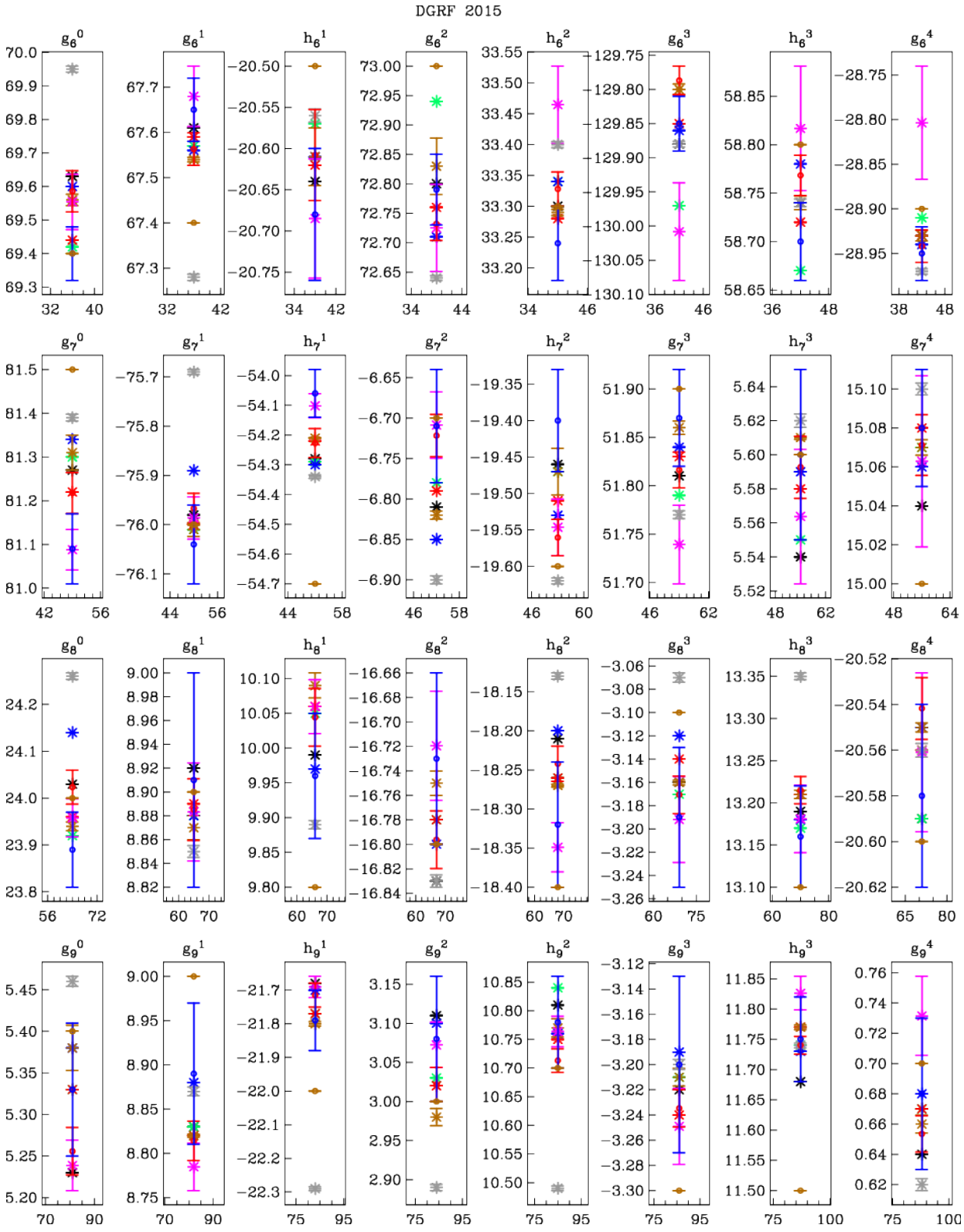
DGRF 2015
g6 0
g6 1
h6 1
g6 2
h6 2
g6 3
h6 3
g6 4
g7 0
g7 1
h7 1
g7 2
h7 2
g7 3
h7 3
g7 4
g8 0
g8 1
h8 1
g8 2
h8 2
g8 3
h8 3
g8 4
g9 0
g9 1
h9 1
g9 2
h9 2
g9 3
h9 3
g9 4

A.2 IGRF 2020

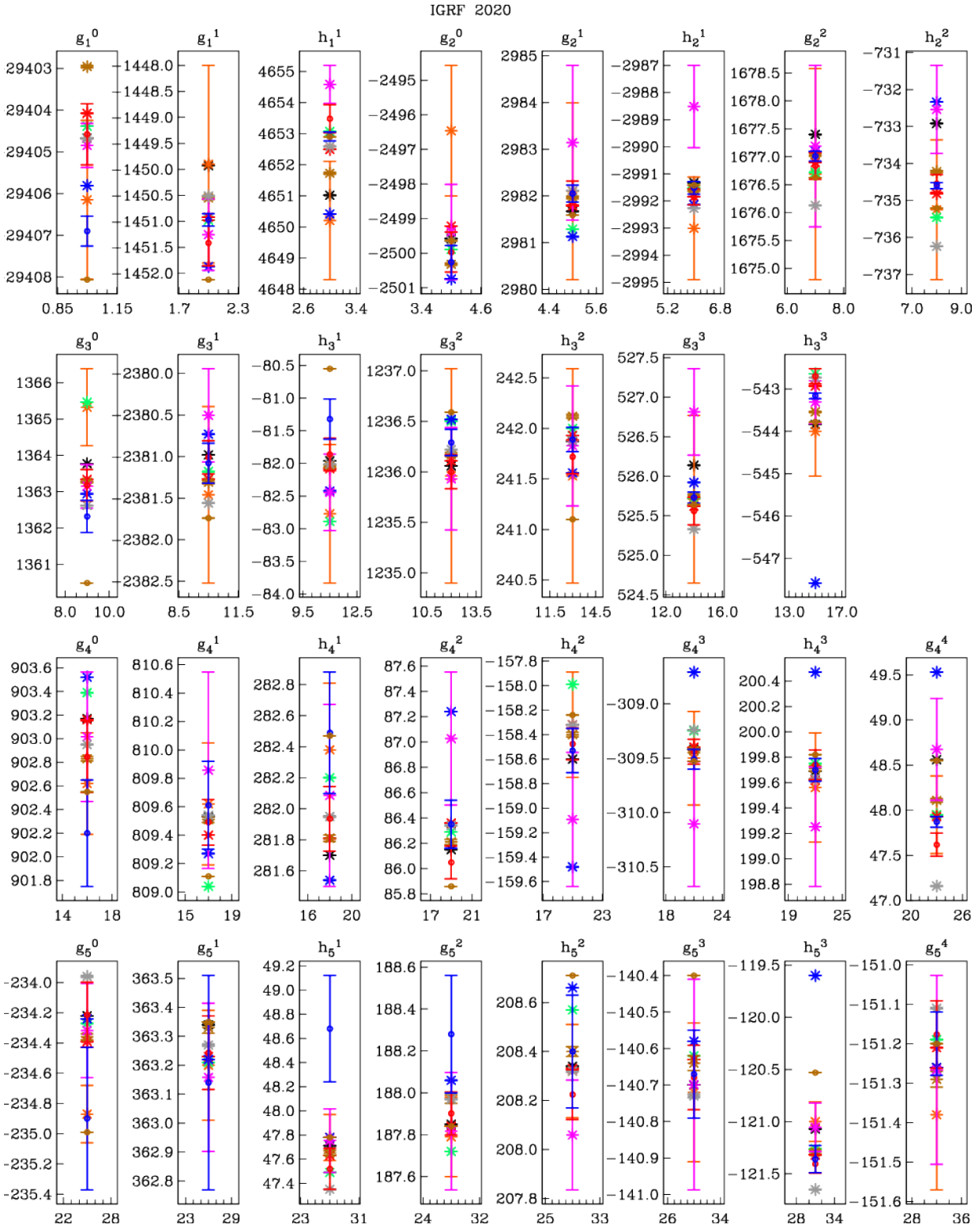
IGRF 2020
g1 0
g1 1
h1 1
g2 0
g2 1
h2 1
g2 2
h2 2
g3 0
g3 1
h3 1
g3 2
h3 2
g3 3
h3 3
g4 0
g4 1
h4 1
g4 2
h4 2
g4 3
h4 3
g4 4
g5 0
g5 1
h5 1
g5 2
h5 2
g5 3
h5 3
g5 4

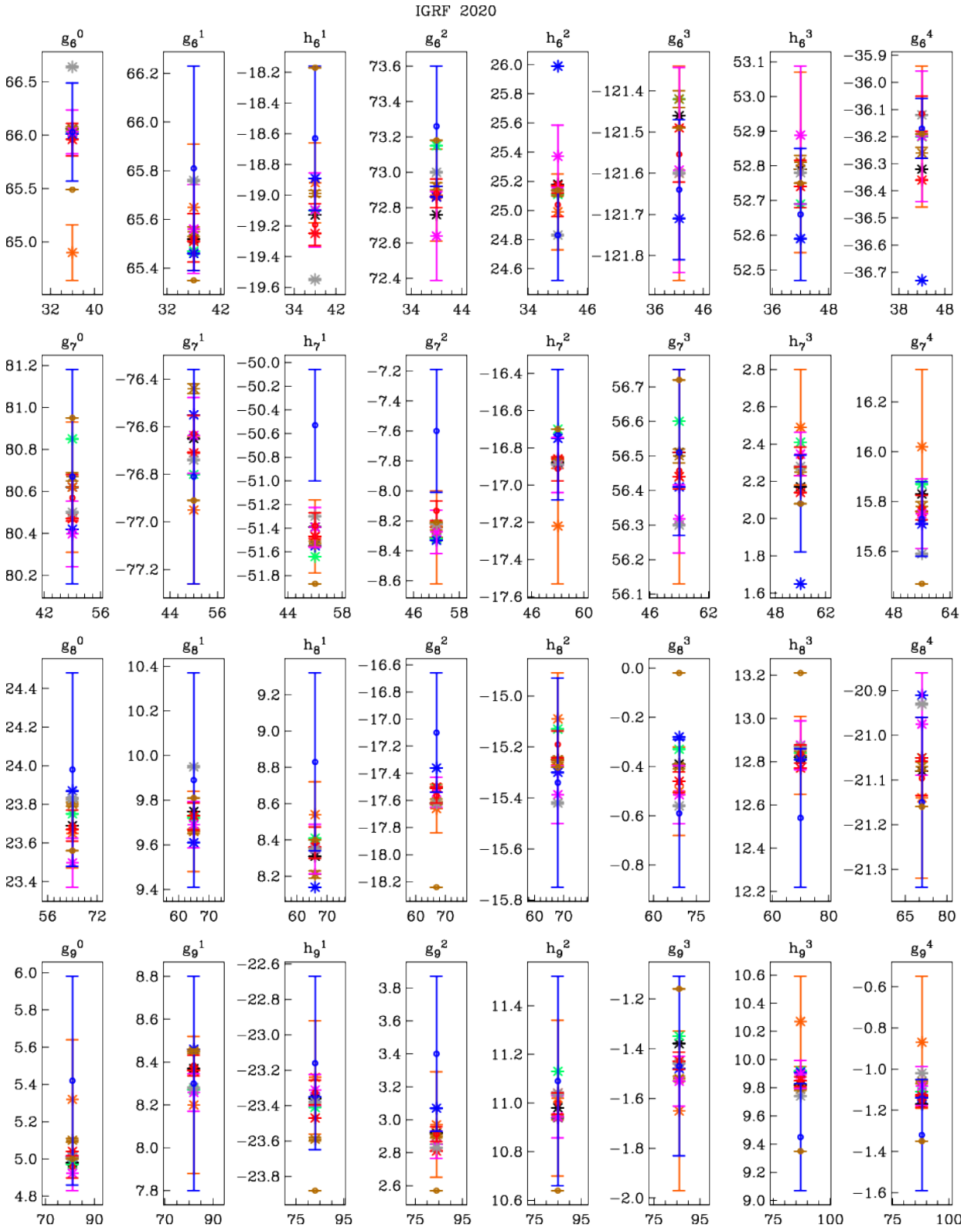
IGRF 2020
g6 0
g6 1
h6 1
g6 2
h6 2
g6 3
h6 3
g6 4
g7 0
g7 1
h7 1
g7 2
h7 2
g7 3
h7 3
g7 4
g8 0
g8 1
h8 1
g8 2
h8 2
g8 3
h8 3
g8 4
g9 0
g9 1
h9 1
g9 2
h9 2
g9 3
h9 3
g9 4

A.3 SV 2020–2025

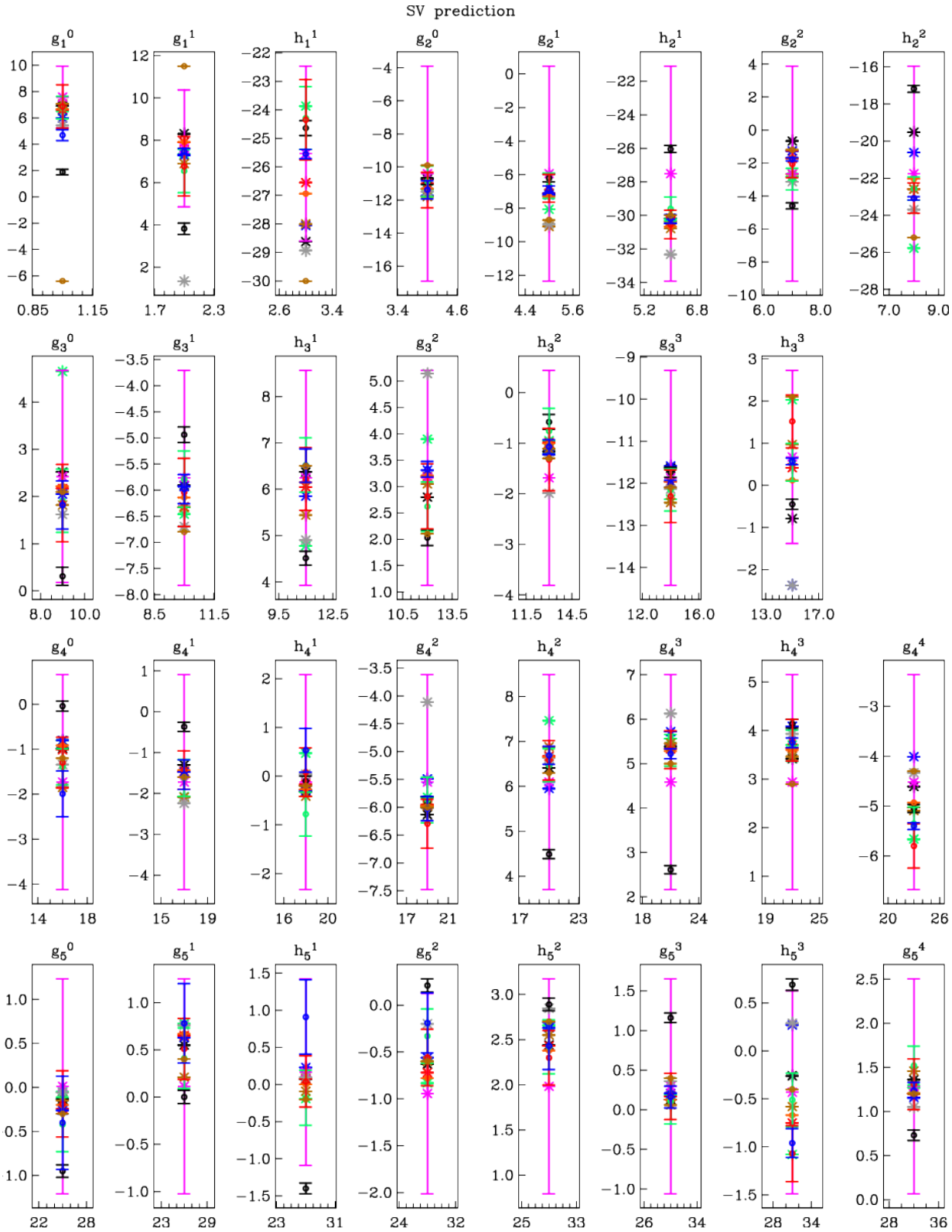

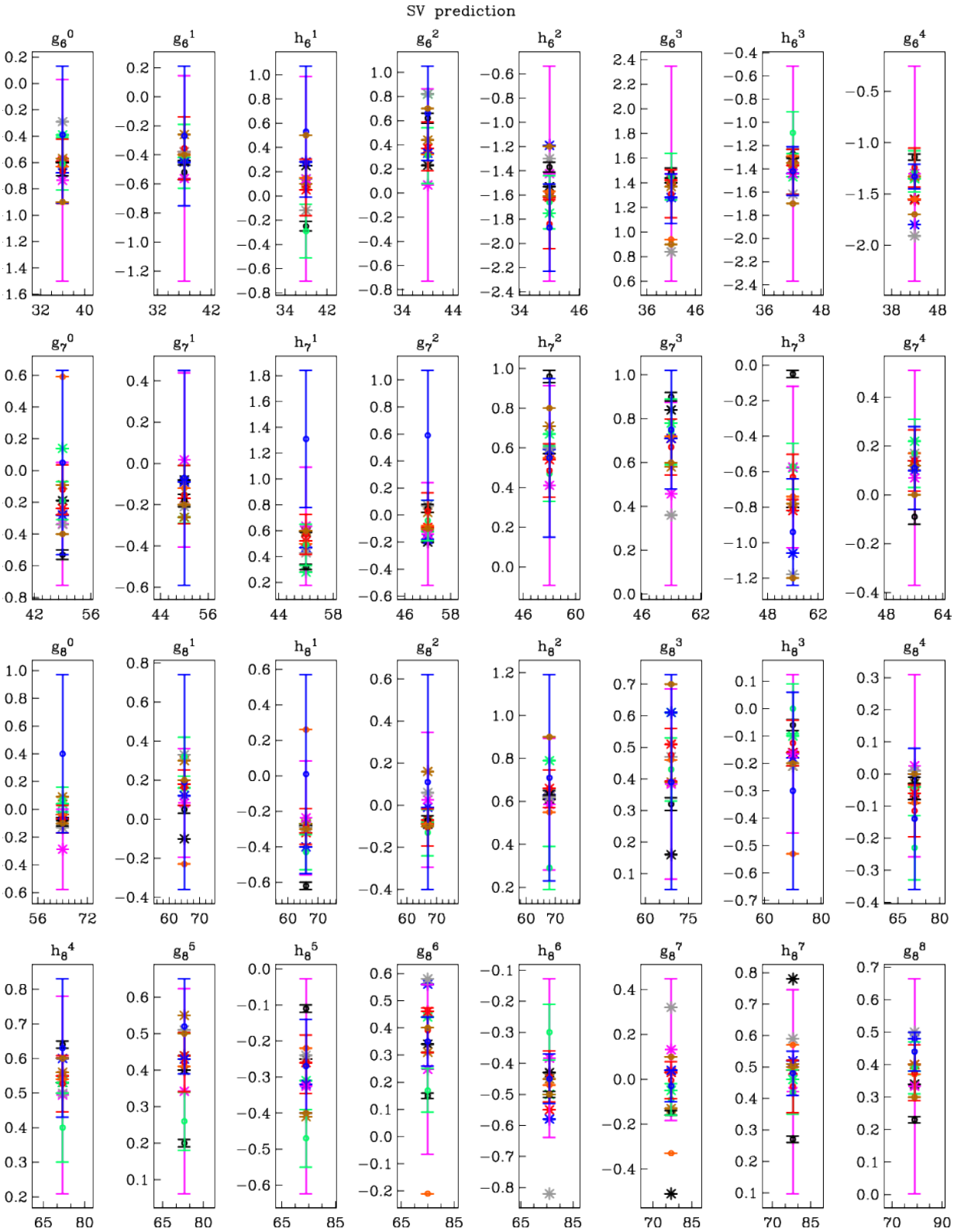
SV prediction
g6^0
g6^1
h6^1
g6^2
h6^2
g6^3
h6^3
g6^4
g7^0
g7^1
h7^1
g7^2
h7^2
g7^3
h7^3
g7^4
g8^0
g8^1
h8^1
g8^2
h8^2
g8^3
h8^3
g8^4
h8^4
g8^5
h8^5
g8^6
h8^6
g8^7
h8^7
g8^8

B Maps of model differences to arithmetic mean

Difference between the individual models and the arithmetic mean for geodetic components intensity (F), vertical down (Z), north (X) and east (Y) at Earth's surface, radial field B_r at the core-mantle boundary (CMB), and surface power spectrum of the differences (as also summarised in section 6). Models and and times according to section and subsection titles.

B.1 DGRF 2015

B.1.1 BGS (A)

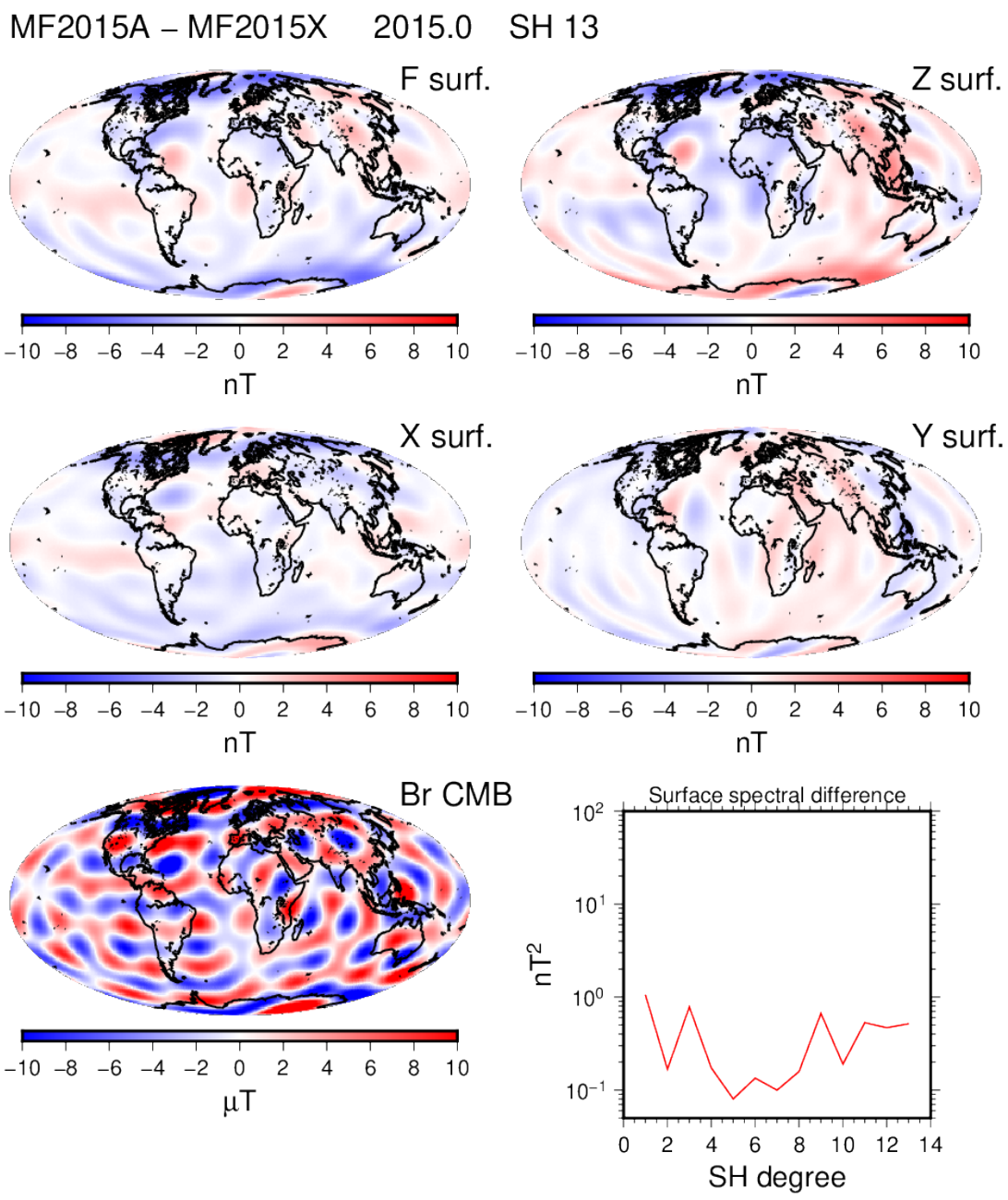

B.1.2 CU/NCEI (C)

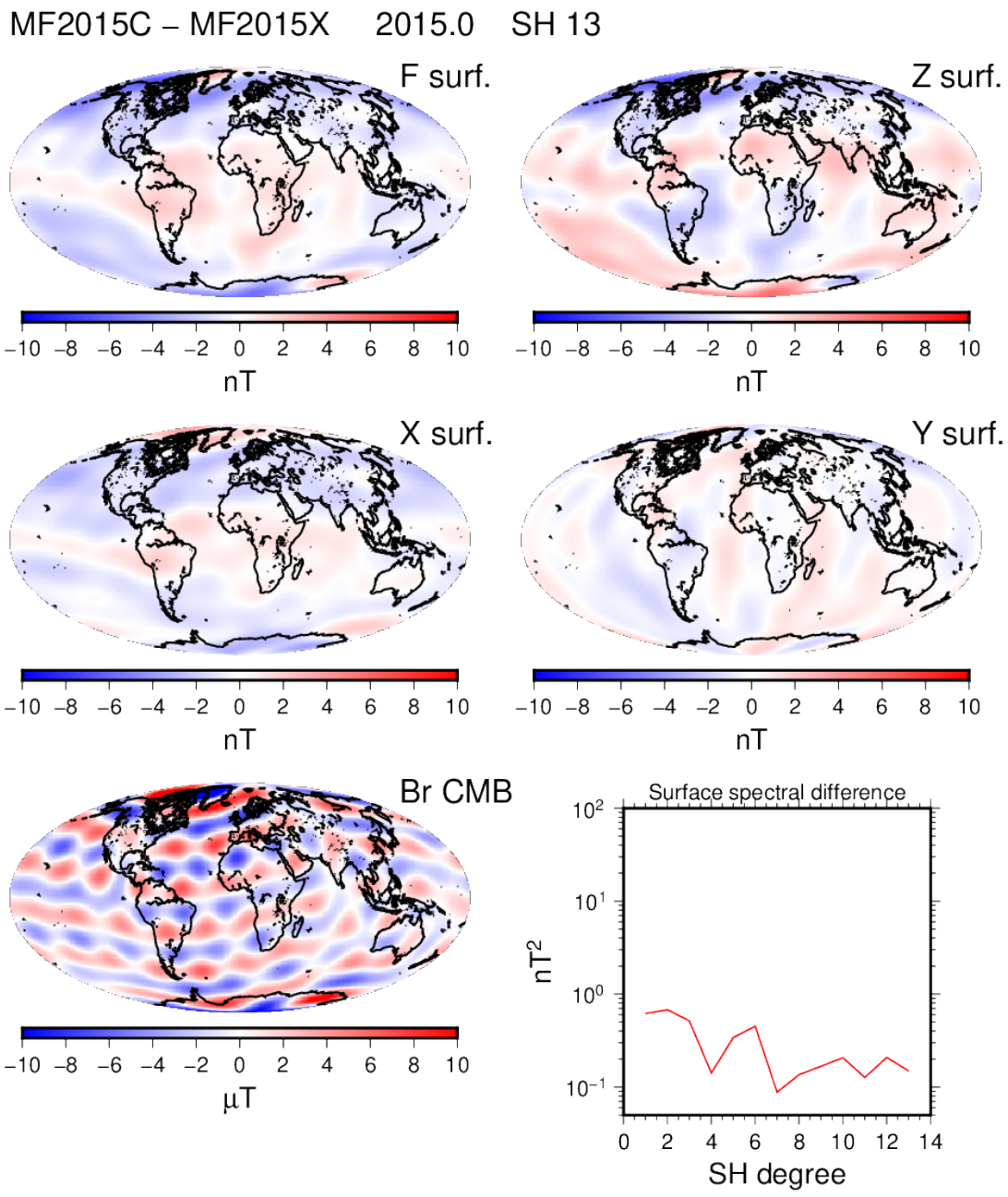
MF2015C – MF2015X 2015.0 SH 13
F surf.
Z surf.
X surf.
Y surf.
Br CMB
−10 −8 −6 −4 −2 0 2 4 6 8 10
nT
μT
Surface spectral difference
nT²
SH degree
0 2 4 6 8 10 12 14

B.1.3 DTU (D)

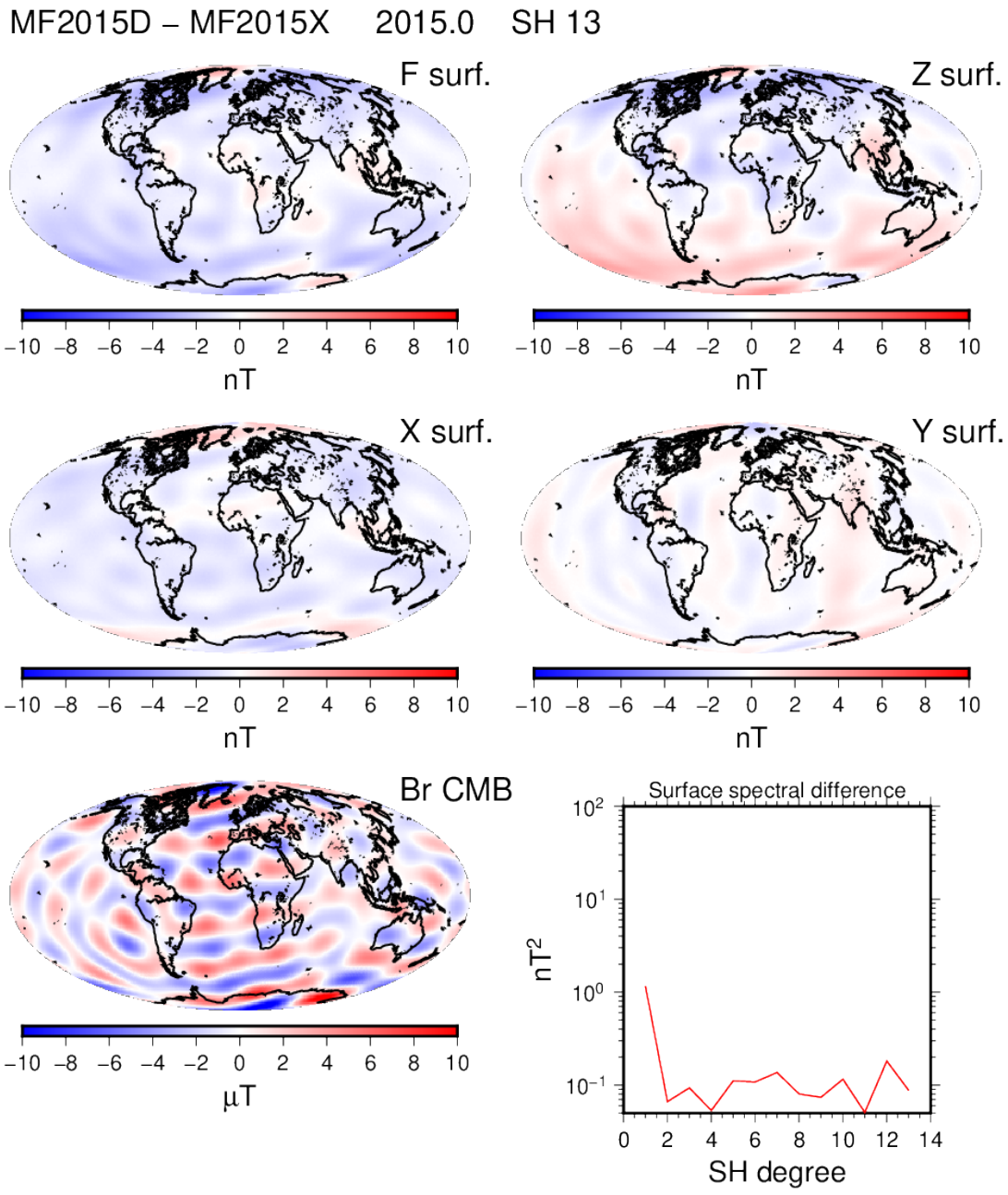
MF2015D – MF2015X 2015.0 SH 13
F surf.
Z surf.
X surf.
Y surf.
Br CMB
−10 −8 −6 −4 −2 0 2 4 6 8 10
nT
μT
Surface spectral difference
nT²
SH degree

B.1.4 GFZ (E)

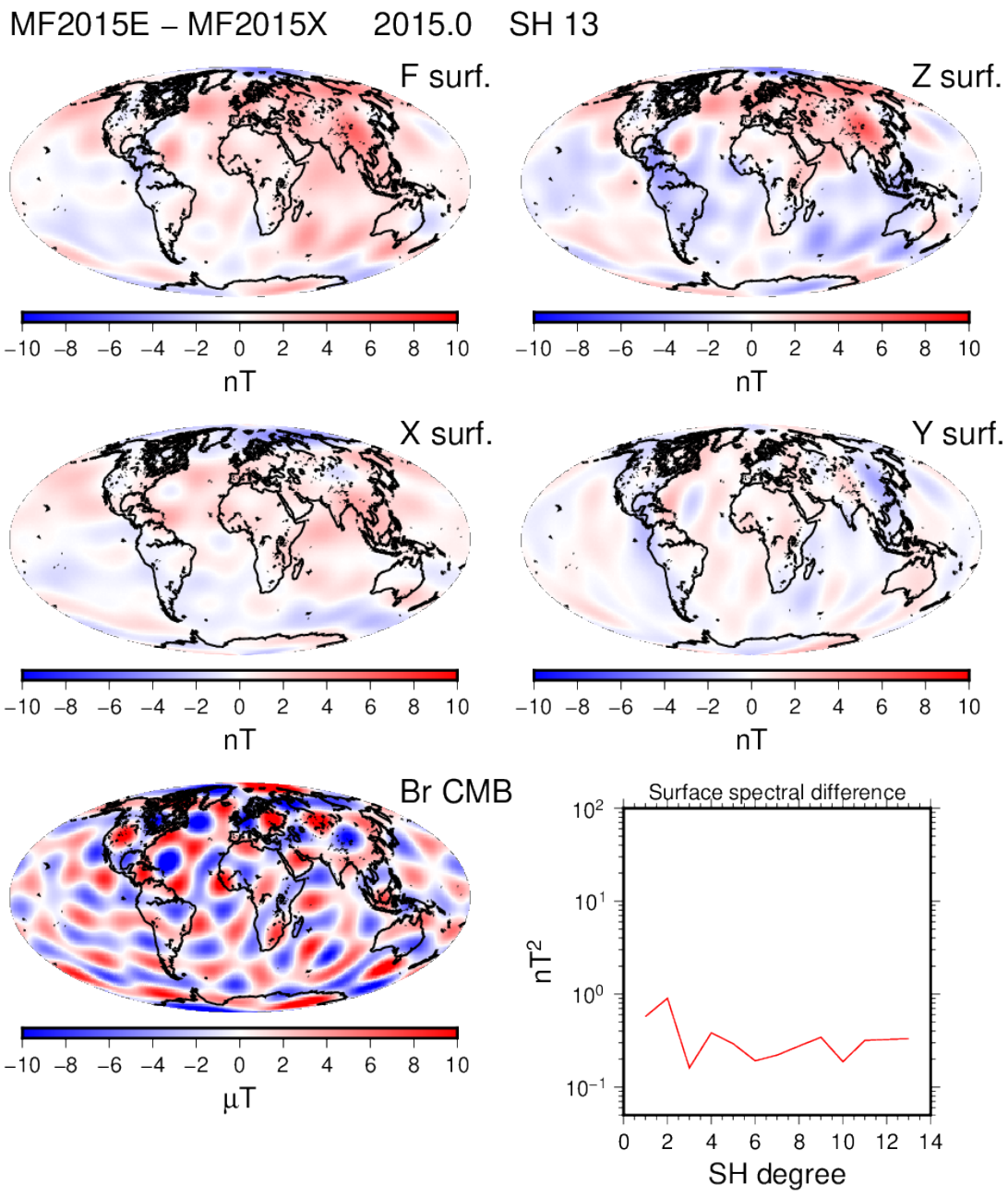
MF2015E – MF2015X 2015.0 SH 13
F surf.
Z surf.
X surf.
Y surf.
Br CMB
−10 −8 −6 −4 −2 0 2 4 6 8 10
nT
μT
Surface spectral difference
nT²
SH degree
0 2 4 6 8 10 12 14

B.1.5 IPGP (F)

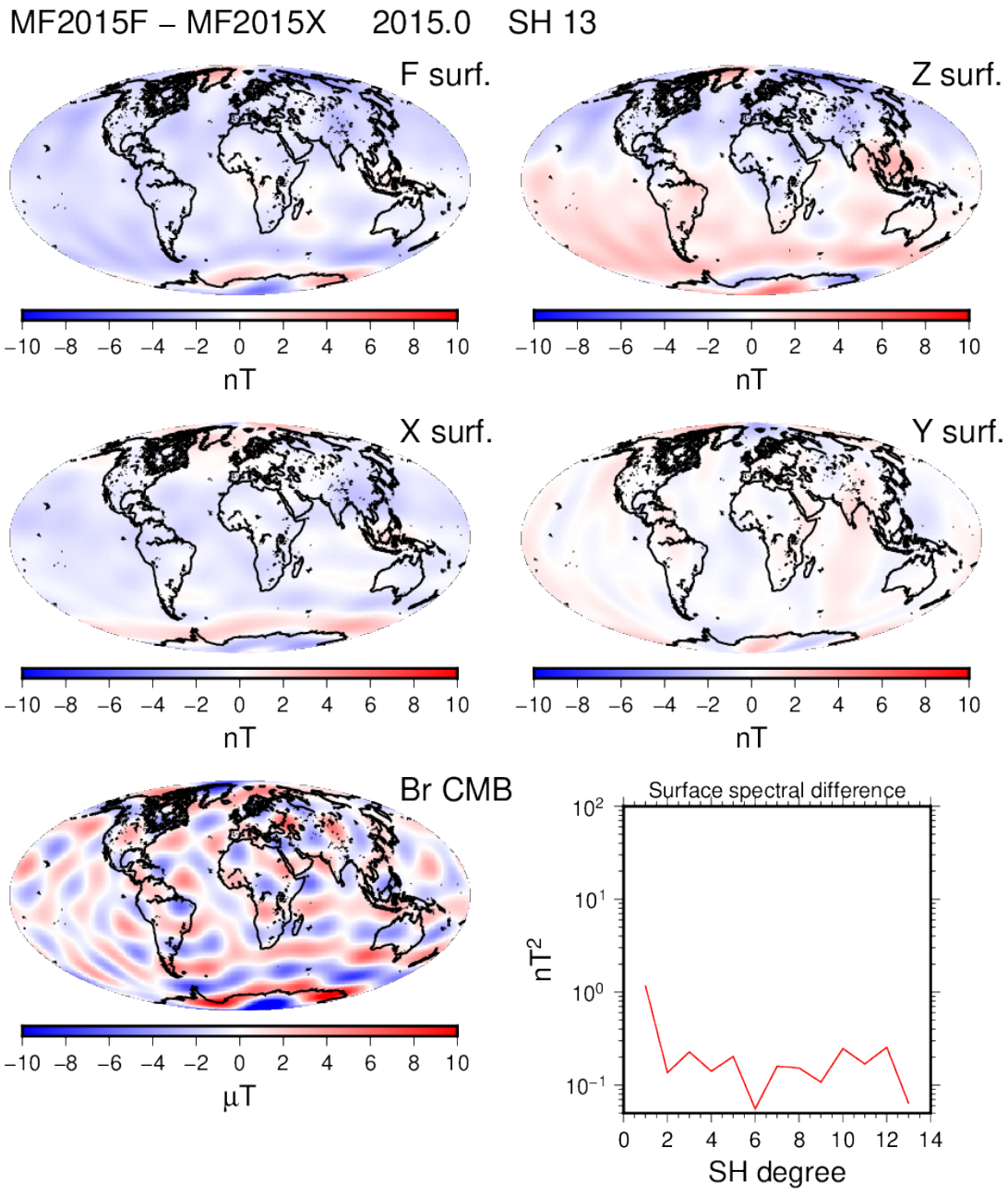
MF2015F – MF2015X 2015.0 SH 13
F surf.
Z surf.
X surf.
Y surf.
Br CMB
−10 −8 −6 −4 −2 0 2 4 6 8 10
nT
μT
Surface spectral difference
nT²
SH degree

B.1.6 `ISTerre` (G)

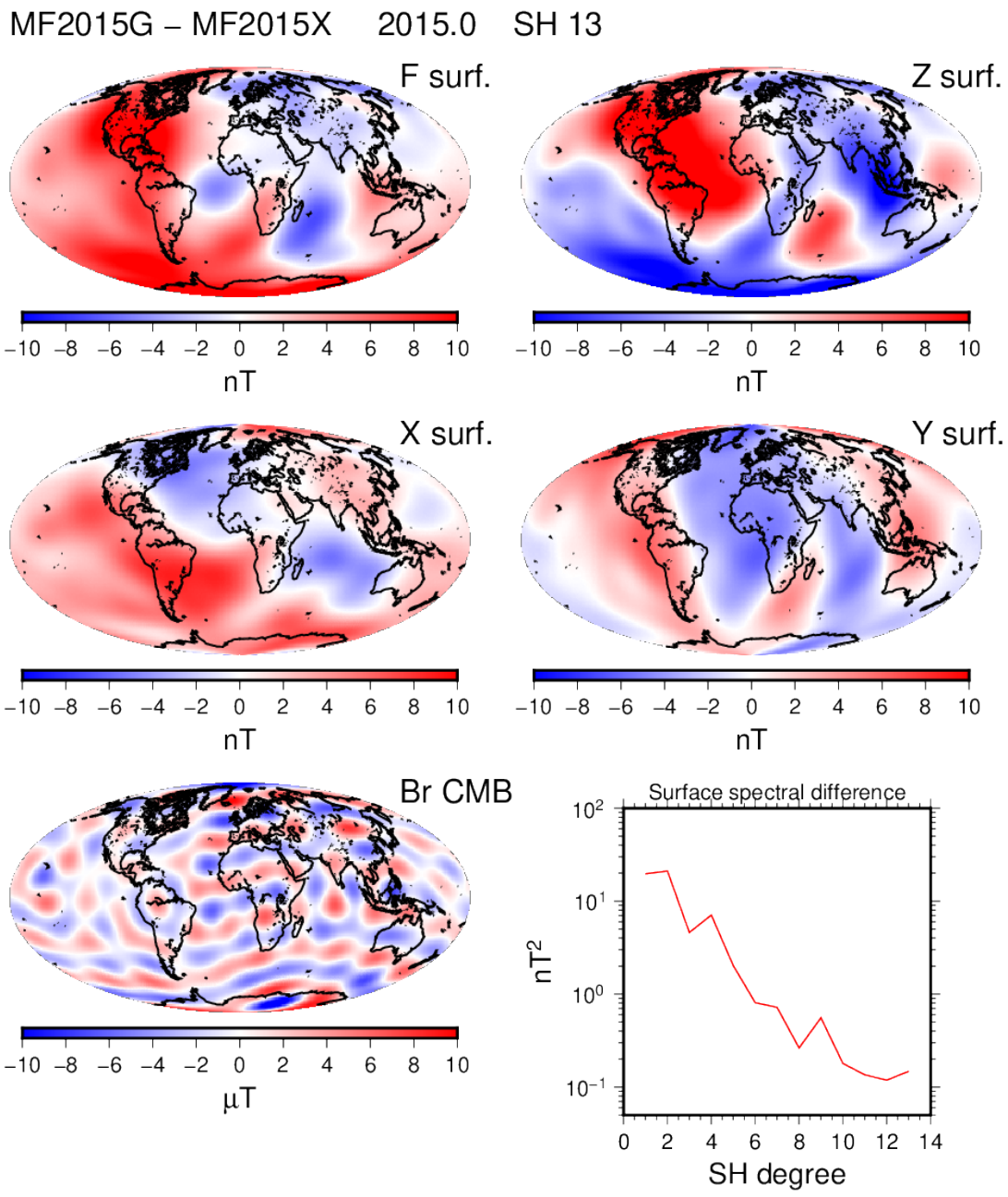

B.1.7 IZMIRAN (H)

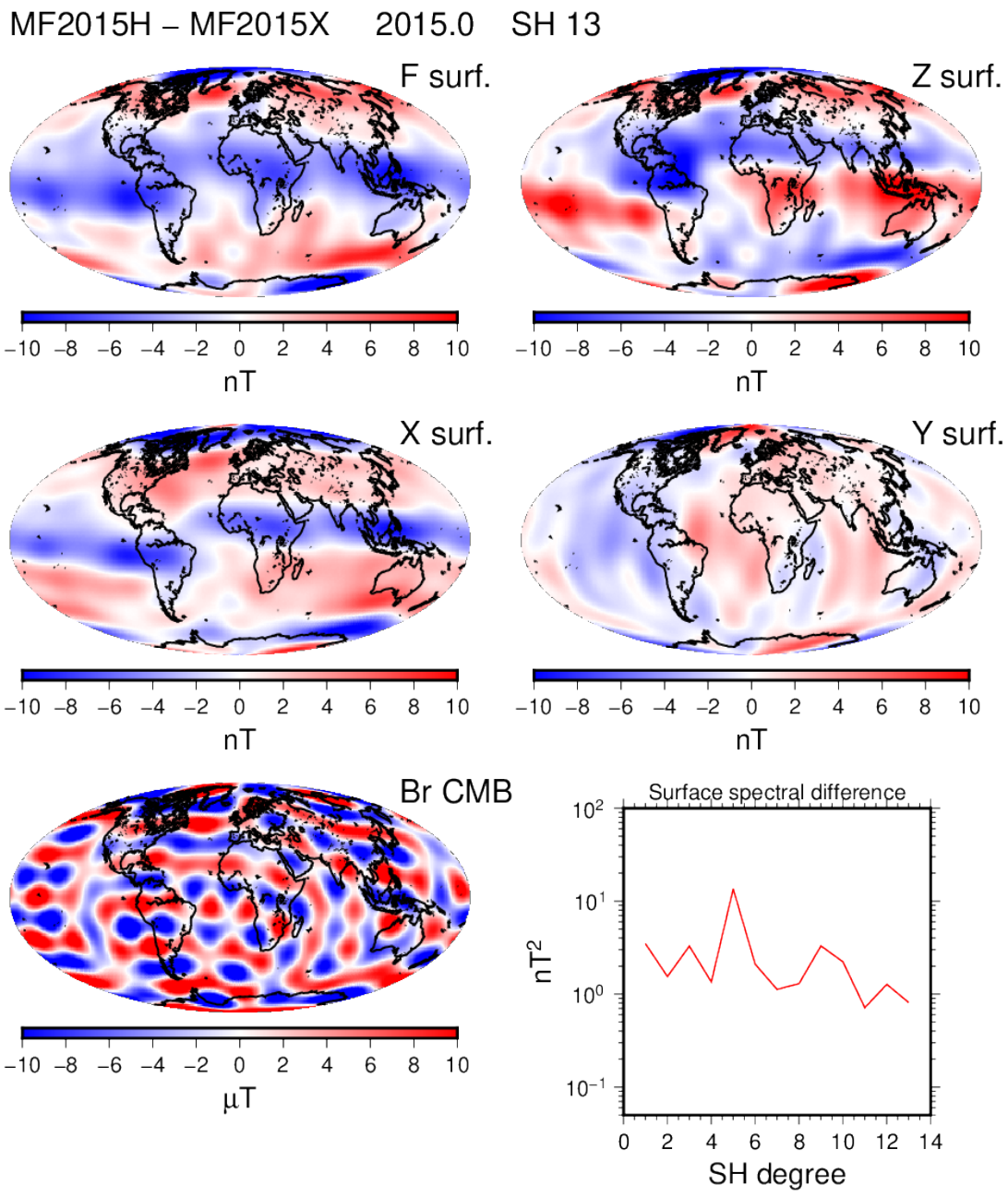

B.1.8 NASA/GSFC (L)

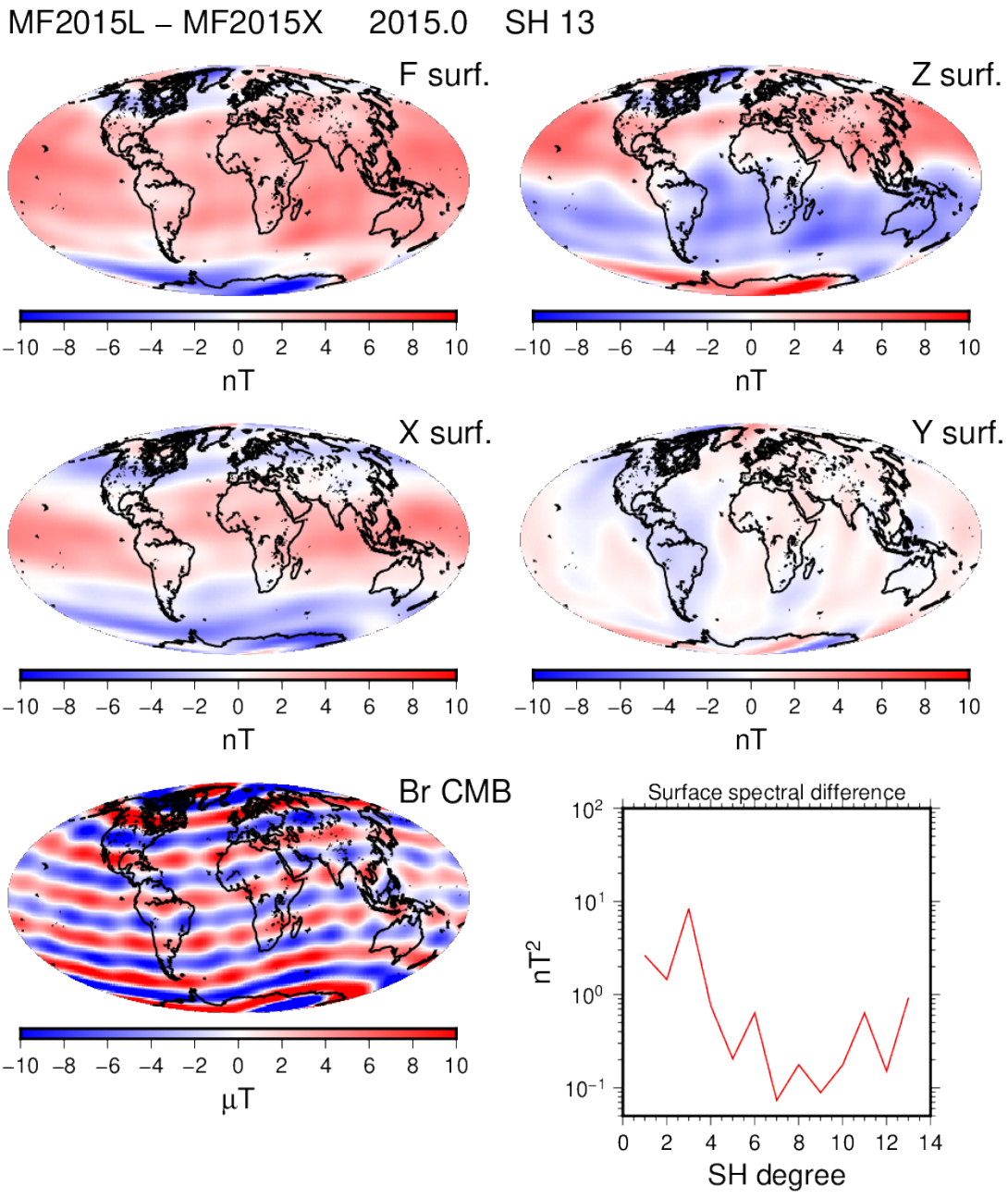

B.1.9 Uni Potsdam/Max Planck (M)

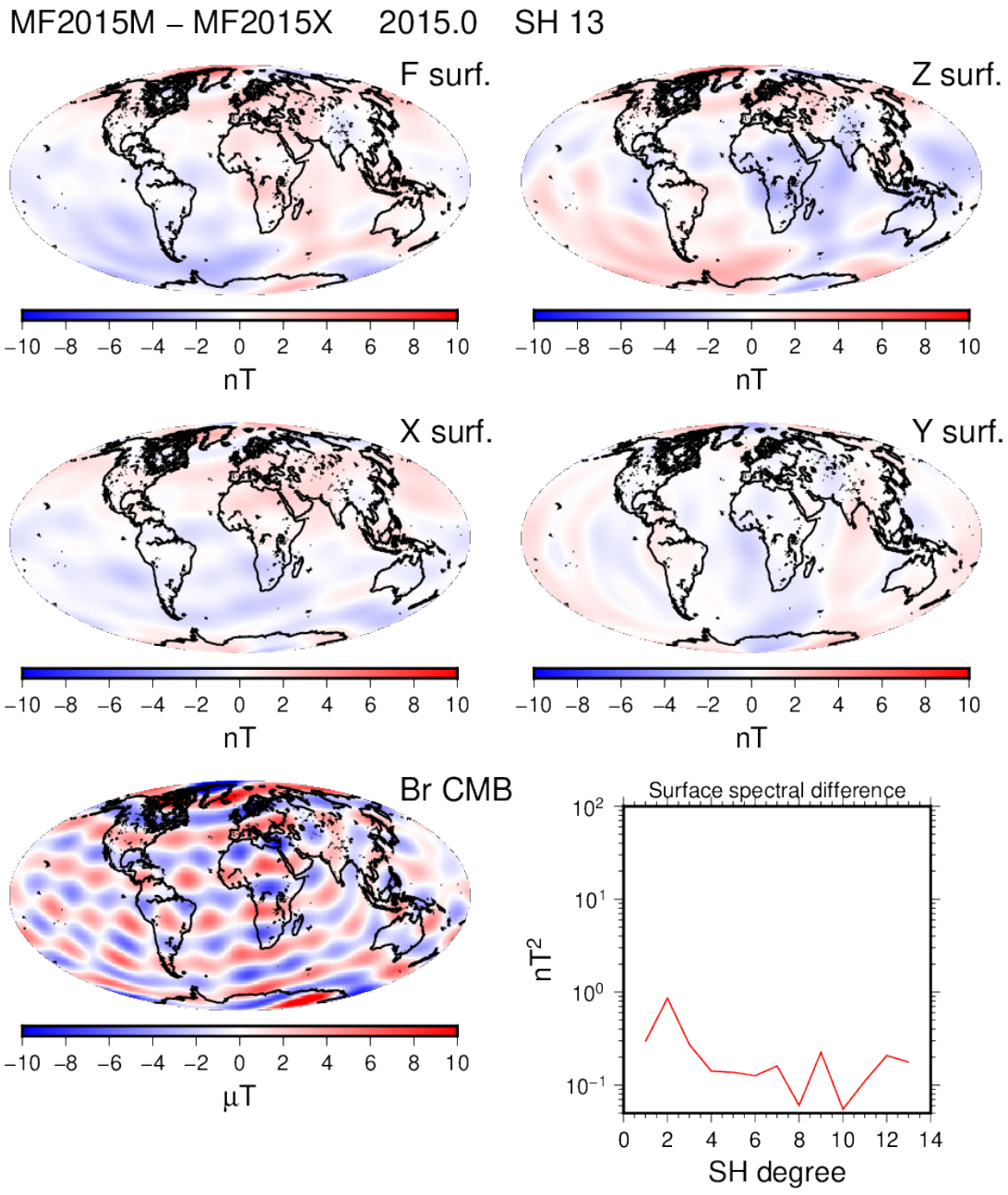

B.1.10 Spanish Team (N)

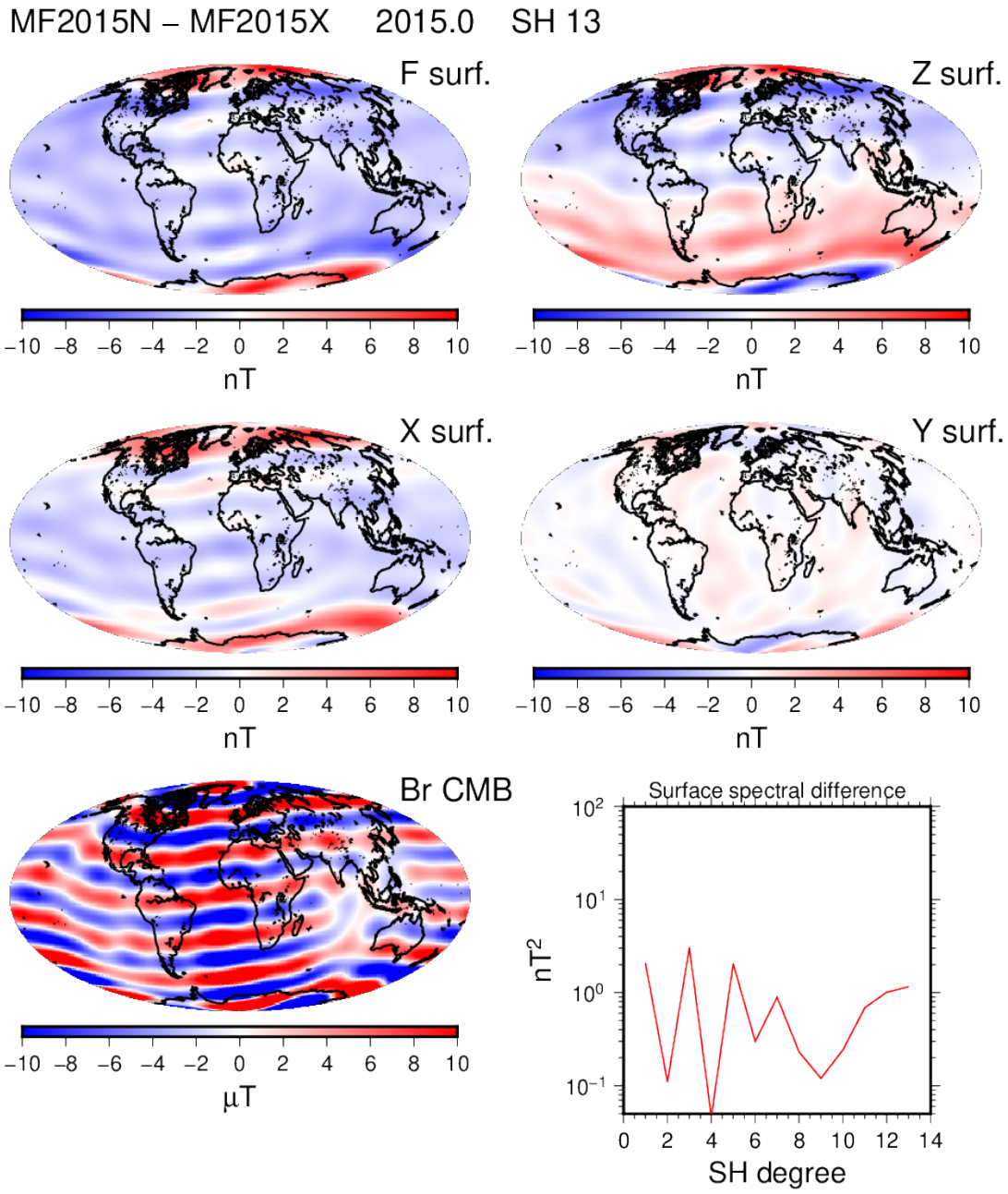

B.1.11 U Strasbourgh (O)

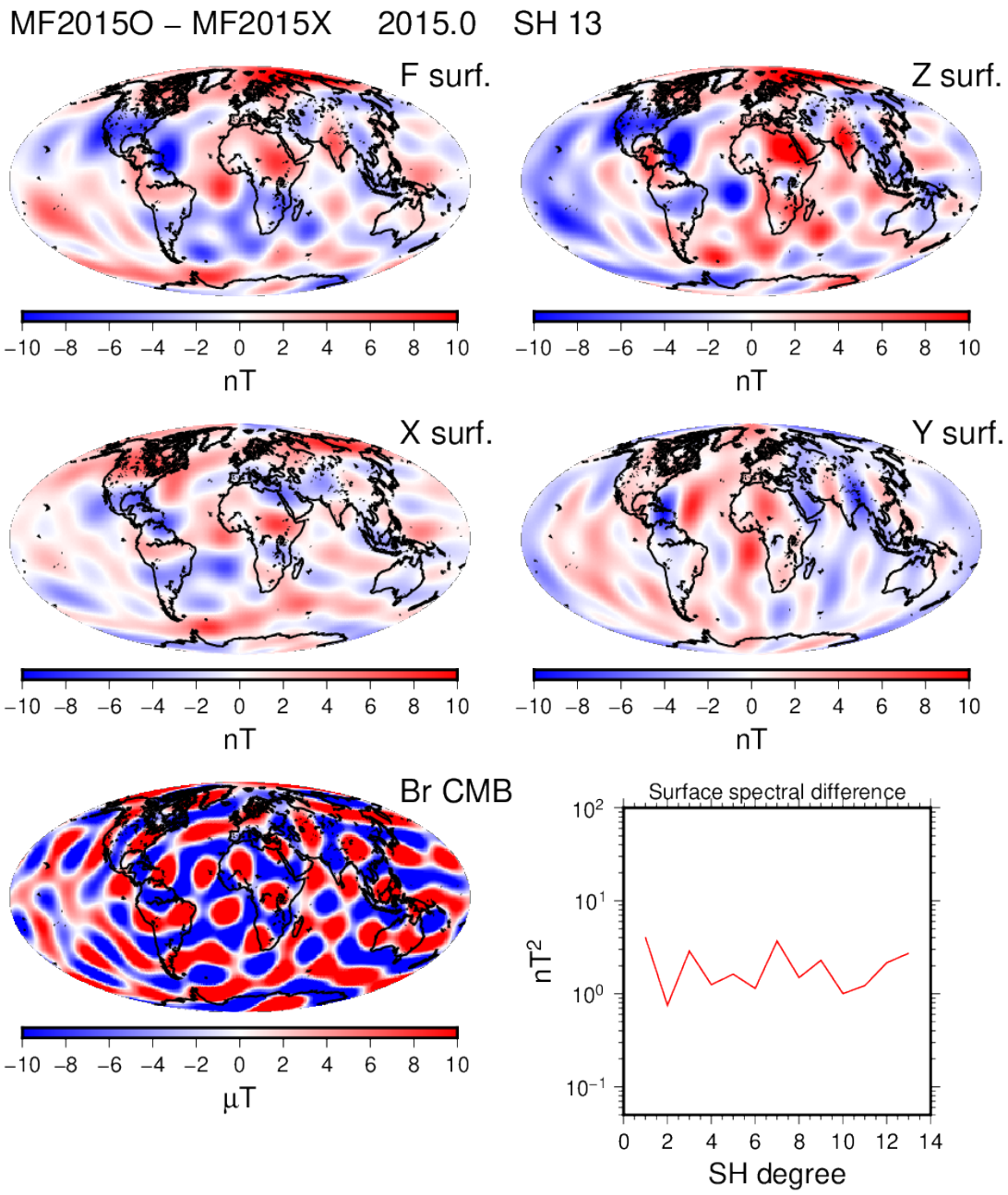

B.2 IGRF 2020

B.2.1 BGS (A)

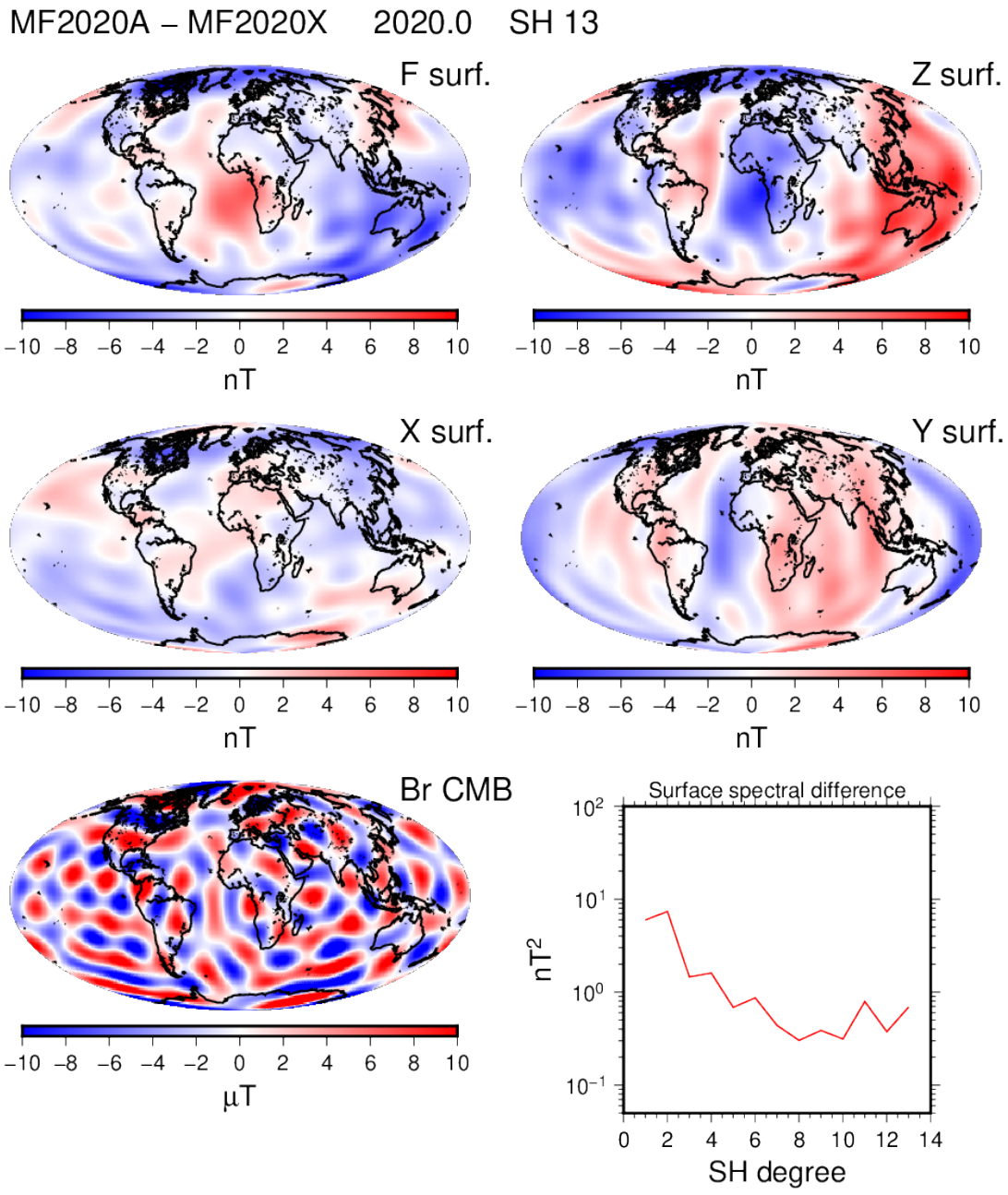

B.2.2 CEA/CSES (B)

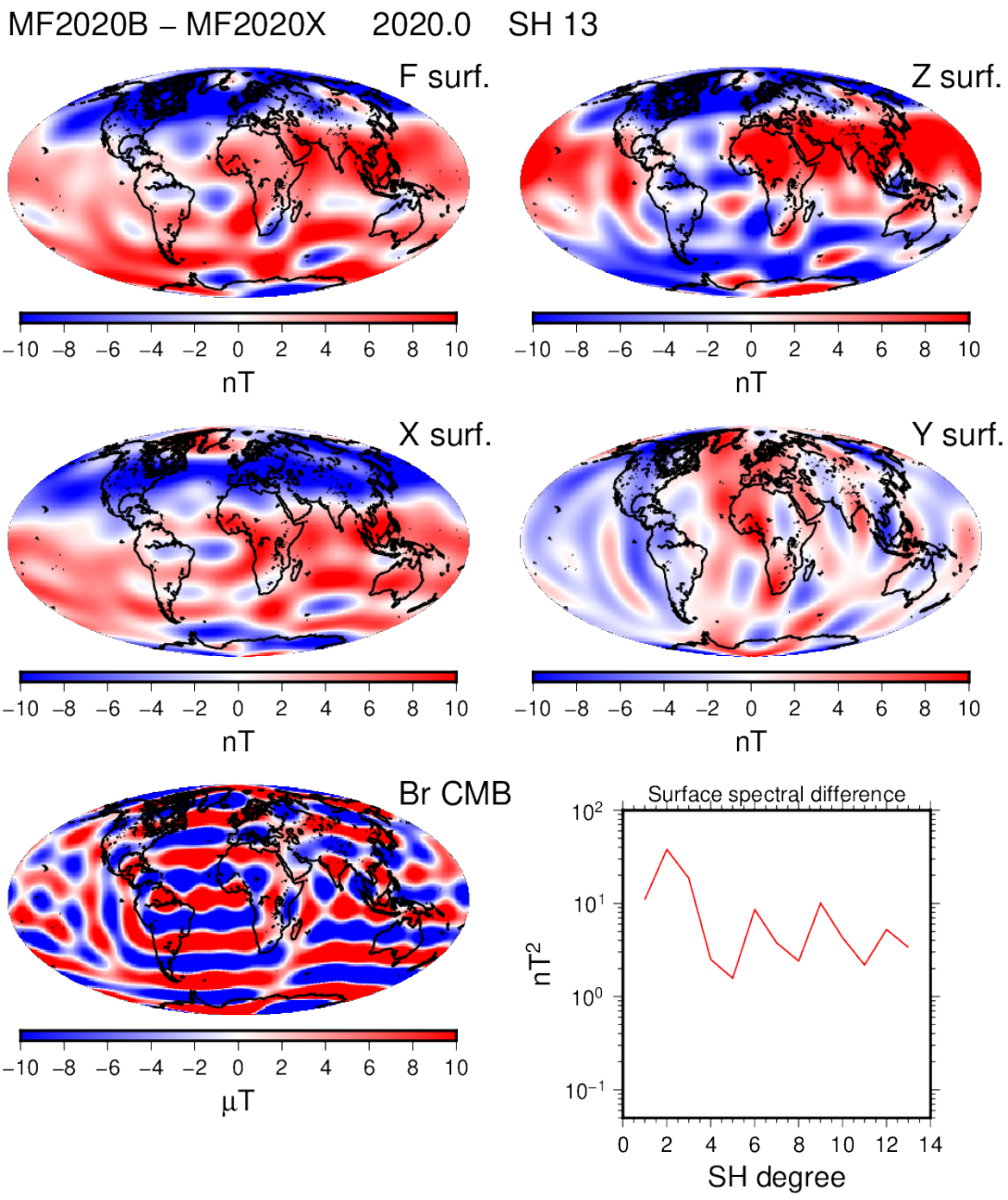

B.2.3 CU/NCEI (C)

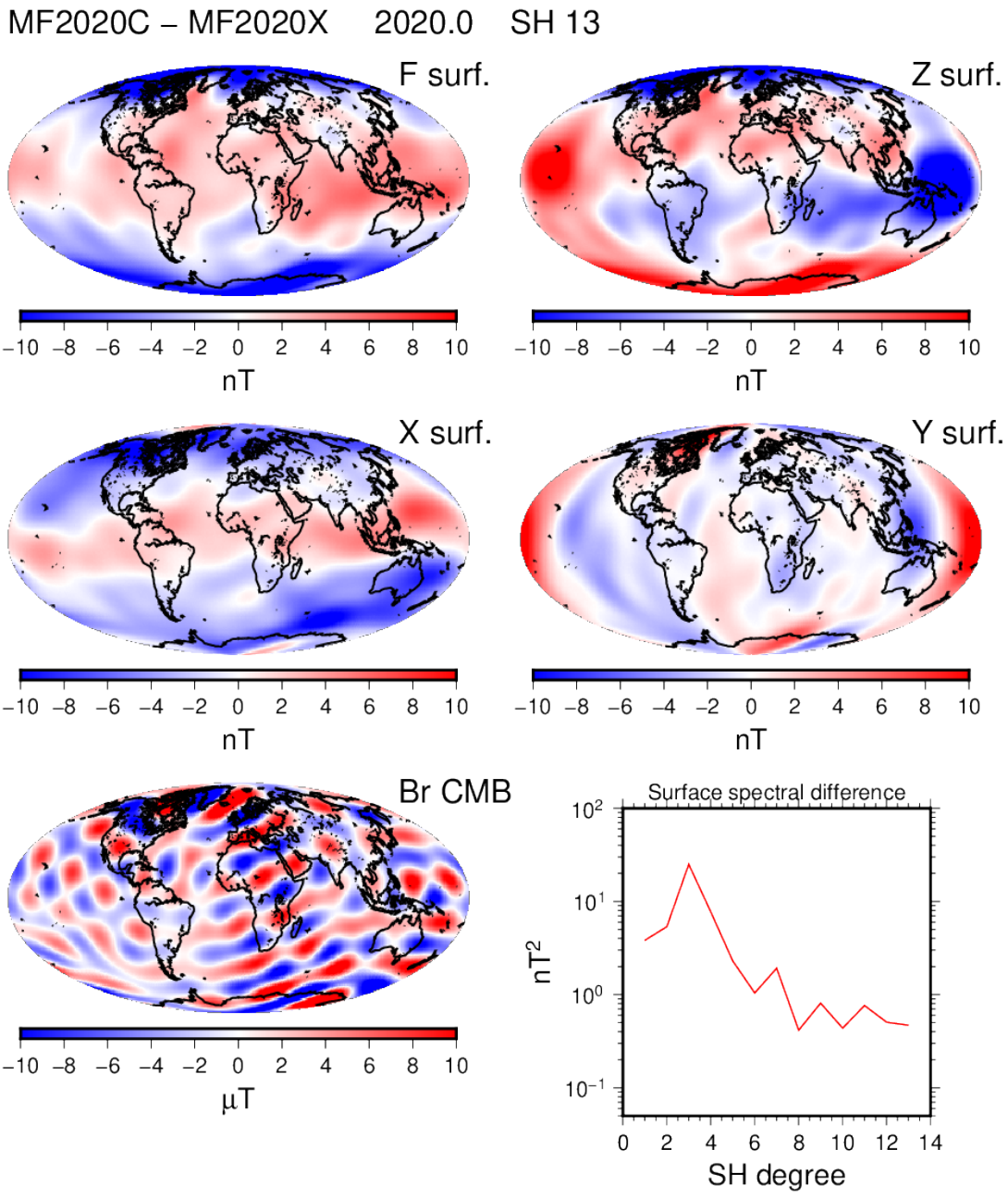
MF2020C – MF2020X 2020.0 SH 13
F surf.
Z surf.
X surf.
Y surf.
Br CMB
−10 −8 −6 −4 −2 0 2 4 6 8 10
nT
μT
Surface spectral difference
nT²
SH degree

B.2.4 DTU (D)

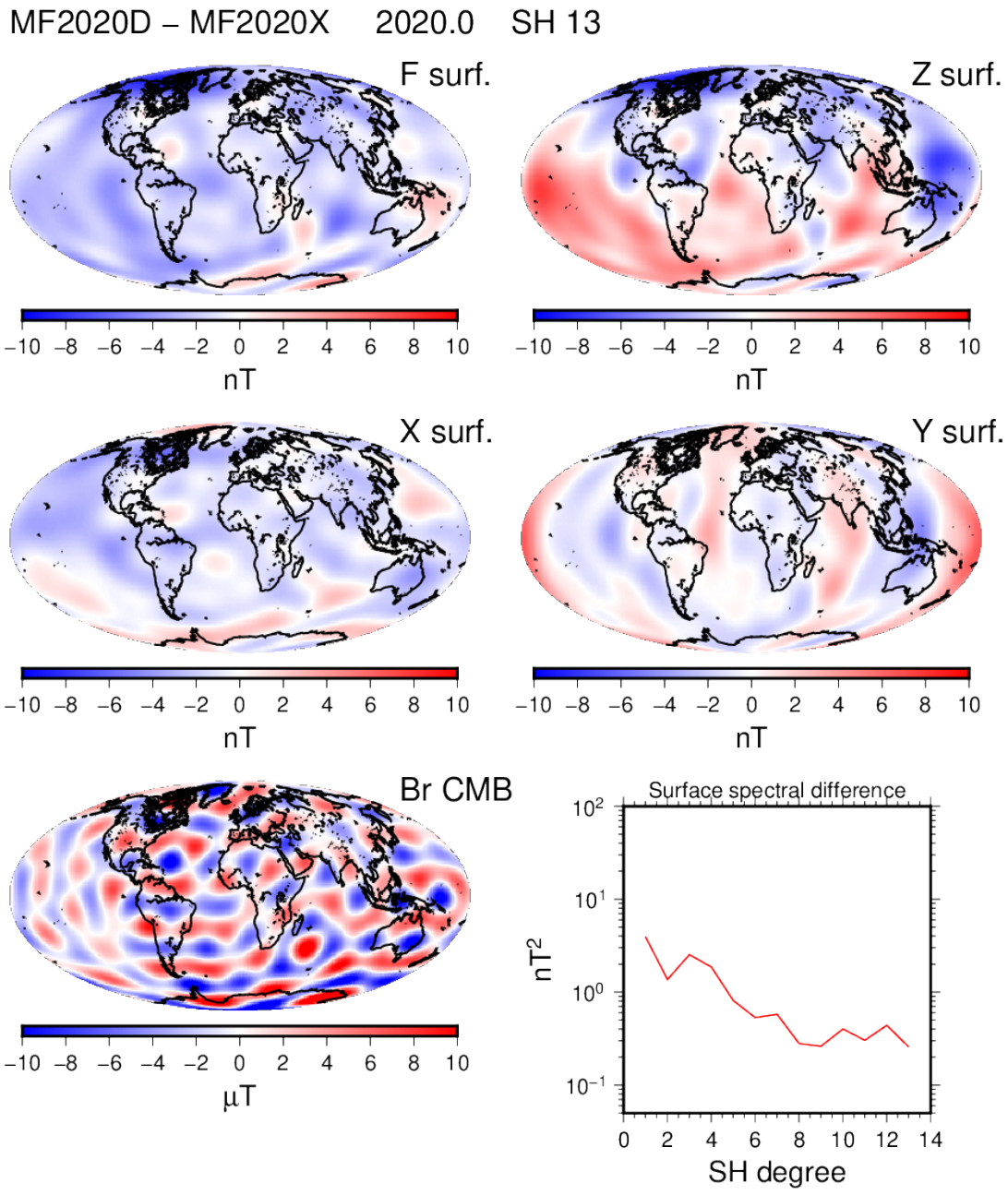
MF2020D – MF2020X 2020.0 SH 13
F surf.
Z surf.
X surf.
Y surf.
Br CMB
−10 −8 −6 −4 −2 0 2 4 6 8 10
nT
μT
Surface spectral difference
nT²
SH degree
0 2 4 6 8 10 12 14

B.2.5 GFZ (E)

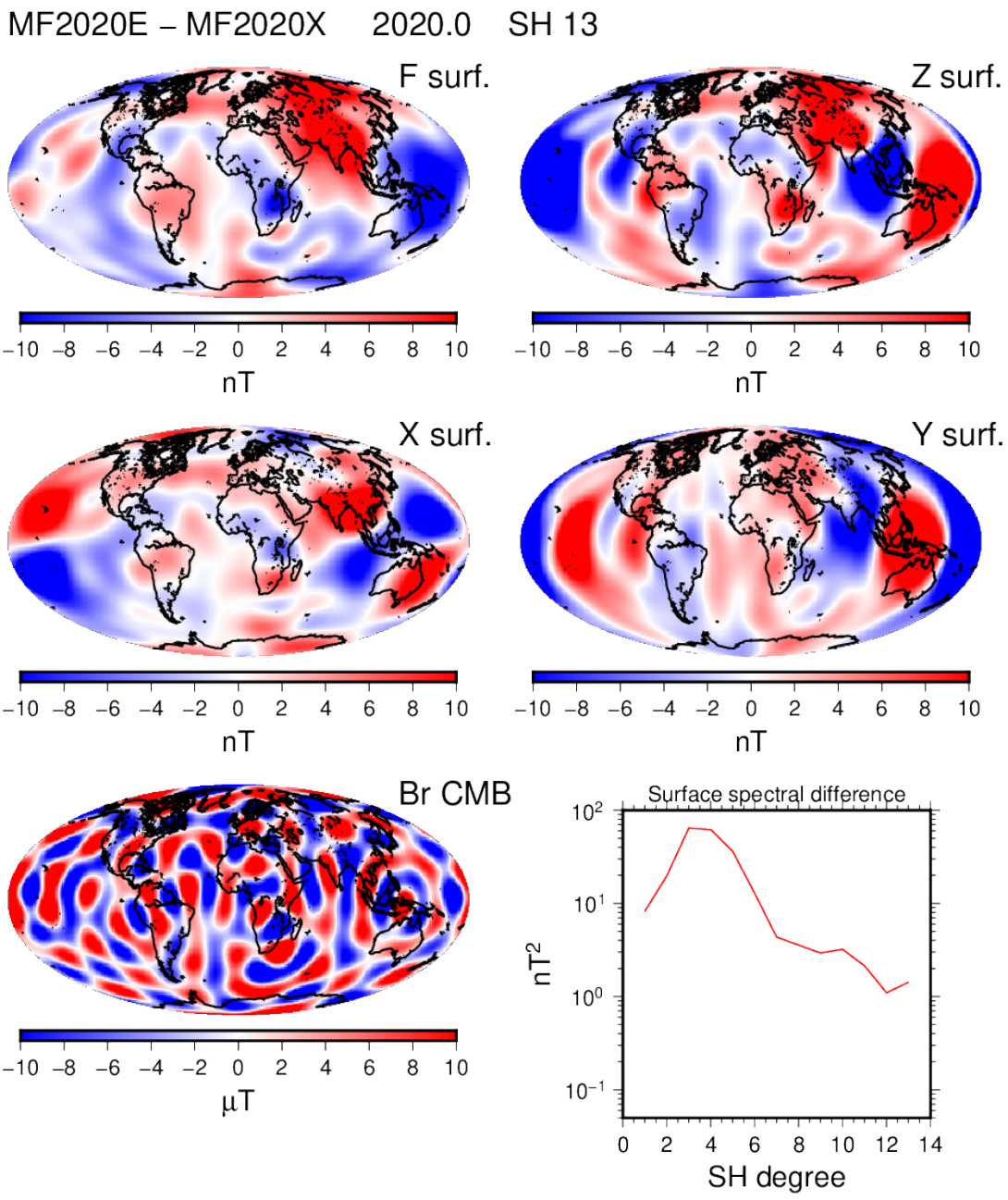
MF2020E – MF2020X 2020.0 SH 13
F surf.
Z surf.
X surf.
Y surf.
Br CMB
−10 −8 −6 −4 −2 0 2 4 6 8 10
nT
μT
Surface spectral difference
nT²
SH degree

B.2.6 IPGP (F)

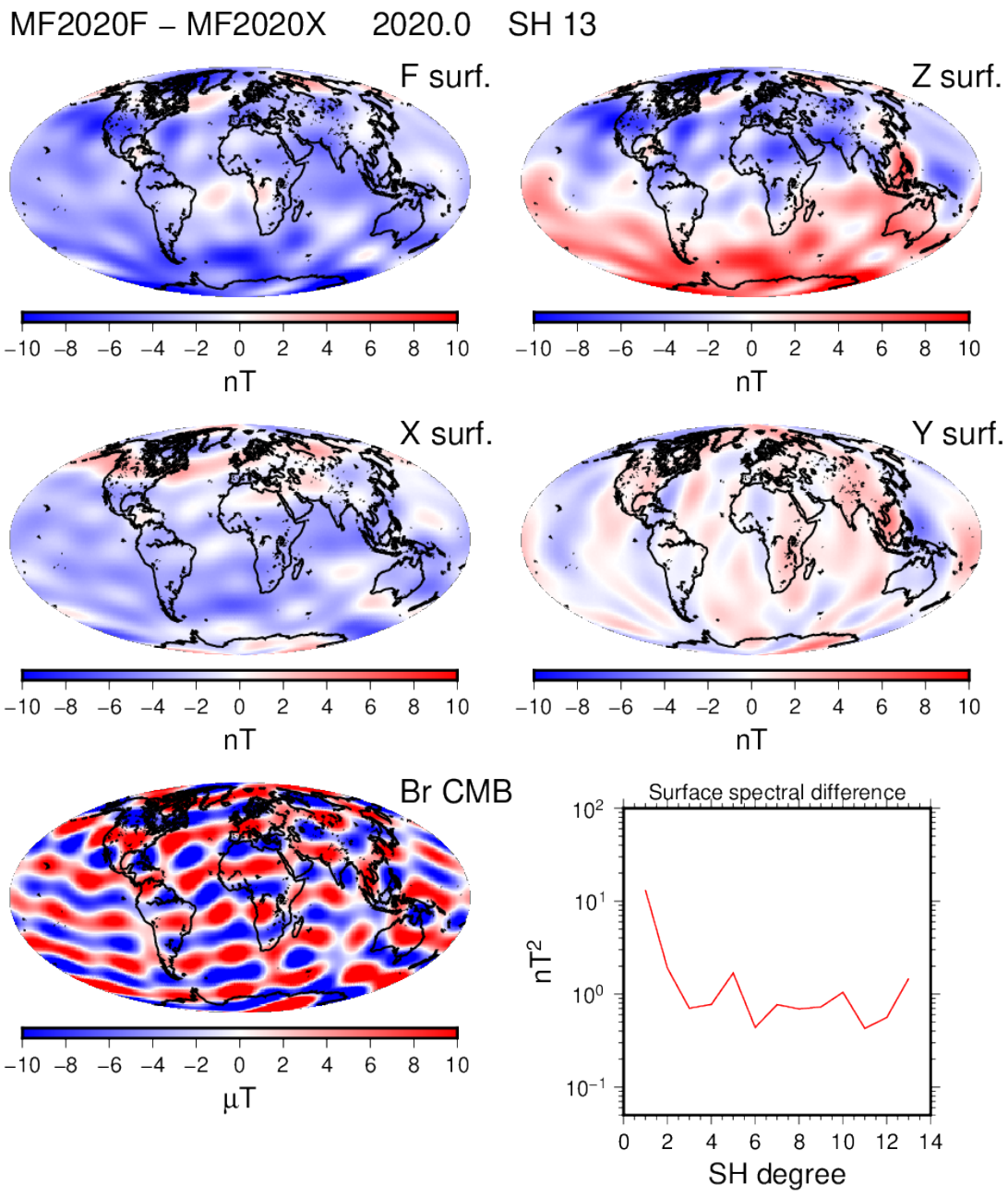
MF2020F – MF2020X 2020.0 SH 13
F surf.
Z surf.
X surf.
Y surf.
Br CMB
−10 −8 −6 −4 −2 0 2 4 6 8 10
nT
μT
Surface spectral difference
nT²
SH degree
0 2 4 6 8 10 12 14

B.2.7 `ISTerre` (G)

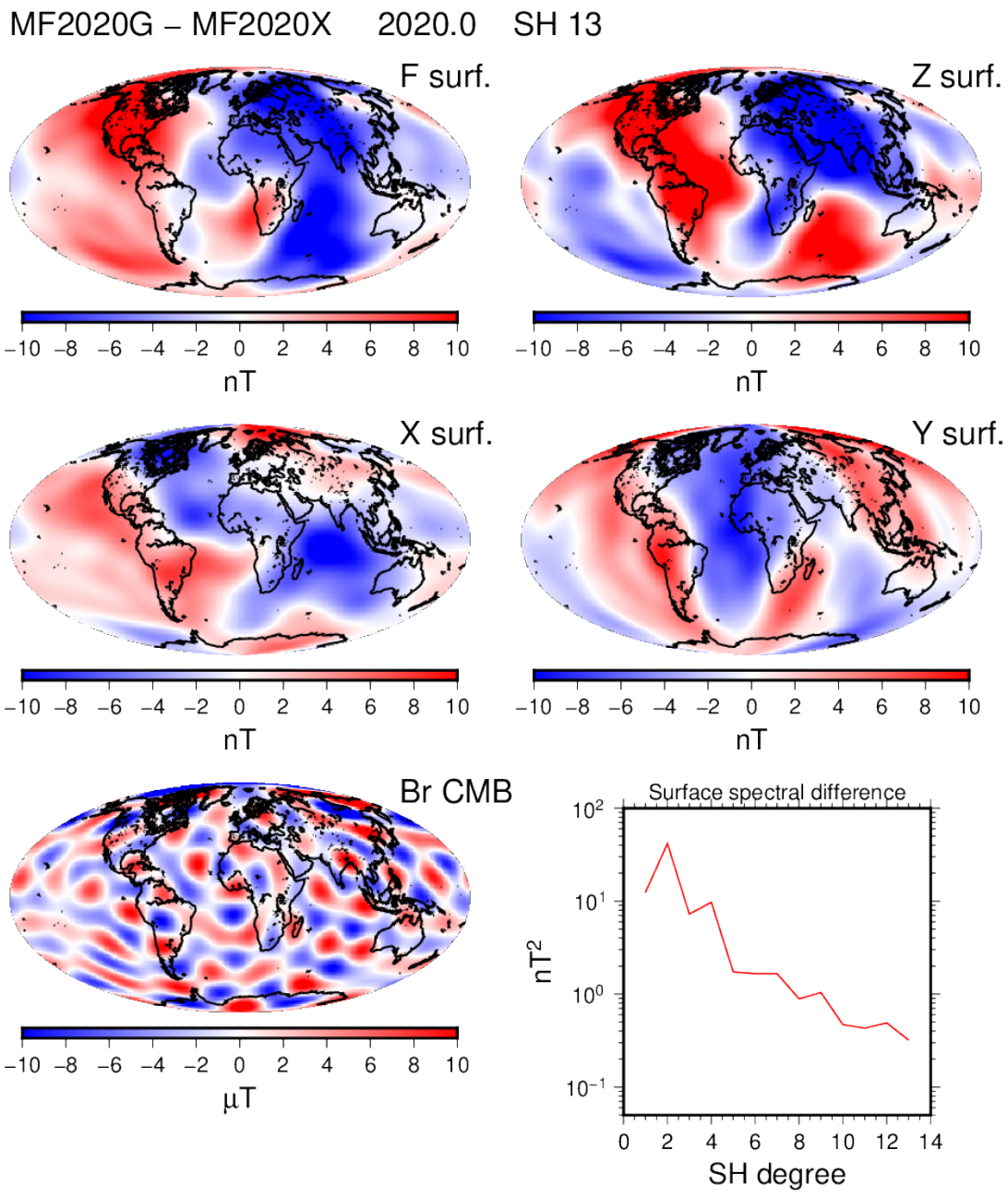

B.2.8 IZMIRAN (H)

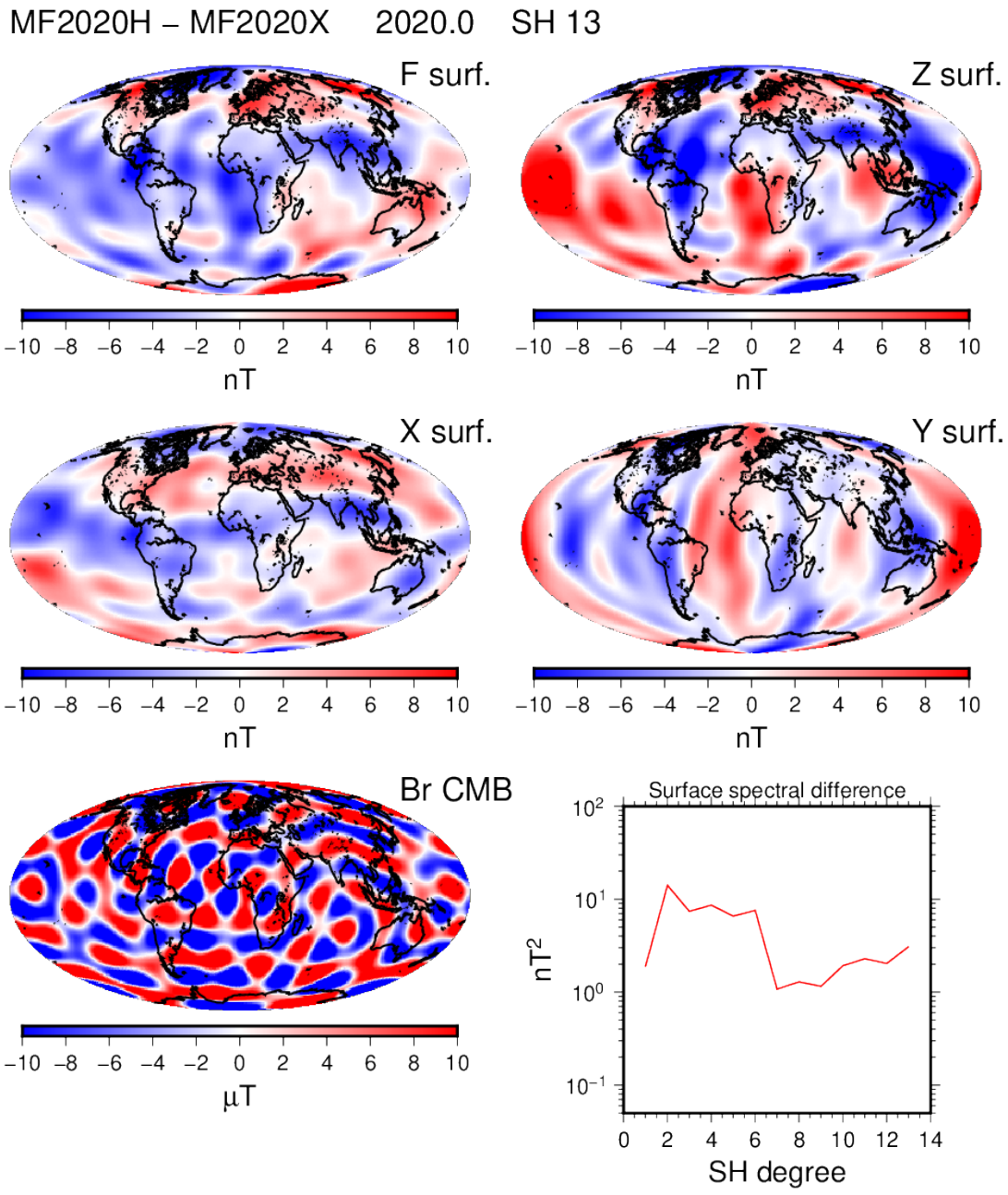

B.2.9 NASA/GSFC (L)

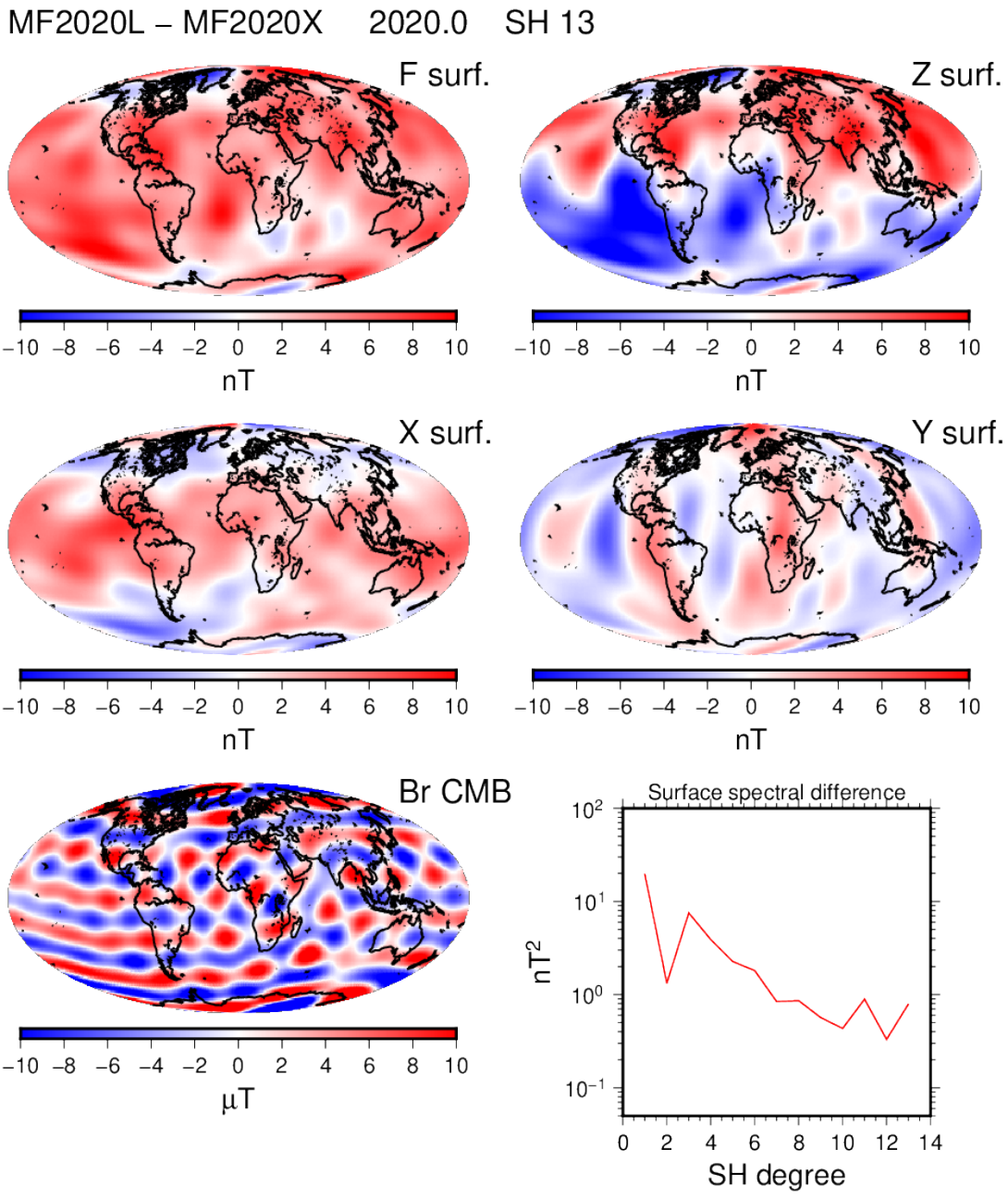

B.2.10 Uni Potsdam/Max Planck (M)

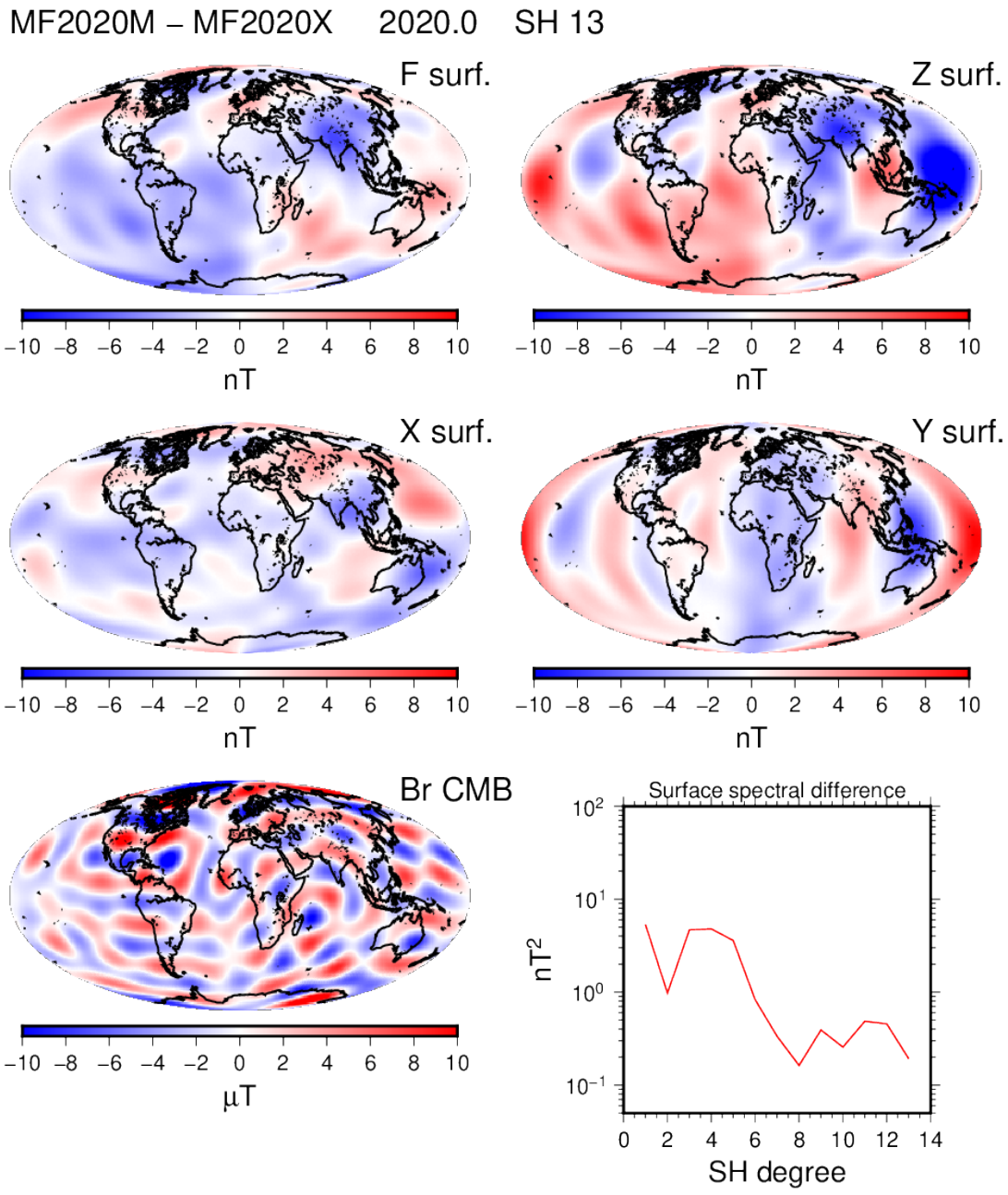

B.2.11 Spanish Team (N)

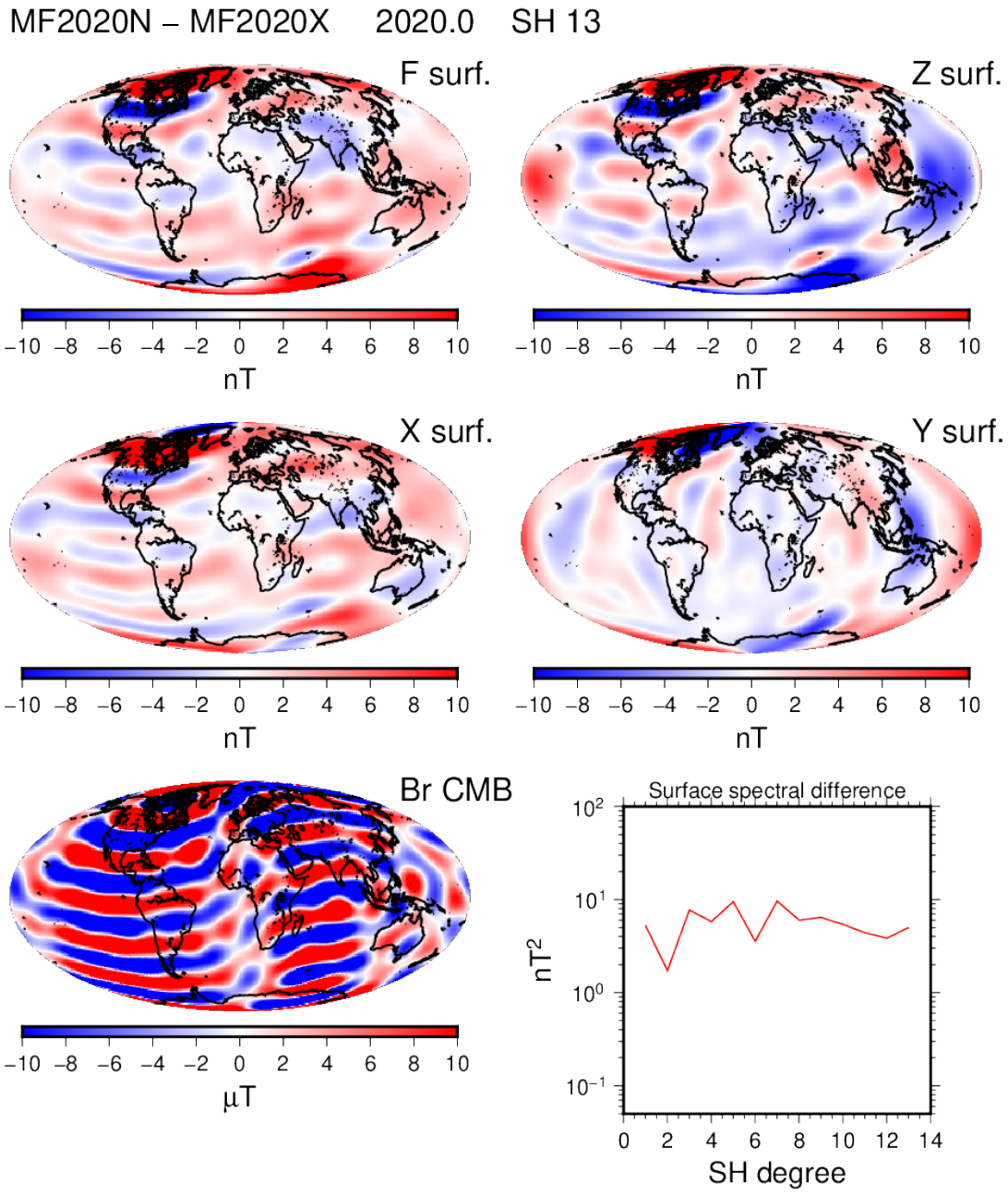

B.2.12 U Strasbourgh (O)

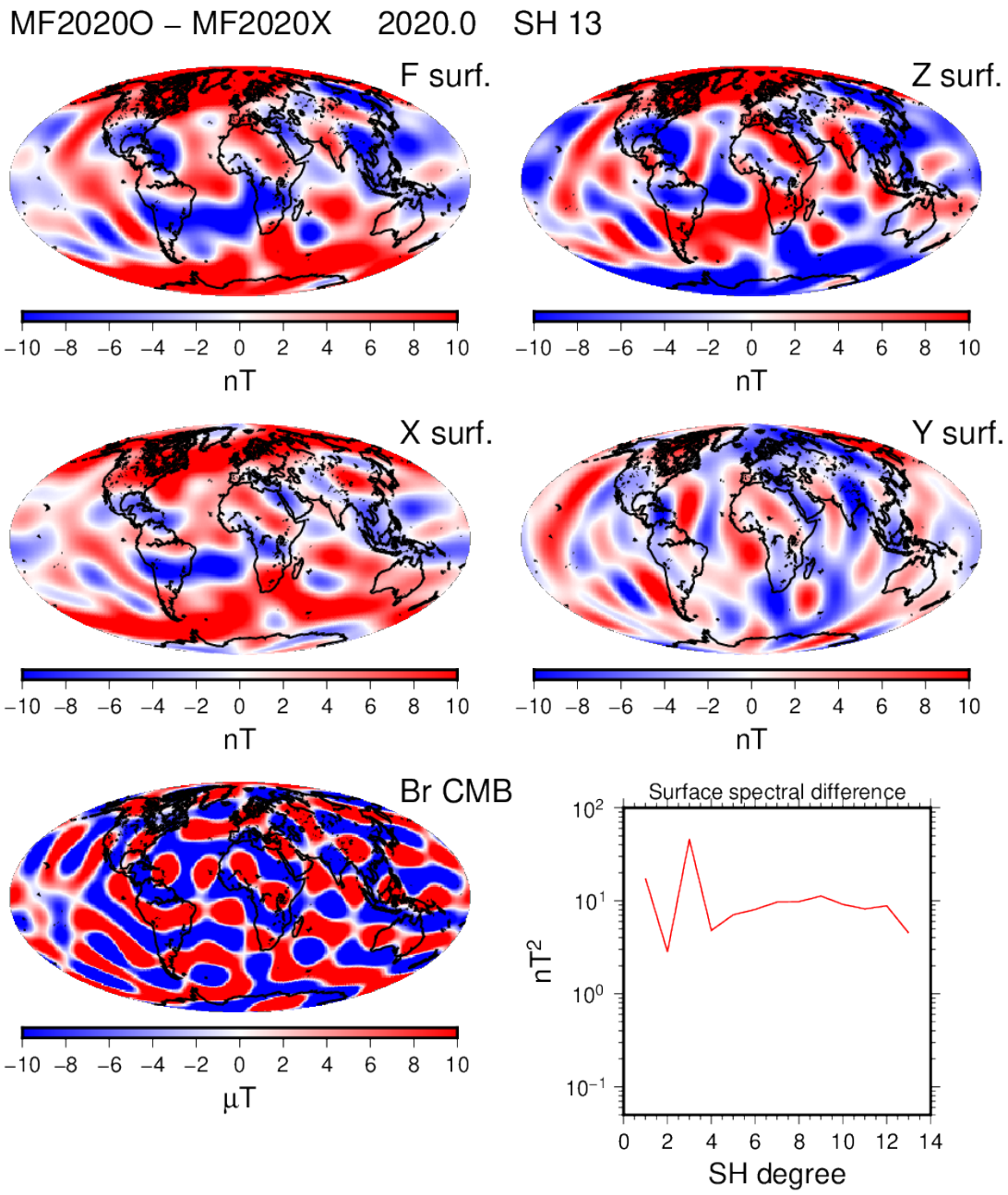

B.3 SV 2020–2025

SVA – SVX

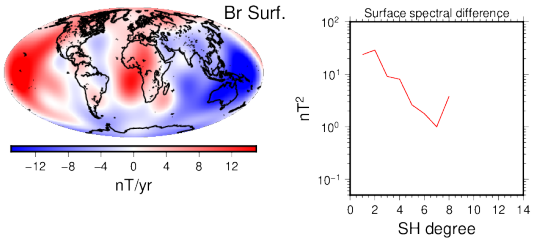

SVC – SVX

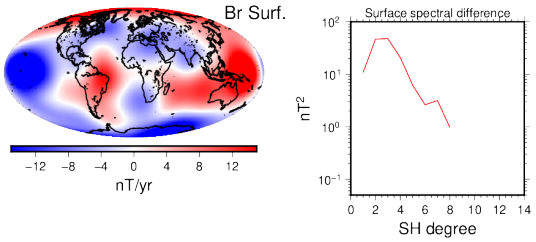

SVD – SVX

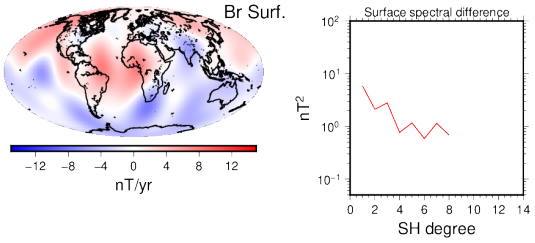

SVE – SVX

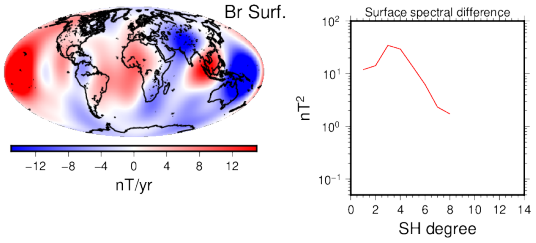

SVF – SVX

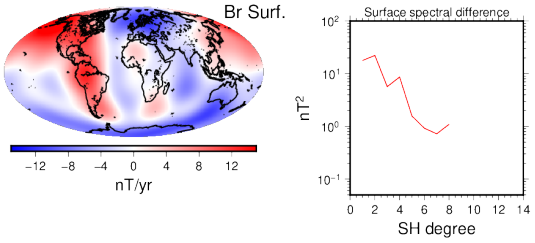

SVG – SVX

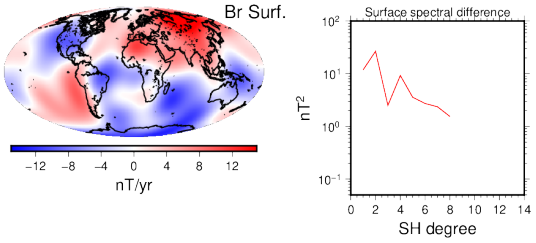

SVH – SVX

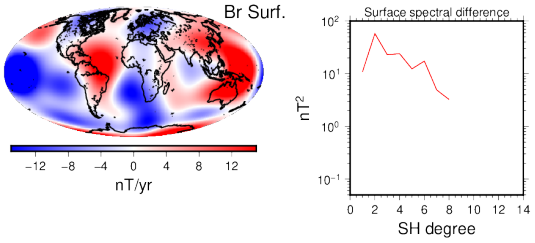

SVI – SVX

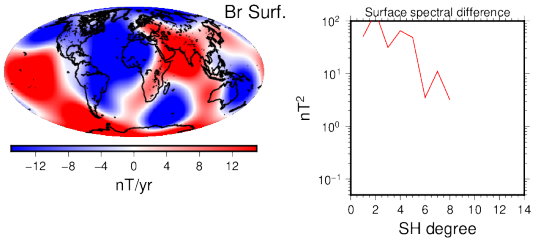

SVJ – SVX

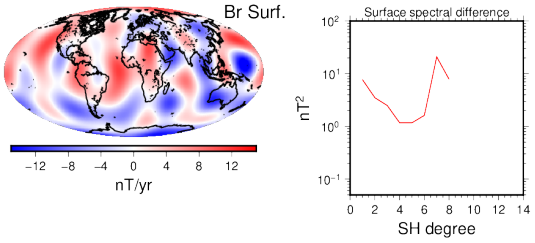

SVK – SVX

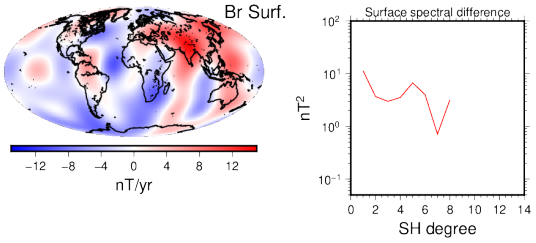

SVL – SVX

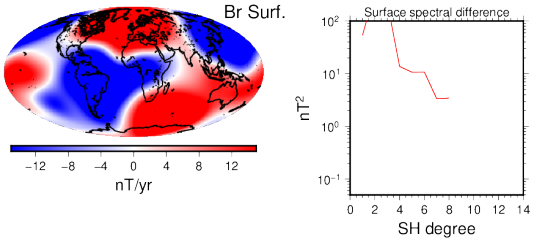

SVM – SVX

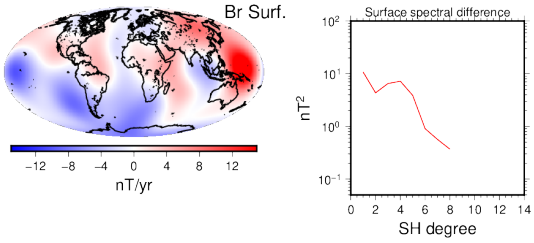

SVN – SVX

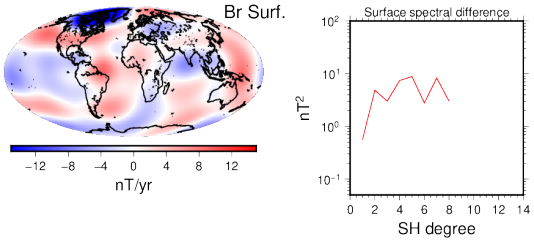

SVO – SVX